

Persistent Homology Captures the Generalization of Neural Networks Without A Validation Set

Asier Gutiérrez-Fandiño*
Barcelona Supercomputing Center
Barcelona, Spain
asier.gutierrez@bsc.es

David Pérez-Fernández*
SEGITTUR
Madrid, Spain
david.perez@inv.uam.es

Jordi Armengol-Estapé
Barcelona Supercomputing Center
Barcelona, Spain
jordi.armengol@bsc.es

Marta Villegas
Barcelona Supercomputing Center
Barcelona, Spain
marta.villegas@bsc.es

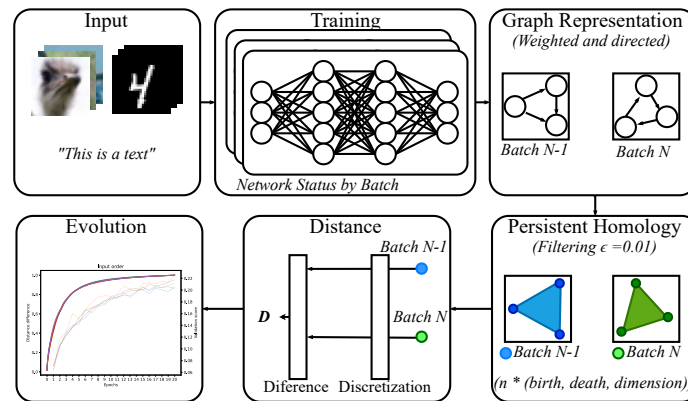


Figure 1: Our proposal.

Abstract

The training of neural networks is usually monitored with a validation (holdout) set to estimate the generalization of the model. This is done instead of measuring intrinsic properties of the model to determine whether it is learning appropriately. In this work, we suggest studying the training of neural networks with Algebraic Topology, specifically Persistent Homology (PH). Using simplicial complex representations of neural networks, we study the PH diagram distance evolution on the neural network learning process with different architectures and several datasets. Results show that the PH diagram distance between consecutive neural network states correlates with the validation accuracy, implying that the generalization error of a neural network could be intrinsically estimated without any holdout set.

*Equal contribution.

1 Introduction

Generalization is what makes a machine learning model useful; the uncertainty of its behaviour with unseen data is what makes it potentially dangerous. Thus, understanding the generalization error of a model can be considered one of the holy grails of the entire machine learning field.

Machine learning practitioners typically monitor some metrics of the model to estimate its generalization error and stop the training even before the numerical convergence to prevent the overfitting of the model. Usually, the error measure or the metric relevant to the task is computed for a holdout set, the validation set. Since these data have not been directly used for updating the parameters, it is assumed that the performance of the model on the validation set can be used as a proxy of the generalization error, provided it is representative of the data that will be used in inference. One can, though, potentially overfit to this holdout set if it is repeatedly used for guiding a hyperparameter search.

Instead of relying on an external set, though, the question of whether it could be possible to estimate the generalization error with some intrinsic property of the model is highly relevant, and it has been barely explored in the literature. On the other hand, Algebraic Topology has recently been gaining momentum as a mathematical tool for studying graphs, machine learning algorithms, and data.

In this work, we have the goal of, once having characterized neural networks as weighted, acyclic graphs, represented as Algebraic Topology objects (following previous works), computing distances between consecutive neural network states. More specifically, we can calculate the Persistent Homology (PH) diagram distances between a give state (i.e., when having a specific weights during the training process) and the next one (i.e., after having updated the weights in a training step) (see Figure 1). We observe that during the training procedure of neural networks we can measure this distance in each learning step, and show that there exists a high correlation with the corresponding validation accuracy of the model. We do so in a diverse set of deep learning benchmarks and model hyperparameters. This shines light on the question of whether the generalization error could be estimated from intrinsic properties of the model, and opens the path towards a better theoretical understanding of the dynamics of the training of neural networks.

In summary, our contributions are as follows:

- Based on principles of Algebraic Topology, we propose measuring the distances (Silhouette and Heat) between the PH persistence diagrams obtained from a given state of a neural network during the training procedure and the one in the immediately previous weights update.
- We empirically show that the evolution of these measures during training correlate with the accuracy in the validation set. We do so in diverse benchmarks (MNIST, CIFAR10, CIFAR100, Reuters text classification), and models (MLPs in MNIST and Reuters, MLPs and CNNs in CIFAR100 and CIFAR100).
- We thus provide empirical proof of the fact that valuable information related to the learning process of neural networks can be obtained from PH distances between persistence diagrams (*homological convergence*). In particular, we show that homological convergence is related to learning process and the generalization properties of neural networks.
- In practice, we provide a new tool for monitoring the training of neural networks, and open the path to estimating their generalization error without a validation set.

The remainder of this article is as follows. In Section 2 we describe the theoretical background of our proposal in terms of Algebraic Topology, while in Section 3 we go through the related work. Then, in Section 4 we formalize our method. Finally, in sections 6 and 7 we present and discuss our empirical results, respectively.

2 Background

In this section we introduce the mathematical foundations of this paper. A detailed mathematical description is included in the Supplementary Material.

A simplicial complex is a set composed of points, line segments, triangles, and their n -dimensional counterparts, named simplex (K). In particular, a simplicial complex must comply with two properties:

1. Every face of a simplex is also in the simplicial complex (of lower dimension). 2. The non-empty intersection of any two simplices contained on a simplicial complex is a face of both. 0,1,2,3-simplex and non simplex examples are shown in Figure 2.

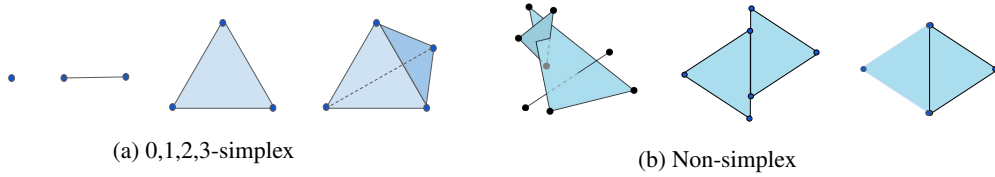


Figure 2: Simplex and non-simplex examples.

We can associate to an undirected graph, $G = (V, E)$, a simplicial complex where all the vertices of G are the 0-simplex of the simplicial complex and the complete subgraphs with i vertices, in G corresponds to a $(i - 1)$ -simplex. This type of construction is usually called a complex clique on the graph G , and is denoted by $Cl(G)$. Figure 3 shows a graph clique complex $Cl(G)$ example.

The boundary function is defined as a map, from an i -simplex to an $(i - 1)$ -simplex, as the sum of its $(i - 1)$ -dimensional faces. A boundary function sample is shown in Figure 4.

In algebraic topology, a k -chain is a combination of k -simplices (sometimes symbolized as a linear combination of simplices that compose the chain). The boundary of a k -chain is a $(k - 1)$ -chain. It is the linear and signed combination of chain element boundary simplices. The space of i -chains is denoted by $C_i(K)$.

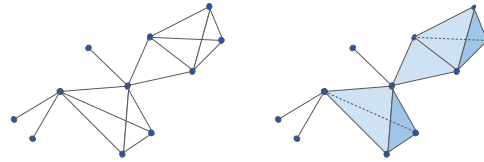


Figure 3: Graph clique complex $Cl(G)$ example.

There are two special cases of chains that will be useful to define homology:

- Closed chain or i -cycle: i -chain with empty boundary. An i -chain c is an i -cycle if and only if $\partial_i c = 0$, i.e. $c \in \ker(\partial_i)$. This subspace of $C_i(K)$ is denoted as $\mathbb{Z}_i(K)$.
- Exact chain or i -boundary: An i -chain c is an i -boundary if there exists an $(i + 1)$ -chain d such that $c = \partial_{i+1}(d)$, i.e. $c \in \text{im}(\partial_{i+1})$. This subspace of $C_i(K)$, the set of all such i -boundaries forms, is denoted by $\mathbb{B}_i(K)$.

Now, if we think in the i -cycles that do not bound an $(i + 1)$ -simplicial complex, this is the definition i -th homology of the simplicial complex K . The precise definition is the quotient space of $\mathbb{B}_i(K)$ a subspace of $\mathbb{Z}_i(K)$ (see Supplementary Material). The number of non equivalent i -cycles (Figure 5) is the dimension of the homology group $H_i(K)$, also named Betti numbers.

We can create a nested family of simplicial complexes, K_ϵ , where at each step t , K_ϵ is embedded in the simplicial complex $K_{\epsilon+1}$. We call this set a simplicial complex filtration.

For each filtration simplicial complex, we can calculate the homology groups. Then, we can look at the birth, that is, when a homology class appears, and death, the time when the homology class disappears. The PH treats the birth and the death of these homological features in K_ϵ for different ϵ values. The lifespan of each homological feature can be represented as an interval (*birth, death*), of

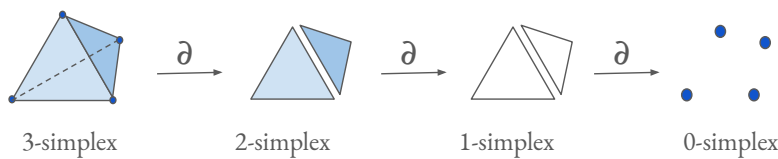


Figure 4: Boundary function sample.

the homological class. Given a filtration, this collection of intervals is named a Persistence Diagram (PD) [5].

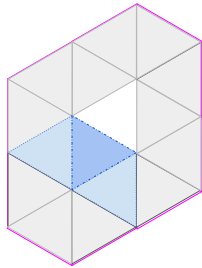


Figure 5: The two blue dashed cycles are homologically equivalent, the pink isn't.

It is possible to compare two PDs using specific distances (Wasserstein and Bottleneck). To efficiently perform this operation, due to the size of these diagrams, it is sometimes necessary to simplify them by means of a discretization process (such as Weighted Silhouette and Heat vectorizations).

3 Related Work

Algebraic Topology and Machine Learning

The use of Algebraic Topology in the fields of data science and machine learning has been gaining momentum in recent years (see Carlsson [5]). Specifically in the case of neural networks, some works have applied topology for improving the training procedure of the models [15, 8],

or pruning the model afterwards [30]. Other works have focused on analyzing the capacity of neural networks [14, 26, 17] or the complexity of input data [17]. Furthermore, recent works have provided topological analysis of the decision boundaries of classifiers based on PH and Betti numbers [24, 22].

Graph and topological representations of neural networks Gebhart et al. [12] suggest a method for computing the PH over the graphical activation neural networks, while Watanabe and Yamana [29] propose representing neural networks via simplicial complexes based on Taylor decomposition, from which one can compute the PH. Chowdhury et al. [7] show that directed homology can be used to represent MLPs. Anonymous [2] concurrently show neural networks, when represented as directed, acyclic graphs, can be associated to an Algebraic Topology object. By computing the PH diagram, one can effectively characterize neural networks, and even compute distances between two given neural networks, which can be used to measure their similarity. This is unlike other works [11, 13] approximating neural networks representations with regard to the input space.

Estimating the generalization and studying the learning process We are, though, specifically interested in the use of PH for analyzing the learning process, especially with the goal of estimating generalization. In this regard, the literature is perhaps more limited. Jiang et al. [16] work on understanding what drives generalization in deep networks from a Bayesian of view. Neyshabur et al. [23] study the generalization gap prediction from the training data and network parameters using a margin distribution, which are the distances of training points to the decision boundary. In Li et al. [21], authors propose an alternative to cross-validation for model selection based on training once on the whole train set, without any data split, deriving a validation set with data augmentation.

Corneanu et al. [10] try to estimate the performance gap between training and testing using PH measures. They claim. However, one can observe some caveats. The first one is that their regression fitted to predict the test error has a considerably high error, making it not usable in practice. The second caveat is that for fitting the regression one needs at least part of the sequestered testing set.

In this work, motivated by the interest of having a better understanding of whether it would be possible to estimate the generalization of neural networks without a holdout set, we suggest using the topological characterization and distances concurrently proposed in Anonymous [2] but, crucially, measured between consecutive weight updates. We will show that the evolution of this distance is similar to the one of the validation accuracy. Unlike Li et al. [21], we do not use any data at all. Unlike [10], we do not build a statistical or machine learning model (linear regression) for predicting the testing error. Instead, we propose a new measure, and we empirically show that it highly correlates with the validation accuracy. Note that in this work we do not work with any input data and activations, but with the parameters of the neural network themselves.

4 Approach

Representation For representing neural networks as graphs, we follow the approach proposed concurrently in Anonymous [2]. We associate to the neural network, at each learning state (defined by its weights), a weighted directed graph that is analyzed as an abstract simplicial complex. It is important to note that abstract simplicial complex are used in opposition to geometric simplicial complex.

For every training state, neural network connections are considered as directed and weighted edges between neurons, represented by graph nodes. Biases are considered as new edges that join to isolate vertices. In this representation, activation functions are lost. Bias information could also have been ignored because, as we will see, it is not very informative in terms of homology, but we decided to preserve it.

Negative edge weights are represented with reverse edges with the same weight absolute value. We discard the use of weight absolute value as neural networks are not invariant under weight sign transformations. This representation is consistent with the fact that every neuron can be replaced by a neuron from which two edges with opposite weights emerge and converge again on another neuron with opposite weights. From an homological point of view, this would be represented as a closed cycle. Weights are normalized following the Equation 1. ζ is a smoothing parameter that we set to $1e-6$. This smoothing parameter is necessary as we want to avoid normalized weights of edges to be 0 (in our representation 0 implies a lack of connection):

$$\max\left(1 - \frac{|w|}{\max(|\max(W)|, |\min(W)|)}, \zeta\right) \quad (1)$$

Algebraic Topology object For each weighted directed graph associated with the state of a neural network, we link a directed flag complex to it. The topological properties of this directed flag complex are studied using homology groups H_n . We calculate the homology groups up to degree 3 (H_0-H_3).

For each state, we use a family of simplicial complexes, K_ε , for a range of values of $\varepsilon \in \mathbb{R}$. The simplicial complex at step ε_t is embedded in the complex at ε_{t+1} , for $\varepsilon_t \leq \varepsilon_{t+1}$, i.e. $K_\varepsilon \subseteq K_{\varepsilon_{t+1}}$. ε is used as a filter that establish the minimum weight of the graph representation edges included on the simplicial complex. This collection of contained simplicial complex (associated to a directed weighted graph), called filtration, $K_{\varepsilon_{min}} \subseteq \dots \subseteq K_{\varepsilon_t} \subseteq K_{\varepsilon_{t+1}} \subseteq \dots \subseteq K_{\varepsilon_{max}}$, where $t \in [0, 1]$ and $\varepsilon_{min} = 0$, $\varepsilon_{max} = 1$ (remember that edge weights are normalized).

The sequence of homology groups is calculated by varying the ε parameter to obtain the persistence homology diagram. In our case, persistent homology calculations are performed on \mathbb{Z}_2 . In other words, once the corresponding filter has been applied to the weight of the edges, all connected edges are considered equally.

Distances between persistence diagrams of consecutive states In this paper, we are interested in comparing PDs between different simplicial complex associated to each training state of the neural network. There are two distances traditionally used to compare PDs, Bottleneck distance (the length of the longest edge) and Wasserstein distance (using the sum of all edges lengths, instead of the maximum). Their stability with respect to perturbations on PDs has been object of different studies [6, 9].

In order to make computations feasible and obviate noisy intervals, we filter the PDs by limiting the minimum PD interval size. We do so by setting a minimum threshold $\eta = 0.01$. Intervals with a lifespan under this value are not considered (spurious homological features). Additionally, for computing distances, we need to remove infinity values. As we are only interested in the deaths until the maximum weight value, we replace all the infinity values by 1.0.

In our case, our neural networks have millions of persistence intervals per Persistence Diagram, while Wasserstein distance calculations are computationally hard for large PDs. In order to make calculations computationally feasible, we will use a vectorized version of PDs, also called PD discretization. This vectorized version summaries have been proposed and used on recent literature [1, 3, 4, 19, 25]. For persistence diagram distance calculation, we use weighted Silhouette and Heat vectorizations, using the Giotto-TDA library [27].

5 Experiments

Data We validate our method in several heterogeneous (vision, natural language), well-known datasets, namely 1. MNIST [20], 2. CIFAR-10, 3. CIFAR-100 [18], and 4. the Reuters dataset [28] (multi-class and multi-label document classification dataset).

Models We experiment with two neural architectures, 1. MLPs and 2. CNNs. In the latter case, we use the convolutional layers as a pre-trained model with frozen weights, and we learn an MLP on top of it. The reason we do so is that our method is based in a representation that, at least in the basic form, does not allow capturing information from convolutional layers. Thus, we need a single (exact same weights) feature extractor, to abstract away distances related to the CNN layers and focus on the MLP.

Conducted experiments We define the *base* MLP architecture as $\{\text{Input}, \text{Linear}(512), \text{Dropout}(0.2), \text{Linear}(512), \text{Dropout}(0.2), \text{Output}\}$. In the case of CNNs, the pre-trained model is defined as 3 convolutional blocks with kernel size 3 (starting with 32 channels), interleaved with max pooling (its linear layers are thrown away after the pre-training). On top of the pre-trained CNN, we also define the same base MLP architecture. Then, for each dataset and model (MLP and CNN), we experiment with varying (while keeping the rest fixed to the base architecture)

1. Layer size (number of units per layer): 4, 16, 32, 128, 256.
2. Number of labels (the other classes are removed): 2, 4, 6, 8, 10.
3. Learning rate: $1e-05$, 0.0001, 0.001, 0.01, 0.1
4. Dropout: 0.0, 0.2, 0.4, 0.5, 0.8.
5. Input order: 5 random input orders. As a control experiment, for each analyzed problem we run the same configuration with 5 different input orders. If the measured distances are, indeed, related with the learning process of neural networks, these variations should not have any noticeable effect.

We run each configuration 5 times with different random seeds (and, thus, weight initializations²) to see if the results are consistent across runs. All models are trained with the RMSProp optimizer with a batch size of 256.

Distances and validation accuracy computation Note that homological distances are obtained at the end of each batch, while validation metrics are only computed on each epoch. The methodology we follow to analyze the learning process on each different problem can be summarized with the following steps:

1. In each training step (i.e., for each batch) we extract the weights from the MLP current state and use them to build an abstract simplicial complex from the associated weighted directed graph.
2. We calculate the homological persistence diagram of the simplicial complex.
3. We then calculate the distance between consecutive persistence diagrams (we will call this sequence *homological convergence*). We use two different distances, namely, Heat and Silhouette.
4. We compare the homological convergence with the evolution of the validation results on neural network learning process.

Hardware All experiments were executed in a machine with 2 NVIDIA V100 of 32GB, 2 Intel(R) Xeon(R) Platinum 8176 CPU @ 2.10GHz, and of 1.5TB RAM, for a total of around 7 days. We note that our method is considerably demanding in terms of both compute and memory.

The code and outputs are fully available³ under MIT License.

²The pre-trained convolutional weights are always identical, though.

³<https://github.com/asier-gutierrez/nn-evolution>

6 Results

In this section, we highlight the main results, omitting the ones with Silhouette (since the obtained results were clearer with Heat). See the Supplementary Material for the full results (plots and correlations), including the ones with Silhouette distance.

We study the relation between the evolution of the PH diagram distances with the one of the validation score with the cumulative values of the distance between homologous persistence diagrams because this value seems much more stable. The information of the distance between the persistence diagrams has been normalized to visualize clearly the type of evolution of each curve on the same scale. Some of the non-normalized plots can be found in the Supplementary Material. Figure 6 shows the cumulative and non-cumulative homology the MNIST experiment with layer size.

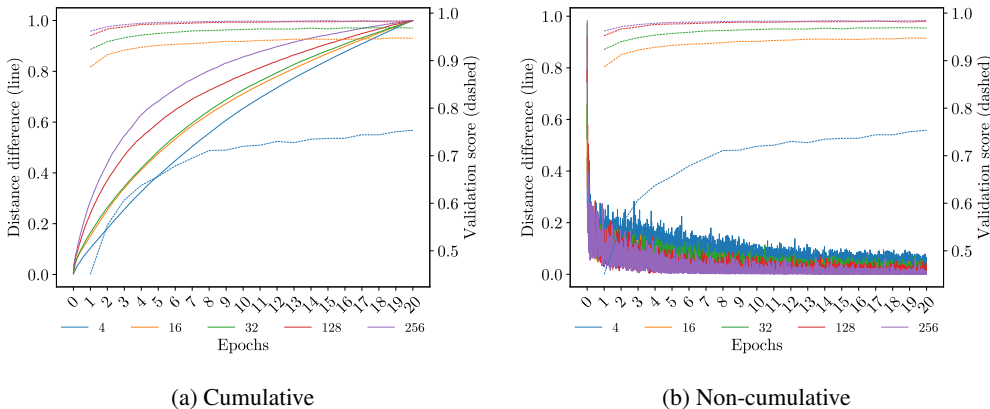


Figure 6: Heat distance and validation accuracy curves on the MNIST experiment with layer size. Normalized.

For each experiment (e.g., layer size in MNIST), we plot both the evolution of the PH diagram distance and the validation score (accuracy). The plotted values are the corresponding means of the 5 repetitions with different seeds. In addition, we compute the Pearson correlation for these values. Plots show on the x-axis each training step (for each batch) of the evolution in the training state of the neural network. On the y-axis, two scales are shown that apply to the distance curves between accumulated persistence diagrams (solid lines), scale on the right side, and the neural network validation (dotted lines), numerical scale on the left side. For each sub-experiment (for example, different values of layer size) a different color was used.

The general result is that the evolution of the homological convergence of the MLPs seems to be very similar to the one of the validation score. This is generally consistent across experiments (see the Supplementary Material). Table 1 shows the mean (and standard deviations) of the Pearson correlations for all datasets. All means are above 0.8, implying that there is strong correlation. Intuitively, this is also observed in the plots, although once the distances are normalized it is not as clear to visualize. Interestingly, we find that the very few exceptions in which the correlation is low corresponds to extreme values (very small number of neurons per layer, very high learning rate, very high dropout), in which the neural network doesn't end up learning properly.

In the case of CNNs, the correlations are lower (although still almost always above 0.8 in experiments such as the one of increasing the number of layers). Recall that in the case of CNN we froze a single convolutional feature extractor, since our method only supports MLPs. We believe these lower correlations can be explained because an important part of the learning process happened in the convolutional layers (in the pre-training), which we do not capture.

Another finding is that the method obtains consistent results across runs, meaning that it is capturing information related to important properties of the networks themselves instead of random artifacts.

When varying the studied hyperparameters, we observe that the curves for each configuration are indeed, different. Remarkably, in the control experiments, this is not the case; results show that the homological convergence during the learning of the same problem with the same model but with

Dataset	Heat distance		Silhouette distance	
	Means mean	Deviations mean	Means mean	Deviations mean
MNIST	0.8910	0.0424	0.8910	0.0424
Reuters	0.6220	0.0700	0.6220	0.0700
CIFAR-10 MLP	0.8233	0.0649	0.8233	0.0649
CIFAR-10 CNN	0.4241	0.1915	0.4241	0.1915
CIFAR-100 MLP	0.8420	0.0566	0.8420	0.0566
CIFAR-100 CNN	0.6130	0.0800	0.6130	0.0800

Table 1: Correlation of validation values with topological difference cumulative. Correlation is computed with 20 points.

different input order is very similar. The alteration of the order of the input doesn't have any effect in the homological convergence. The results of two of these experiments are shown in Figure 7.

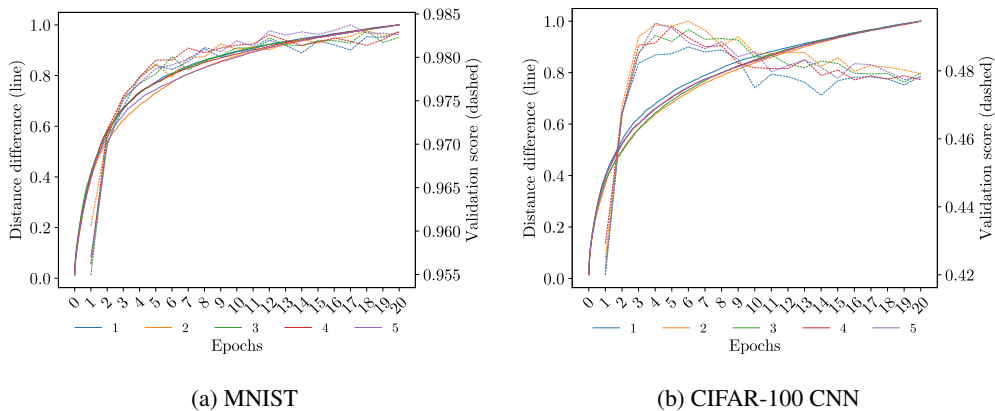


Figure 7: Learning evolution on input order experiments (control experiments). Normalized.

In addition, we observe that when the neural network learns the given problem, homological convergence occurs. For example, when the layer size is modified, the capacity of the neural network to learn the problem changes (Figure 6). When it can't learn the problem, because the network does not have sufficient capacity (the layer size is too small, 4 units), the homology does not seem to converge.

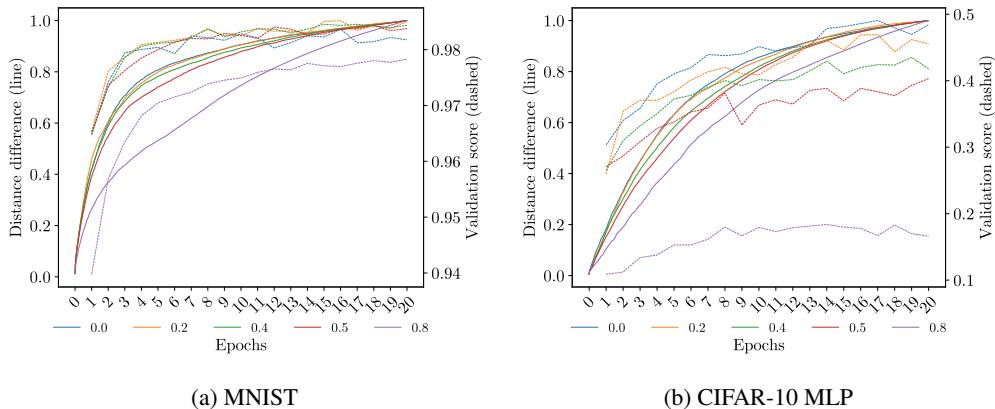


Figure 8: Learning evolution when dropout parameter is changed. Normalized.

Regarding the learning rate, the results are coherent with the intuition that it is a fundamental parameter that controls how much to change the model in response to the estimated error during the learning process. A too small learning rate may result in a long training process that could be stalled,

while a too large value may fall in a fast suboptimal solution or an unstable training process. Using homological convergence we find similar behaviour, as can be seen in Figure 9.

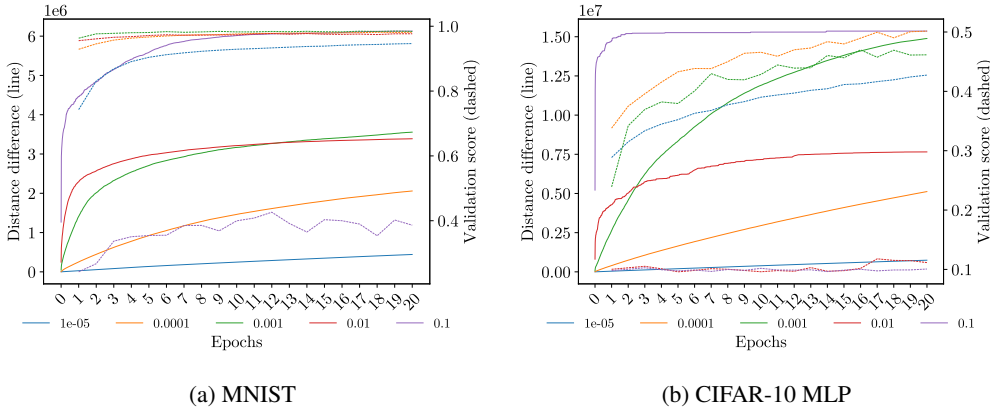


Figure 9: Learning evolution when modifying the learning rate parameter. Not normalized.

Finally, we note that even if the two convergences (validation and homological convergence) are correlated, they are not the same process. This is especially visible in the case of the learning rate experiments. For instance, in Figure 9, homological convergence is reached before the stabilization of the validation accuracy. Presumably, they are not capturing the exact same information; specifically, we believe that the difference is due to the fact that the validation accuracy depends on the specifics of the data sampled in the validation subset, while the homological convergence is independent of the validation data.

7 Discussion

We posed the question whether homological convergence (in terms of distances between PH diagrams in consecutive neural network states) is related to the learning process of neural networks. We have seen that, indeed, it is the case, with strong empirical results backing our claim.

This finding has a remarkable implication. If the homological convergence evolution mirrors the validation accuracy curve, one could ignore the validation set to monitor the training. This opens the path towards estimating the generalization of neural networks without the need of any holdout set. Researchers have wondered for a long time whether generalization could be predicted from intrinsic properties of the model or training data alone (i.e., without a holdout set), and in fact other works have claimed to do so. Although we do not provide any predictive model, we show that our proposed measures strongly correlate with the validation accuracy. In addition, we do so by not using any data at all; we just look at the neural network itself.

Our contribution aims pushing towards having a better understanding of the learning process of neural networks, not targeting any specific direct application. However, we note that it can be effectively used for monitoring the training of neural networks in terms of convergence expected generalization, as we have extensively shown in the experiments. Apart from the cases without access to a validation set, this is relevant because depending on a validation set has the risk of overfitting to it. Having an intrinsic, well-principled measure should be more robust to random noise in a specific data sample.

The main limitation of our method is its computational scalability. As we said in Section 5, our method took more than 7 days of compute in a HPC machine, even if we restricted the experiments to small datasets and parameter count. However, we note that our approach computes the *exact* persistence diagram distances, that is, we do not simplify the graph representation of the neural networks (we keep every single neuron and connections) and we do not approximate any computation. This leaves room for finding efficient approximations, opening a new research line. In addition, this lack of scalability has prevented us from validating our method on bigger models and datasets.

Finally, we note that instead of computing correlations, serving as a basic quantitative study, it would be interesting to perform a time-series analysis to gain more insights on how the two curves vary

together. Moreover, it would have been interesting to investigate how to build a predictive model of the validation accuracy from the PH distances, but it is was of the scope of this work.

8 Conclusions & Future Work

In this work, we have provided an empirical proof of the fact that homological convergence is related to the learning process and generalization properties of neural networks. Furthermore, we have shown that it can be used to monitor the training of a neural network (and potentially estimating its generalization) without a validation set. As future work, we suggest generalizing our representation to other neural architectures and scaling up the experiments to larger models and datasets, for which finding efficient approximations of our method will be crucial.

References

- [1] H. Adams, T. Emerson, M. Kirby, R. Neville, C. Peterson, P. Shipman, S. Chepushtanova, E. Hanson, F. Motta, and L. Ziegelmeier. Persistence images: A stable vector representation of persistent homology. *J. Mach. Learn. Res.*, 18:8:1–8:35, 2017.
- [2] A. Anonymous. Characterizing and measuring the similarity of neural networks with persistent homology, 2021.
- [3] E. Berry, Y.-C. Chen, J. Cisewski-Kehe, and B. T. Fasy. Functional summaries of persistence diagrams. *Journal of Applied and Computational Topology*, 4:211–262, 2020.
- [4] P. Bubenik. Statistical topological data analysis using persistence landscapes. *J. Mach. Learn. Res.*, 16:77–102, 2015.
- [5] G. Carlsson. Topology and data. *Bulletin of the American Mathematical Society*, 46:255–308, 2009.
- [6] F. Chazal, V. D. Silva, and S. Oudot. Persistence stability for geometric complexes. *Geometriae Dedicata*, 173:193–214, 2012.
- [7] S. Chowdhury, T. Gebhart, S. Huntsman, and M. Yutin. Path homologies of deep feedforward networks. *2019 18th IEEE International Conference On Machine Learning And Applications (ICMLA)*, pages 1077–1082, 2019.
- [8] J. Clough, I. Öksüz, N. Byrne, V. Zimmer, J. A. Schnabel, and A. P. King. A topological loss function for deep-learning based image segmentation using persistent homology. *IEEE transactions on pattern analysis and machine intelligence*, PP, 2020.
- [9] D. Cohen-Steiner, H. Edelsbrunner, and J. Harer. Stability of persistence diagrams. *Proceedings of the twenty-first annual symposium on Computational geometry*, 2005.
- [10] C. Corneanu, M. Madadi, S. Escalera, and A. Martínez. Computing the testing error without a testing set. *2020 IEEE/CVF Conference on Computer Vision and Pattern Recognition (CVPR)*, pages 2674–2682, 2020.
- [11] C. A. Corneanu, M. Madadi, S. Escalera, and A. M. Martinez. What does it mean to learn in deep networks? and, how does one detect adversarial attacks? In *2019 IEEE/CVF Conference on Computer Vision and Pattern Recognition (CVPR)*, pages 4752–4761, 2019. doi: 10.1109/CVPR.2019.00489.
- [12] T. Gebhart, P. Schrater, and A. Hylton. Characterizing the shape of activation space in deep neural networks. *2019 18th IEEE International Conference On Machine Learning And Applications (ICMLA)*, pages 1537–1542, 2019.
- [13] W. H. Guss and R. Salakhutdinov. On characterizing the capacity of neural networks using algebraic topology. *CoRR*, abs/1802.04443, 2018. URL <http://arxiv.org/abs/1802.04443>.
- [14] W. H. Guss and R. Salakhutdinov. On characterizing the capacity of neural networks using algebraic topology. *ArXiv*, abs/1802.04443, 2018.
- [15] C. Hofer, F. Graf, M. Niethammer, and R. Kwitt. Topologically densified distributions. *ArXiv*, abs/2002.04805, 2020.
- [16] Y. Jiang, D. Krishnan, H. Mobahi, and S. Bengio. Predicting the generalization gap in deep networks with margin distributions. *ArXiv*, abs/1810.00113, 2019.
- [17] E. Konuk and K. Smith. An empirical study of the relation between network architecture and complexity. *2019 IEEE/CVF International Conference on Computer Vision Workshop (ICCVW)*, pages 4597–4599, 2019.
- [18] A. Krizhevsky. Learning multiple layers of features from tiny images. 2009.
- [19] P. Lawson, A. Sholl, J. Brown, B. T. Fasy, and C. Wenk. Persistent homology for the quantitative evaluation of architectural features in prostate cancer histology. *Scientific Reports*, 9, 2019.
- [20] Y. LeCun and C. Cortes. MNIST handwritten digit database. 2010. URL <http://yann.lecun.com/exdb/mnist/>.
- [21] W. Li, C. Geng, and S. Chen. Leave zero out: Towards a no-cross-validation approach for model selection. *CoRR*, abs/2012.13309, 2020. URL <https://arxiv.org/abs/2012.13309>.

- [22] G. Naitzat, A. Zhitnikov, and L. Lim. Topology of deep neural networks. *J. Mach. Learn. Res.*, 21:184:1–184:40, 2020.
- [23] B. Neyshabur, S. Bhojanapalli, D. McAllester, and N. Srebro. Exploring generalization in deep learning. In *NIPS*, 2017.
- [24] K. Ramamurthy, K. R. Varshney, and K. Mody. Topological data analysis of decision boundaries with application to model selection. *ArXiv*, abs/1805.09949, 2019.
- [25] B. A. Rieck, F. Sadlo, and H. Leitte. Topological machine learning with persistence indicator functions. *ArXiv*, abs/1907.13496, 2019.
- [26] B. A. Rieck, M. Togninalli, C. Bock, M. Moor, M. Horn, T. Gumbsch, and K. Borgwardt. Neural persistence: A complexity measure for deep neural networks using algebraic topology. *ArXiv*, abs/1812.09764, 2019.
- [27] G. Tauzin, U. Lupo, L. Tunstall, J. B. Pérez, M. Caorsi, A. Medina-Mardones, A. Dassatti, and K. Hess. giotto-tda: A topological data analysis toolkit for machine learning and data exploration, 2020.
- [28] M. Thoma. The reuters dataset, July 2017. URL <https://martin-thoma.com/nlp-reuters>.
- [29] S. Watanabe and H. Yamana. Topological measurement of deep neural networks using persistent homology. In *ISAIM*, 2020.
- [30] S. Watanabe and H. Yamana. Deep neural network pruning using persistent homology. In *2020 IEEE Third International Conference on Artificial Intelligence and Knowledge Engineering (AIKE)*, pages 153–156. IEEE, 2020.

Persistent Homology Captures the Generalization of Neural Networks Without A Validation Set

Supplementary Material

Asier Gutiérrez-Fandiño*
Barcelona Supercomputing Center
Barcelona, Spain
asier.gutierrez@bsc.es

David Pérez-Fernández*
SEGITTUR
Madrid, Spain
david.perez@inv.uam.es

Jordi Armengol-Estapé
Barcelona Supercomputing Center
Barcelona, Spain
jordi.armengol@bsc.es

Marta Villegas
Barcelona Supercomputing Center
Barcelona, Spain
marta.villegas@bsc.es

Appendix I

Mathematical definitions are contained in this Appendix.

Definition 1 (simplex) *A k -simplex is a k -dimensional polytope which is the convex hull of its $k + 1$ vertices. i.e. the set of all convex combinations $\lambda_0 v_0 + \lambda_1 v_1 + \dots + \lambda_k v_k$ where $\lambda_0 + \lambda_1 + \dots + \lambda_k = 1$ and $0 \leq \lambda_j \leq 1 \ \forall j \in \{0, 1, \dots, k\}$.*

Some examples of simplices are points (0-simplex), line segments (1-simplex), triangles (2-simplex) or tetrahedrons (3-simplex).

Definition 2 (simplicial complex) *We define a simplicial complex \mathcal{K} is a set of simplices that satisfies the following conditions:*

1. *Every subset (or face) of a simplex in \mathcal{K} also belongs to \mathcal{K} .*
2. *For any two simplices σ_1 and σ_2 in \mathcal{K} , if $\sigma_1 \cap \sigma_2 \neq \emptyset$, then $\sigma_1 \cap \sigma_2$ is a common subset, or face, of both σ_1 and σ_2 .*

Definition 3 (directed flag complex) *The directed flag complex (for example, on a directed graph $G = (V, E)$), $FC(G)$, is defined to be the ordered simplicial complex whose k -simplices are all ordered $(k + 1)$ -cliques, i.e., $(k + 1)$ -tuples $\sigma = (v_0, v_1, \dots, v_k)$, such that $v_i \in V \ \forall i$, and $(v_i, v_j) \in E$ for $i < j$.*

Boundary function, denoted by ∂ symbol, is a function that maps i -simplex to the sum of its $(i-1)$ -dimensional faces. Formally speaking, for an i -simplex $\sigma = [v_0, \dots, v_i]$, its *boundary* (∂) is:

$$\partial_i \sigma = \sum_{j=0}^i [v_0, \dots, \hat{v}_j, \dots, v_i] \quad (1)$$

where the hat indicates the v_j is omitted.

This definition can be expanded to i -chains. For an i -chain $c = c_i \sigma_i$, $\partial_i(c) = \sum_i c_i \partial_i \sigma_i$.

*Equal contribution.

We can now distinguish two special types of chains using the boundary map that will be useful to define homology:

- The first one is an i -cycle, which is defined as an i -chain with empty boundary. In other words, an i -chain c is an i -cycle if and only if $\partial_i(c) = 0$, i.e. $c \in \text{Ker}(\partial_i)$.
- An i -chain c is i -boundary if there exists an $(i + 1)$ -chain d such that $c = \partial_{i+1}(d)$, i.e. $c \in \text{Im}(\partial_{i+1})$.

Definition 4 (graph) A graph G is a pair (V, E) , where V is a finite set referred to as the vertices or nodes of G , and E is a subset of the set of unordered pairs $e = \{u, v\}$ of distinct points in V , which we call the edges of G . Geometrically the pair $\{u, v\}$ indicates that the vertices u and v are adjacent in G . A directed graph, or a digraph, is similarly a pair (V, E) of vertices V and edges E , except the edges are ordered pairs of distinct vertices, i.e., the pair (u, v) indicates that there is an edge from u to v in G . In a digraph, we allow reciprocal edges, i.e., both (u, v) and (v, u) may be edges in G , but we exclude loops, i.e., edges of the form (v, v) .

Definition 5 (homology group) Given these two special subspaces, i -cycles $Z_i(K)$ and i -boundaries $B_i(K)$ of $C_i(K)$, we now take the quotient space of $B_i(K)$ as a subset of $Z_i(K)$. In this quotient space, there are only the i -cycles that do not bound an $(i + 1)$ -complex, or i -voids of K . This quotient space is called i -th homology group of the simplicial complex K :

$$H_i(K) = \frac{Z_i(K)}{B_i(K)} = \frac{\text{Ker}(\partial_i)}{\text{Im}(\partial_{i+1})} \quad (2)$$

where Ker and Im are the function kernel and image respectively.

The dimension of i -th homology is called the i -th Betti number of K , $\beta_i(K)$, where:

$$\beta_i(K) = \dim(\text{Ker}(\partial_i)) - \dim(\text{Im}(\partial_{i+1})) \quad (3)$$

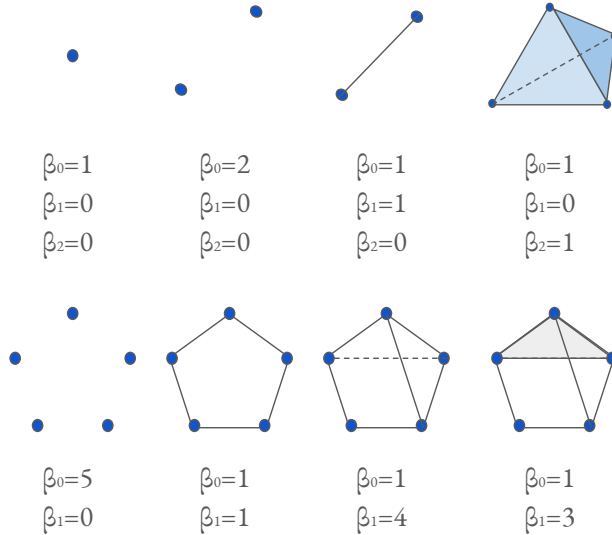


Figure 1: Betti numbers example

Definition 6 (Wasserstein distance) The p -Wasserstein distance between two PDs D_1 and D_2 is the infimum over all bijections: $\gamma : D_1 \rightarrow D_2$ of:

$$d_W(D_1, D_2) = \left(\sum_{x \in D_1} \|x - \gamma(x)\|_\infty^p \right)^{1/p} \quad (4)$$

where $\| \cdot \|_\infty$ is defined for $(x, y) \in \mathbb{R}^2$ by $\max\{|x|, |y|\}$. The limit $p \rightarrow \infty$ defines the Bottleneck distance. More explicitly, it is the infimum over the same set of bijections of the value

$$d_B(D_1, D_2) = \sup_{x \in D_1} \|x - \gamma(x)\|_\infty. \quad (5)$$

Definition 7 (Persistence landscape) Given a collection of intervals $\{(b_i, d_i)\}_{i \in I}$ that compose a PD, its persistence landscape is the set of functions $\lambda_k : \mathbb{R} \rightarrow \overline{\mathbb{R}}$ defined by letting $\lambda_k(t)$ be the k -th largest value of the set $\{\Lambda_i(t)\}_{i \in I}$ where:

$$\Lambda_i(t) = [\min\{t - b_i, d_i - t\}]_+ \quad (6)$$

and $c_+ := \max(c, 0)$. The function λ_k is referred to as the k -layer of the persistence landscape.

Now we define a vectorization of the set of real-valued function that compose PDs on $\mathbb{N} \times \mathbb{R}$. For any $p = 1, \dots, \infty$ we can restrict attention to PDs D whose associated persistence landscape λ is p -integrable, that is to say,

$$\|\lambda\|_p = \left(\sum_{i \in \mathbb{N}} \|\lambda_i\|_p^p \right)^{1/p} \quad (7)$$

is finite. In this case, we refer to Equation (7) as the p -landscape norm of D . For $p = 2$, we define the value of the landscape kernel or similarity of two vectorized PDs D and E as

$$\langle \lambda, \mu \rangle = \left(\sum_{i \in \mathbb{N}} \int_{\mathbb{R}} |\lambda_i(x) - \mu_i(x)|^2 dx \right)^{1/2} \quad (8)$$

where λ and μ are their associated persistence landscapes.

λ_k is geometrically described as follows. For each $i \in I$, we draw an isosceles triangle with base the interval (b_i, d_i) on the horizontal t -axis, and sides with slope 1 and -1 . This subdivides the plane into a number of polygonal regions that we label by the number of triangles contained on it. If P_k is the union of the polygonal regions with values at least k , then the graph of λ_k is the upper contour of P_k , with $\lambda_k(a) = 0$ if the vertical line $t = a$ does not intersect P_k .

Definition 8 (Weighted Silhouette) Let $D = \{(b_i, d_i)\}_{i \in I}$ be a PD and $w = \{w_i\}_{i \in I}$ a set of positive real numbers. The Silhouette of D weighted by w is the function $\phi : \mathbb{R} \rightarrow \mathbb{R}$ defined by:

$$\phi(t) = \frac{\sum_{i \in I} w_i \Lambda_i(t)}{\sum_{i \in I} w_i}, \quad (9)$$

where

$$\Lambda_i(t) = [\min\{t - b_i, d_i - t\}]_+ \quad (10)$$

and $c_+ := \max(c, 0)$ When $w_i = |d_i - b_i|^p$ for $0 < p \leq \infty$ we refer to ϕ as the p -power-weighted Silhouette of D . It defines a vectorization of the set of PDs on the vector space of continuous real-valued functions on \mathbb{R} .

Definition 9 (Heat vectorizations) Considering PD as the support of Dirac deltas, one can construct, for any $t > 0$, two vectorizations of the set of PDs to the set of continuous real-valued function on the first quadrant $\mathbb{R}_{>0}^2$. The Heat vectorization is constructed for every PD D by solving the heat equation:

$$\begin{aligned} \Delta_x(u) &= \partial_t u && \text{on } \Omega \times \mathbb{R}_{>0} \\ u &= 0 && \text{on } \{x_1 = x_2\} \times \mathbb{R}_{\geq 0} \\ u &= \sum_{p \in D} \delta_p && \text{on } \Omega \times 0 \end{aligned} \quad (11)$$

where $\Omega = \{(x_1, x_2) \in \mathbb{R}^2 \mid x_1 \leq x_2\}$, then solving the same equation after precomposing the data of Equation (11) with the change of coordinates $(x_1, x_2) \mapsto (x_2, x_1)$, and defining the image of D to be the difference between these two solutions at the chosen time t .

We recall that the solution to the Heat equation with initial condition given by a Dirac delta supported at $p \in \mathbb{R}^2$ is:

$$\frac{1}{4\pi t} \exp\left(-\frac{\|p - x\|^2}{4t}\right) \quad (12)$$

To highlight the connection with normally distributed random variables, it is customary to use the change of variable $\sigma = \sqrt{2t}$.

For a complete reference on vectorized persistence summaries and PH approximated metrics, see [1] and Giotto-TDA package documentation appendix².

Appendix II

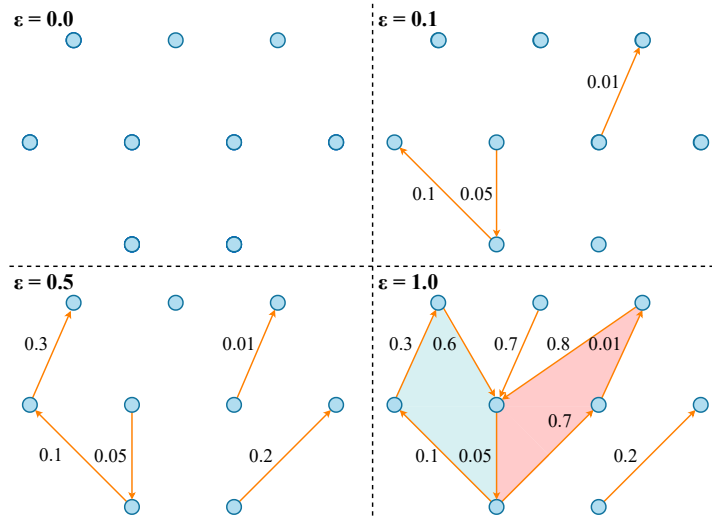


Figure 2: MLP Simplicial complex filtration example.

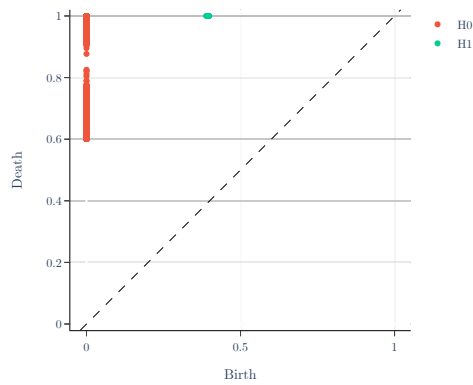


Figure 3: An example of Persistence Homology diagram

²<https://giotto-ai.github.io/gtda-docs/0.3.1/theory/glossary.html#persistence-landscape>

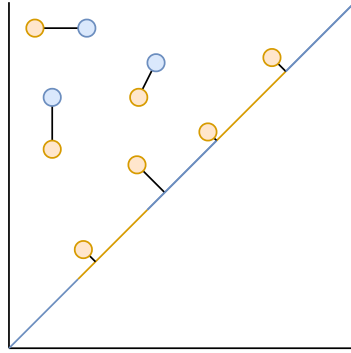


Figure 4: Persistence Homology diagram distance example.

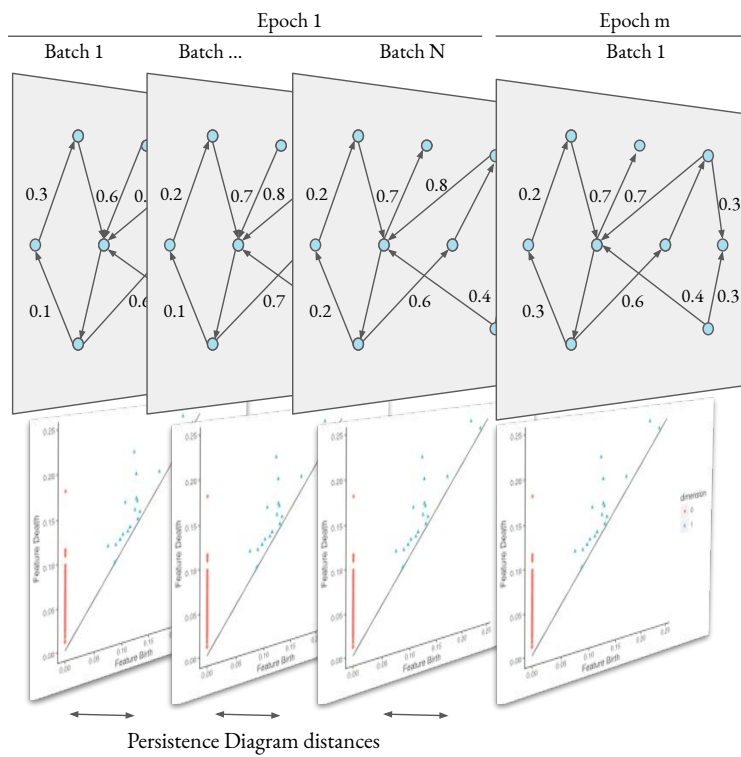


Figure 5: MLP learning evolution PD similarity process.

Appendix III

Cumulative plots

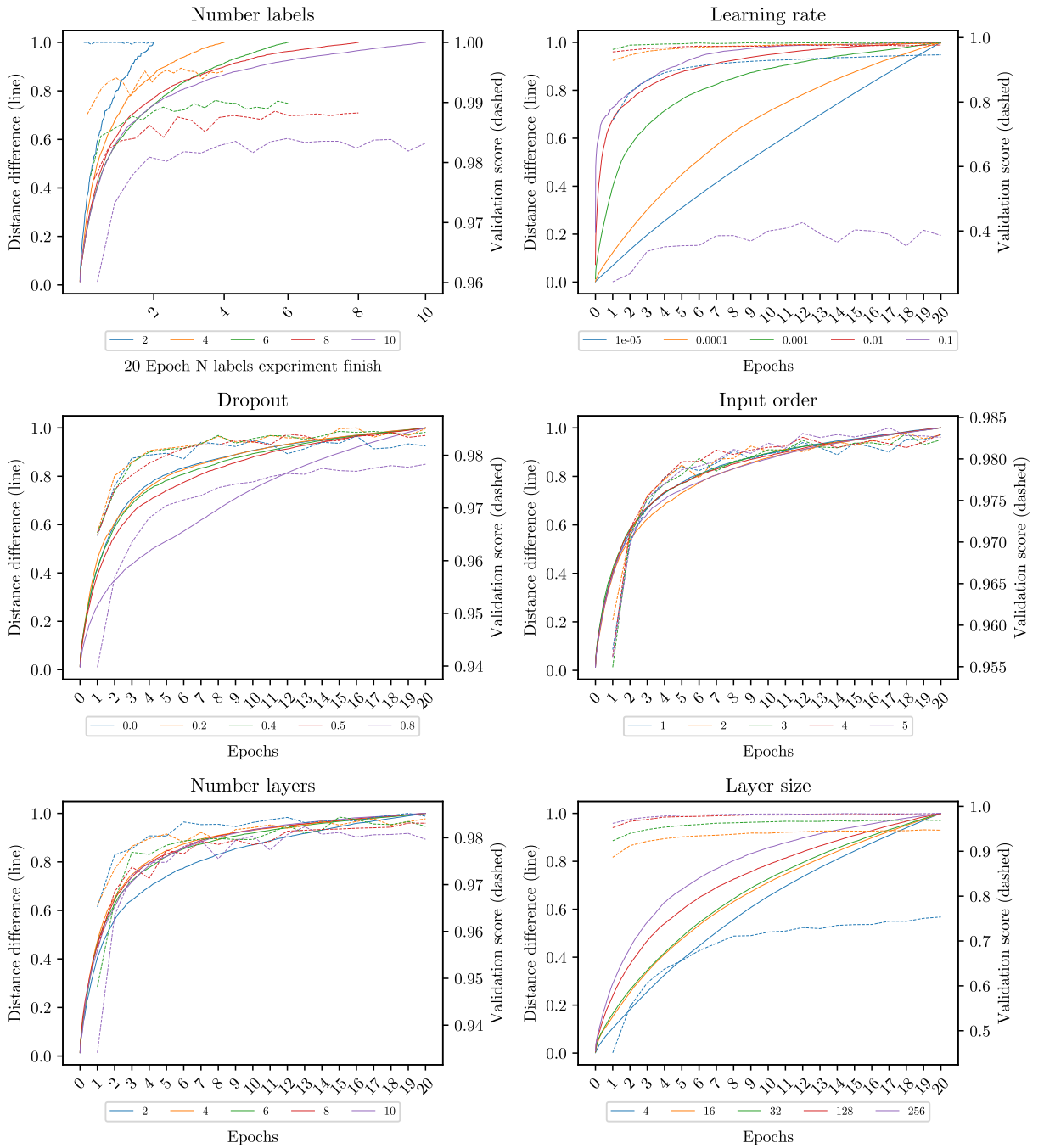


Figure 6: MNIST cumulative using Heat discretization.

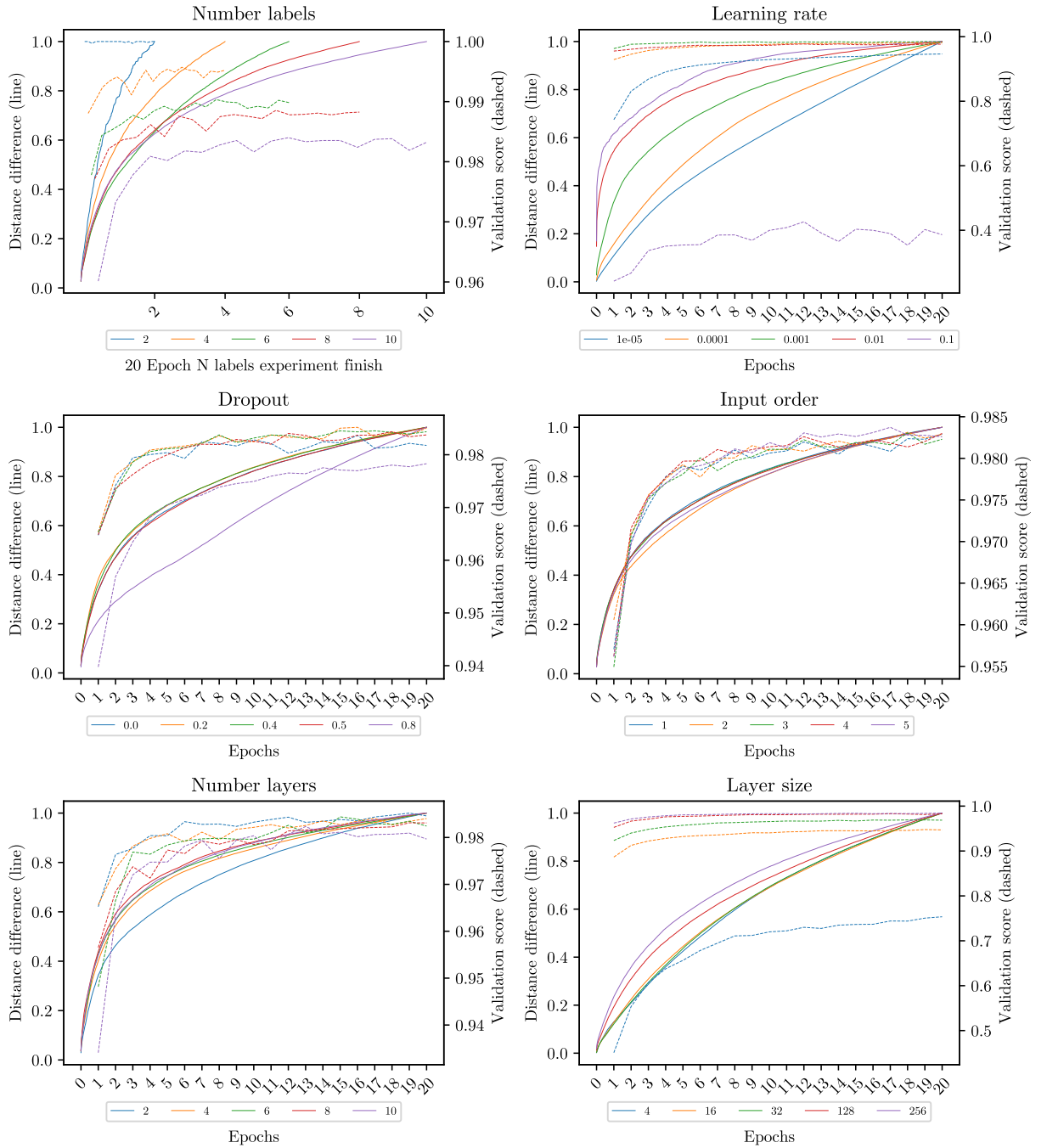


Figure 7: MNIST cumulative using Silhouette discretization.

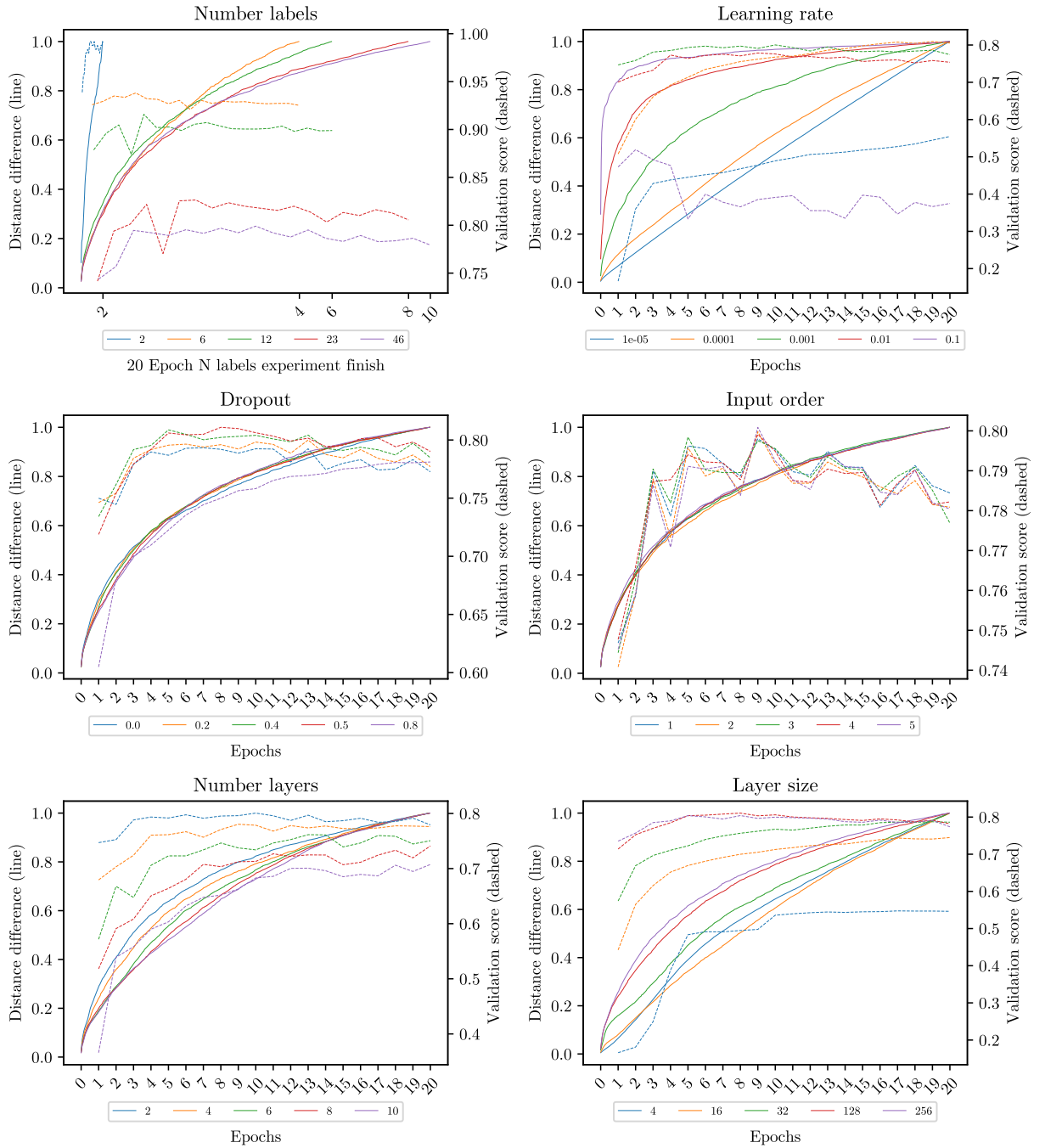


Figure 8: Reuters cumulative using Heat discretization.

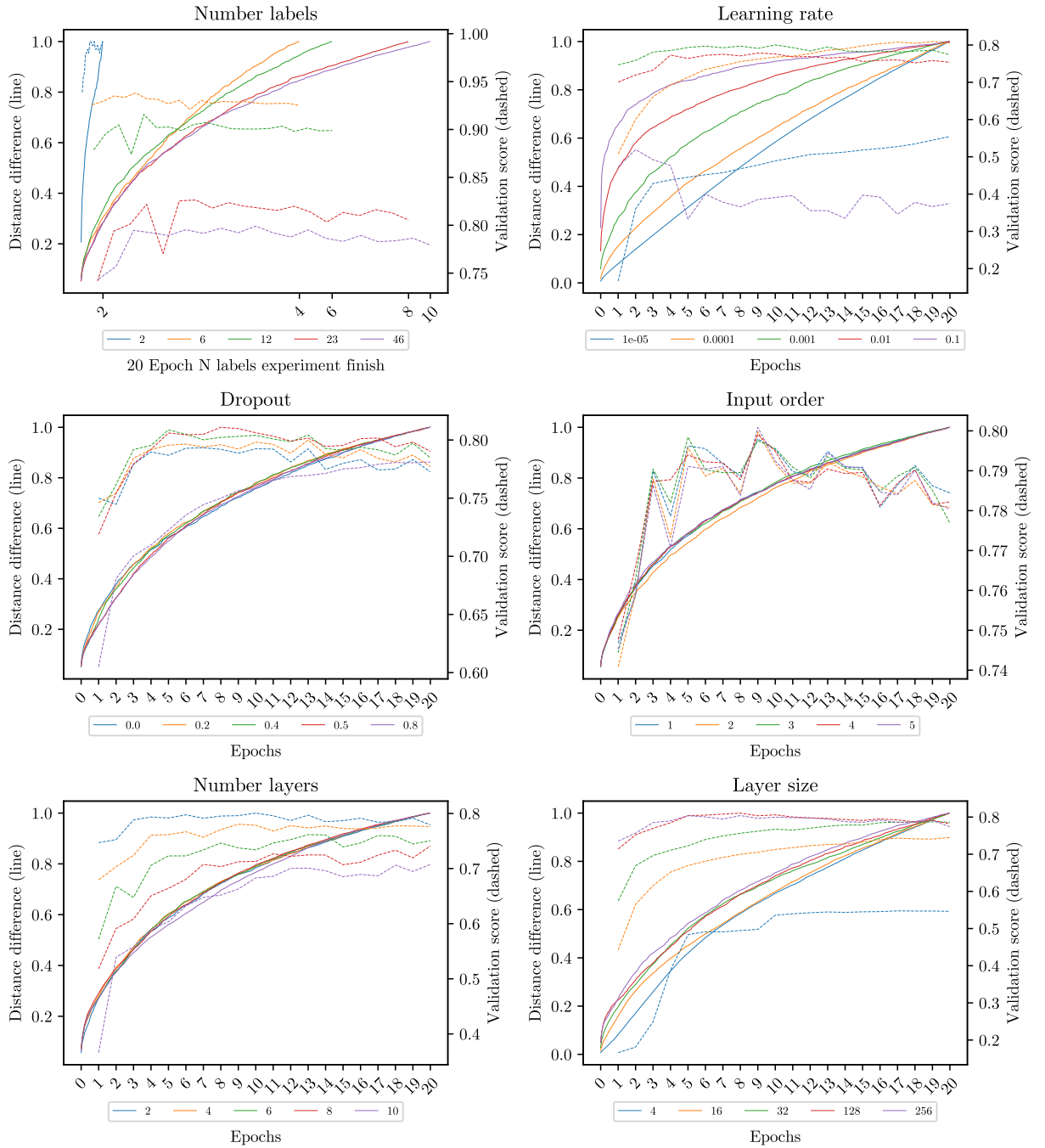


Figure 9: Reuters cumulative using Silhouette discretization.

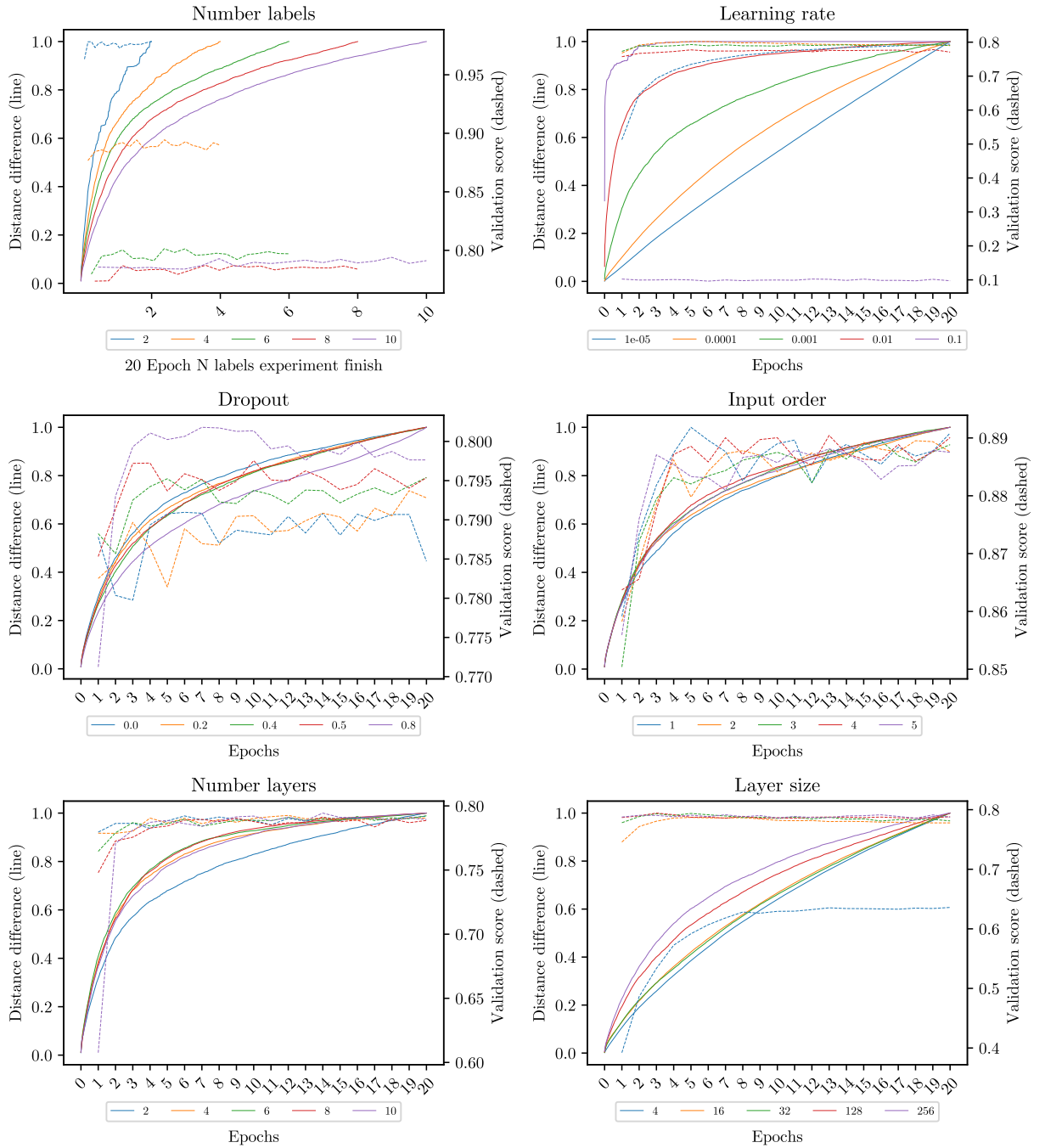


Figure 10: CIFAR-10 CNN cumulative using Heat discretization.

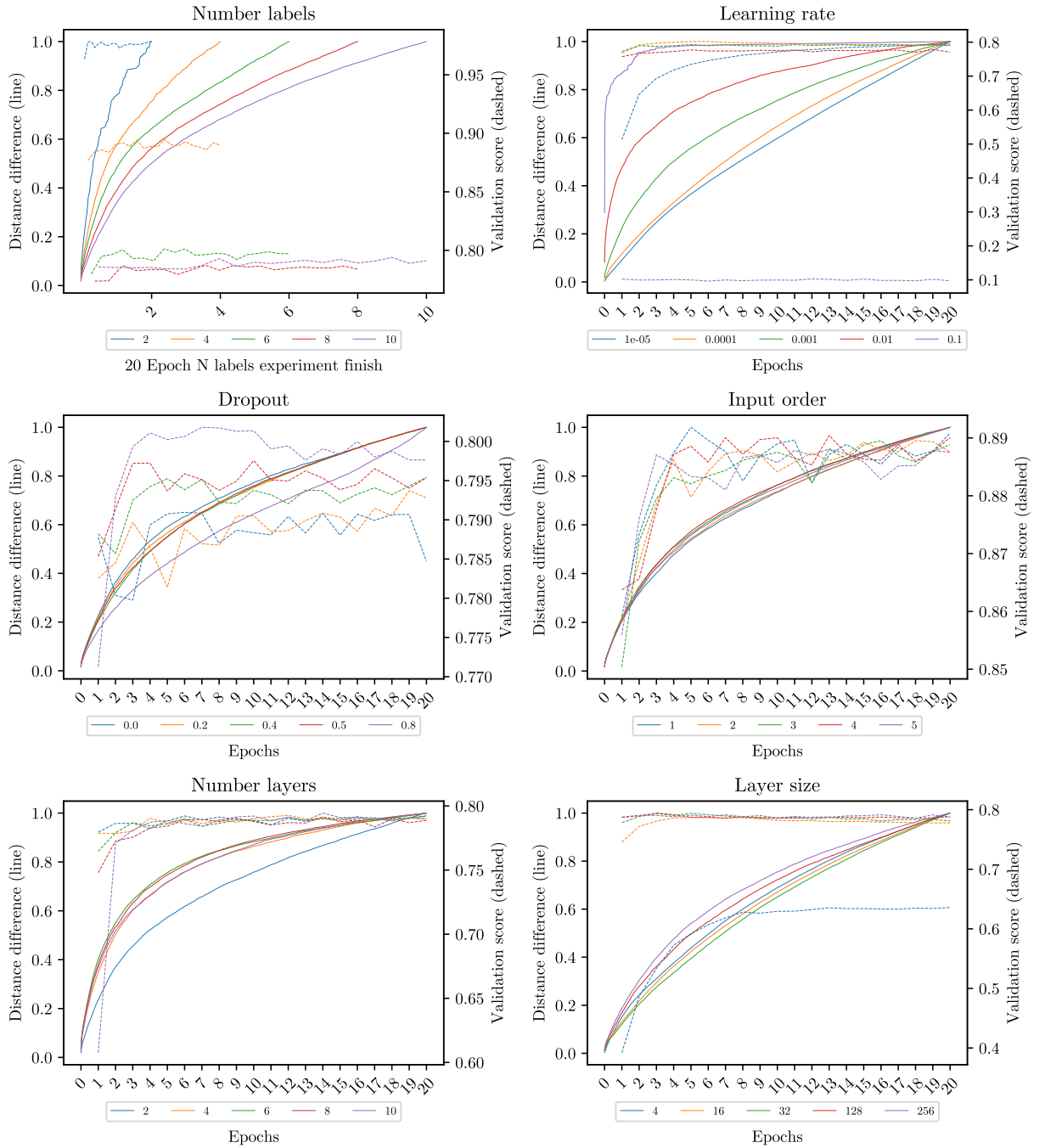


Figure 11: CIFAR-10 CNN cumulative using Silhouette discretization.

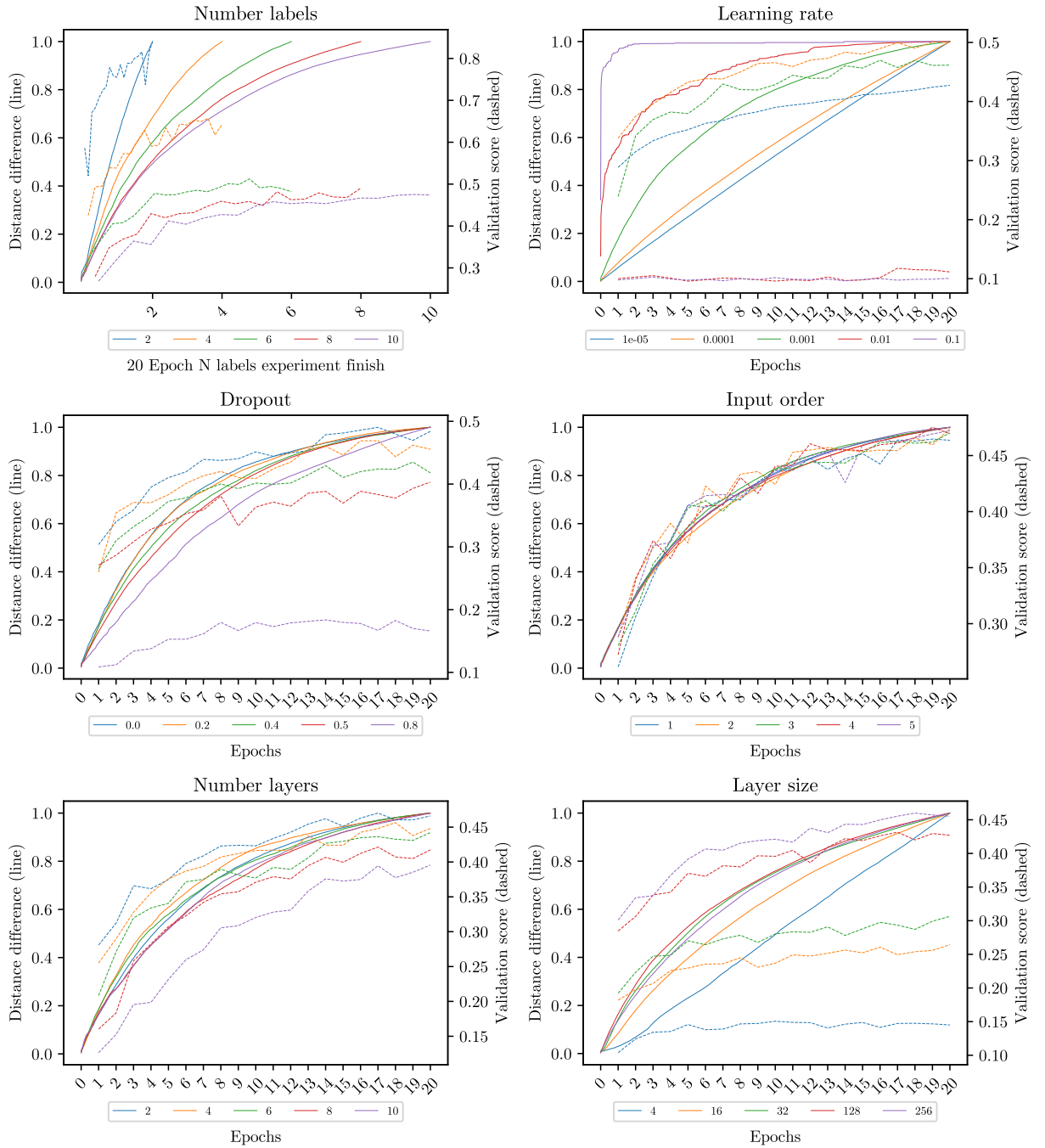


Figure 12: CIFAR-10 MLP cumulative using Heat discretization.

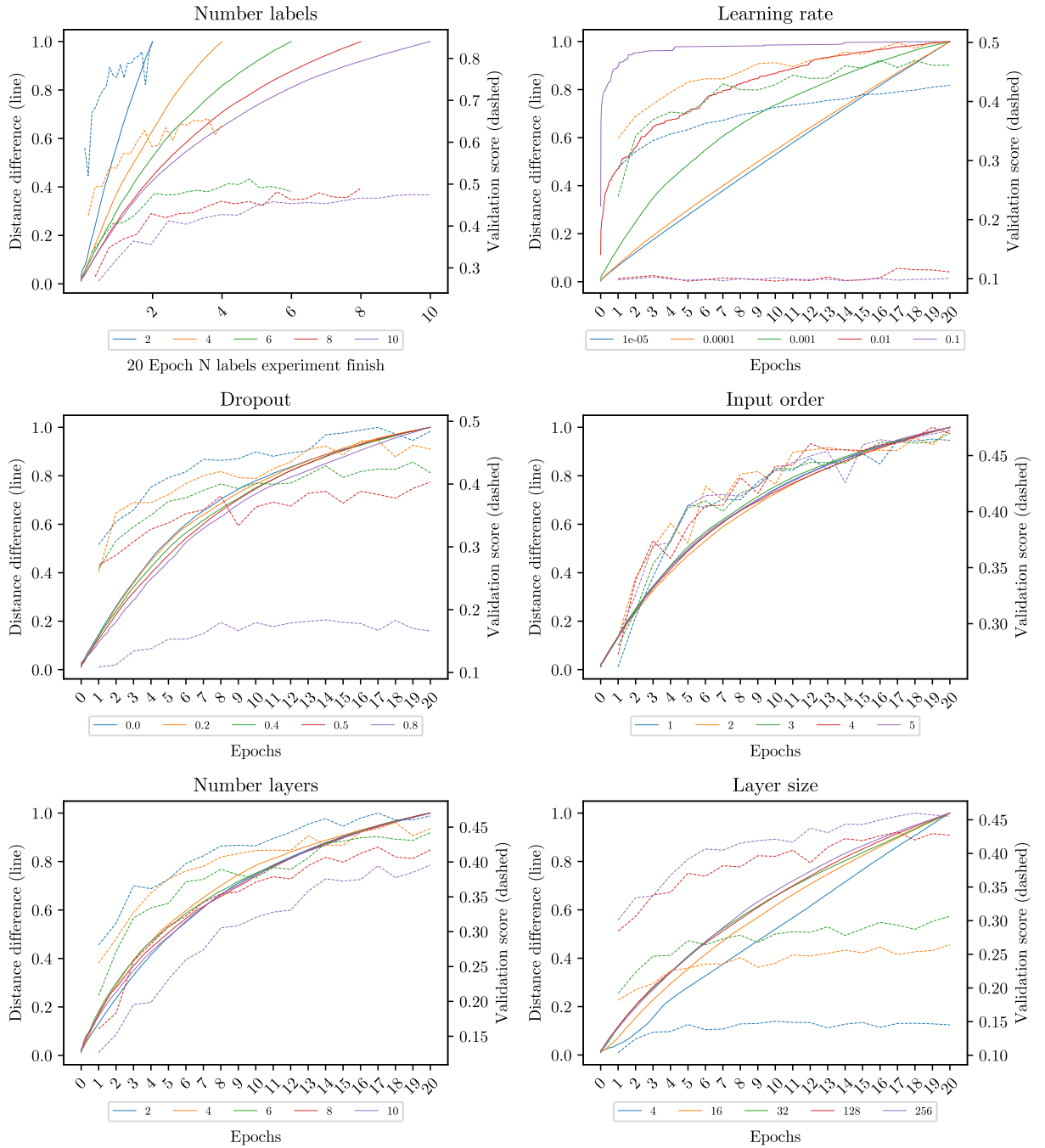


Figure 13: CIFAR-10 MLP cumulative using Silhouette discretization.

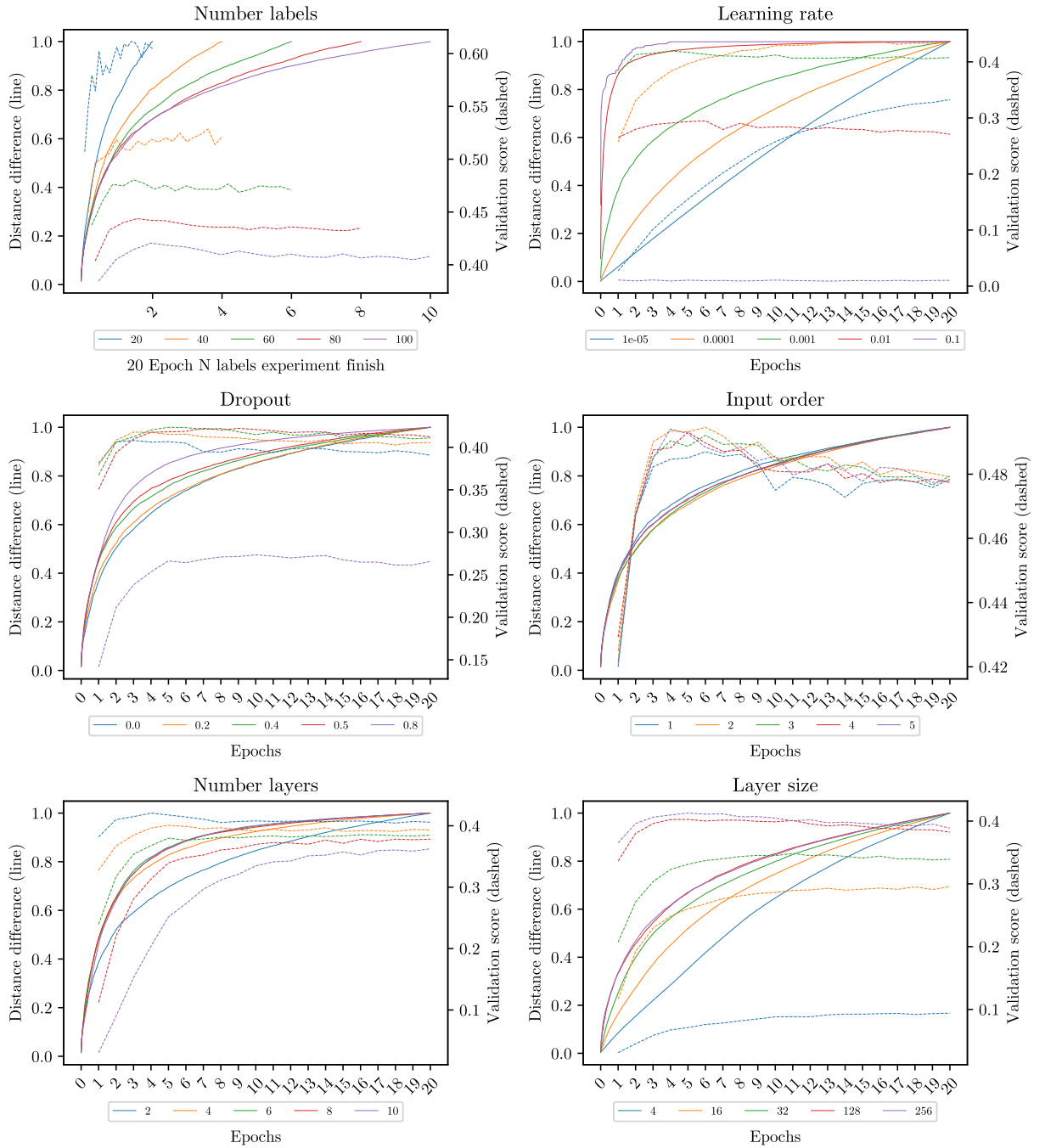


Figure 14: CIFAR-100 CNN cumulative using Heat discretization.

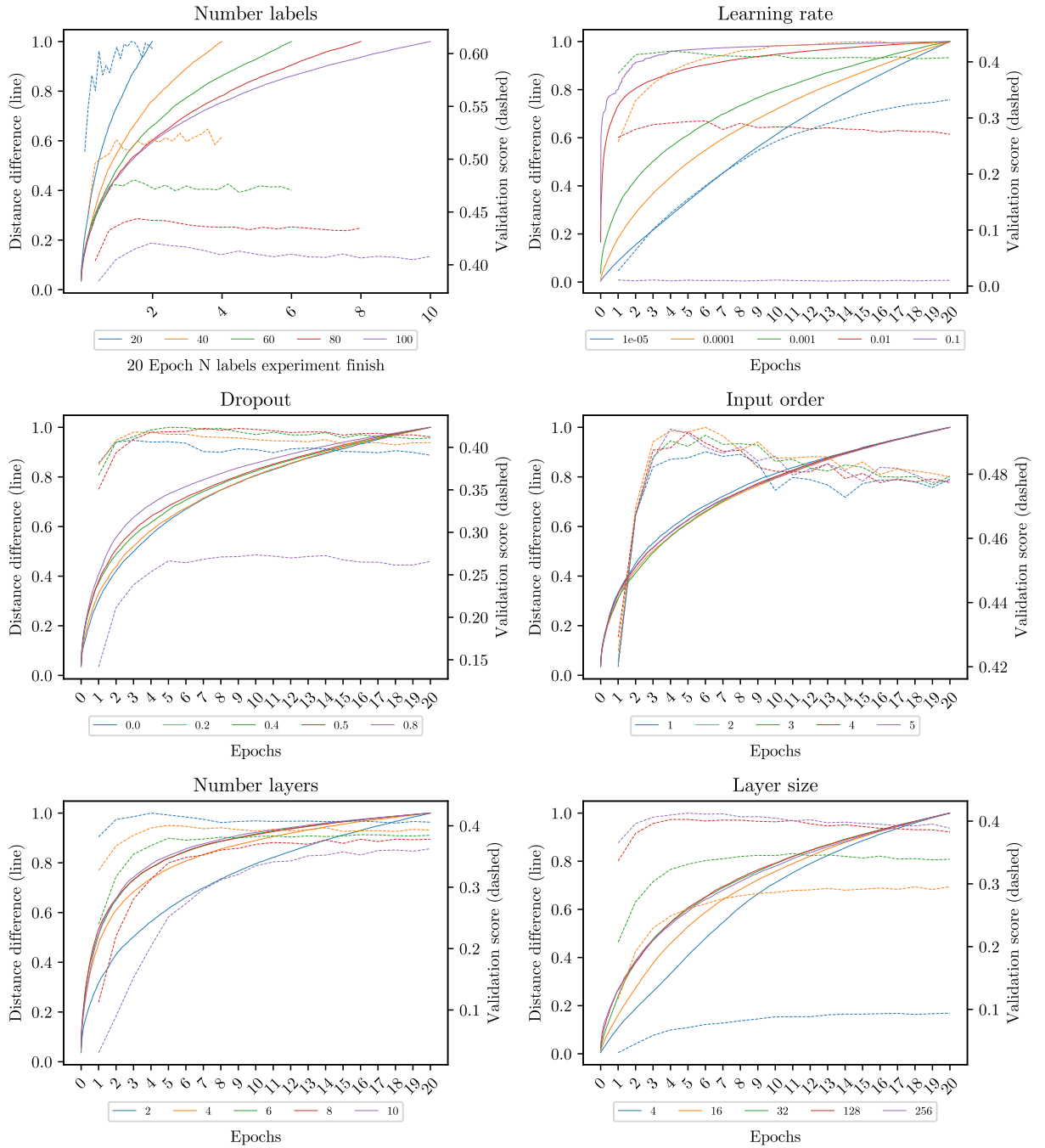


Figure 15: CIFAR-100 CNN cumulative using Silhouette discretization.

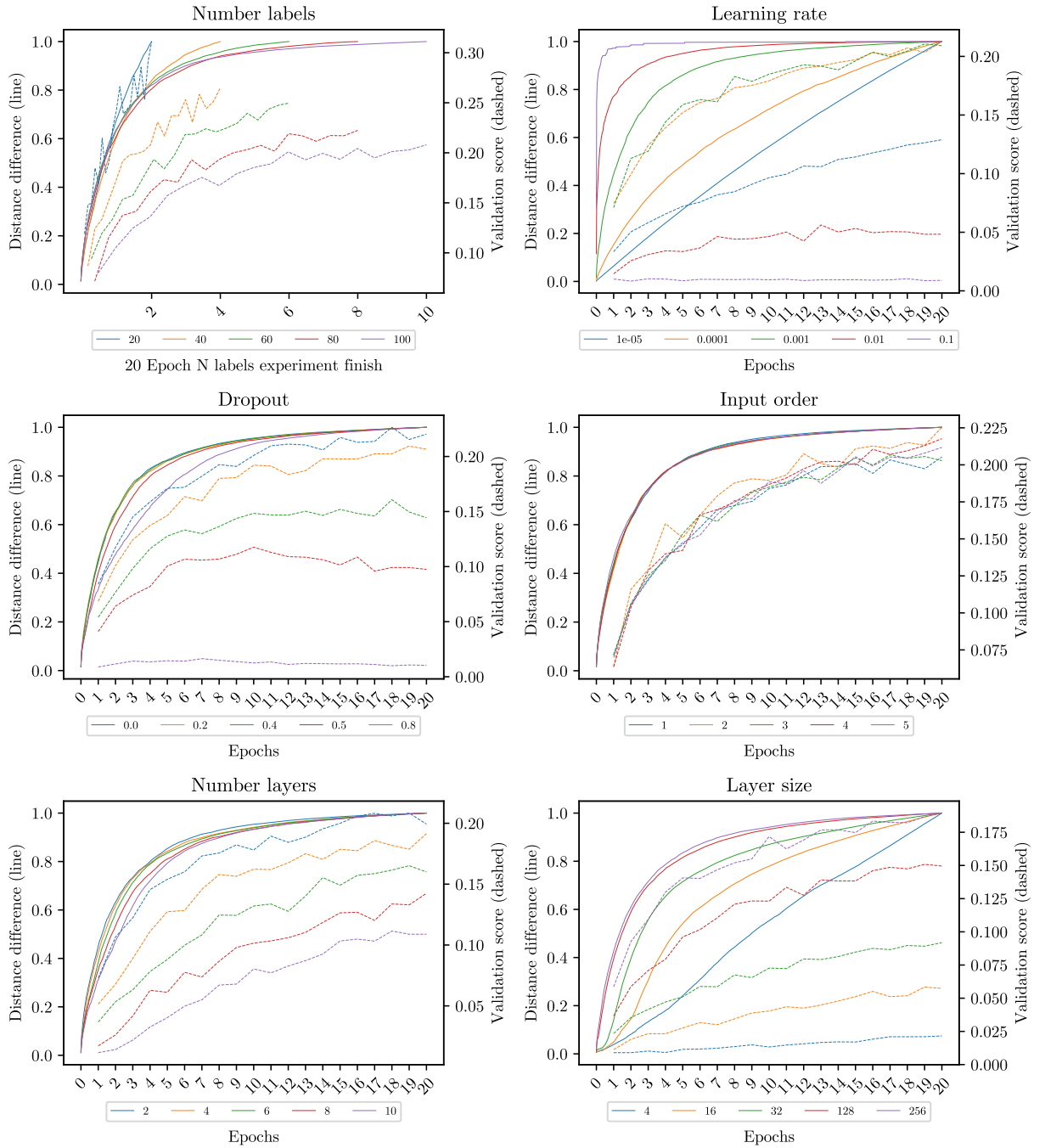


Figure 16: CIFAR-100 MLP cumulative using Heat discretization.

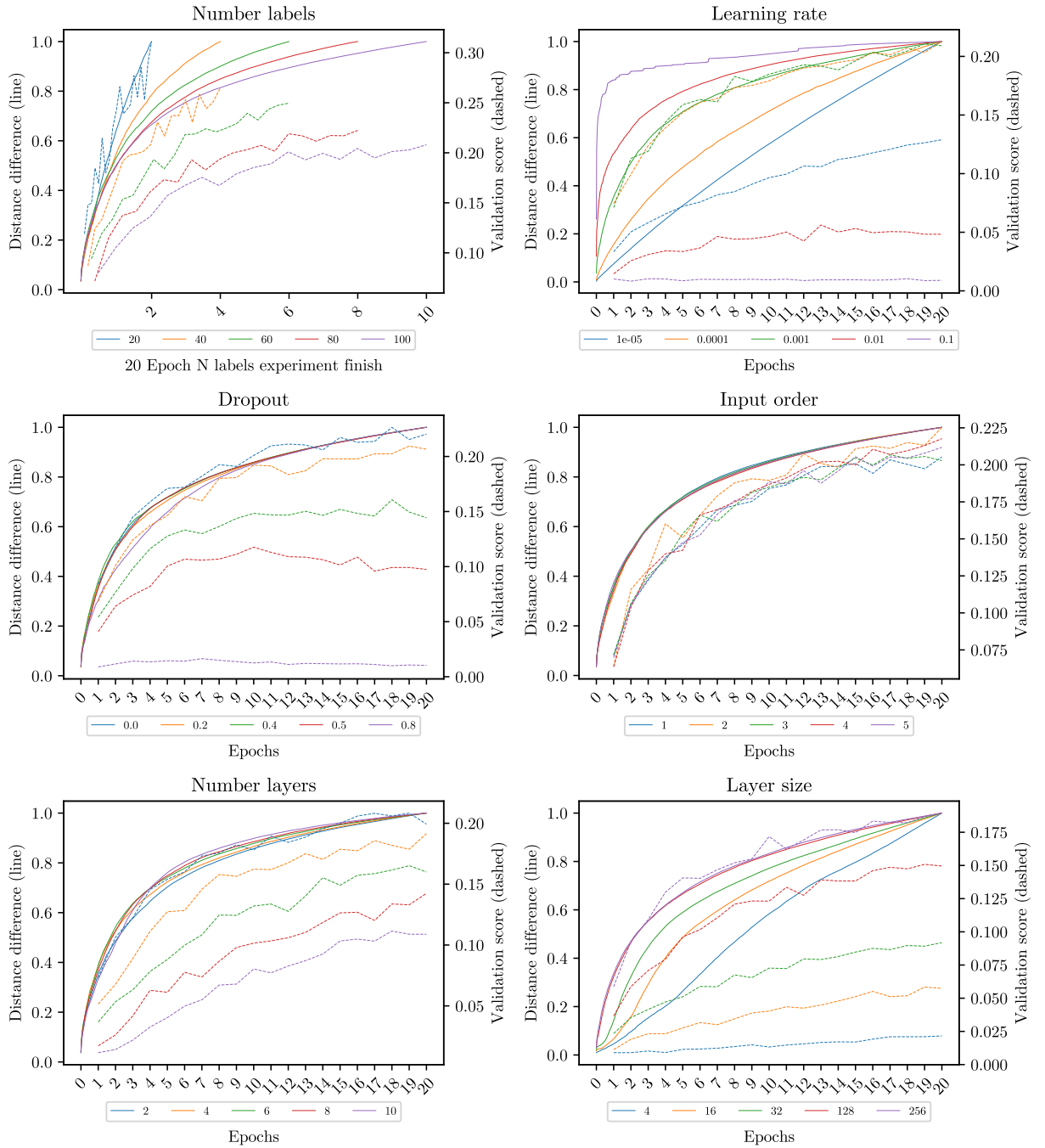


Figure 17: CIFAR-100 MLP cumulative using Silhouette discretization.

Cumulative plots without normalization

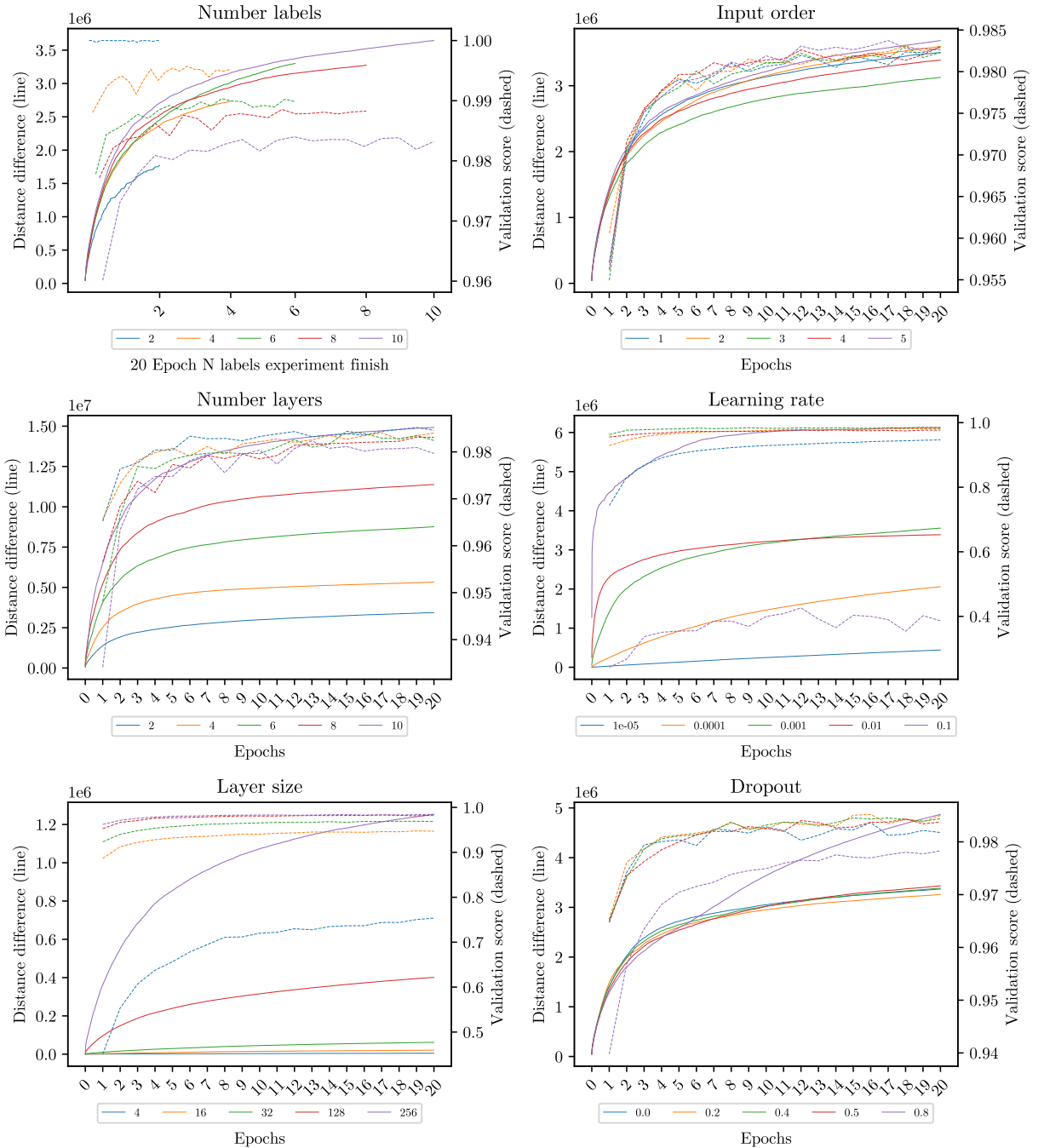


Figure 18: MNIST cumulative using Heat discretization.

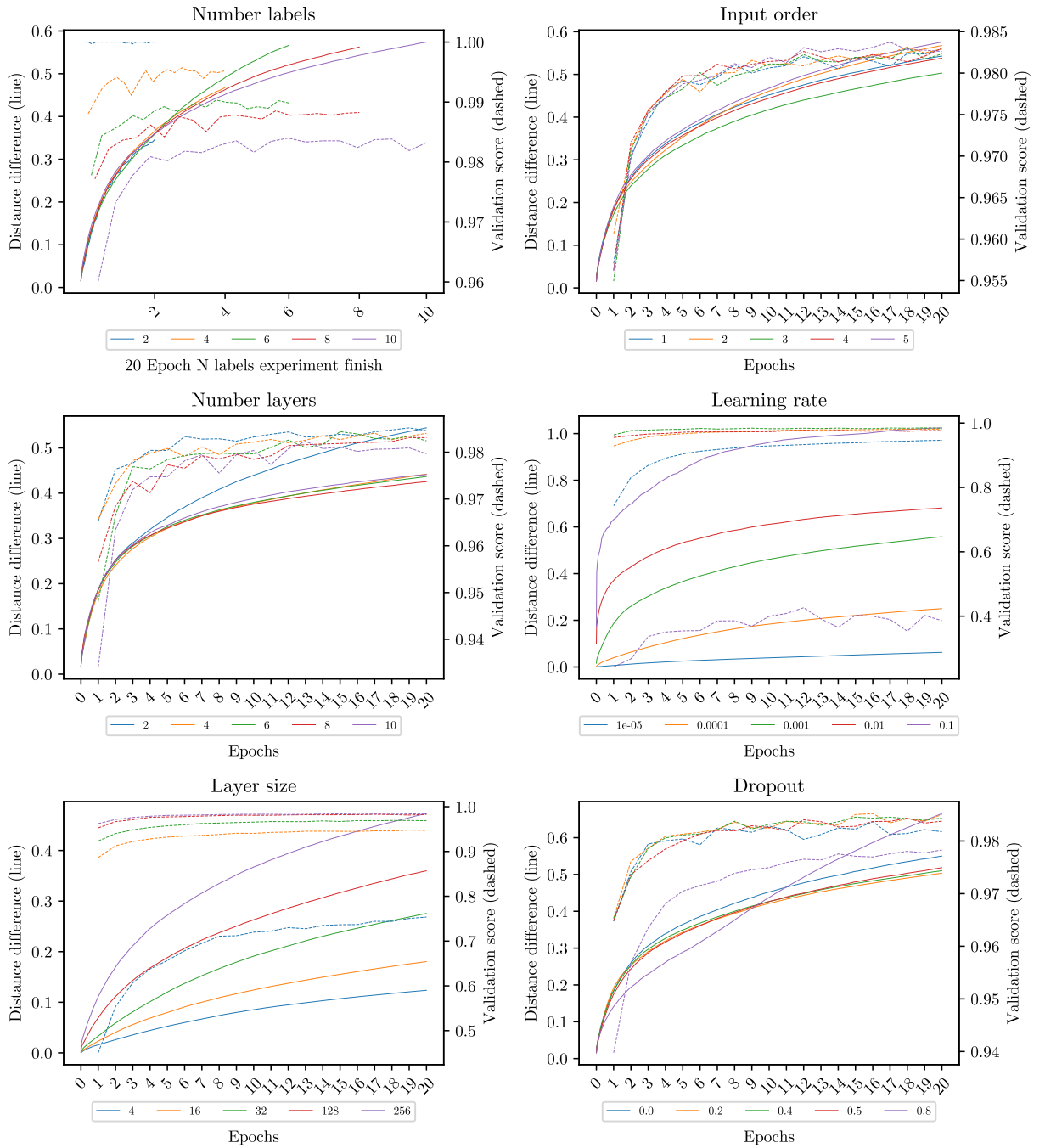


Figure 19: MNIST cumulative using Silhouette discretization.

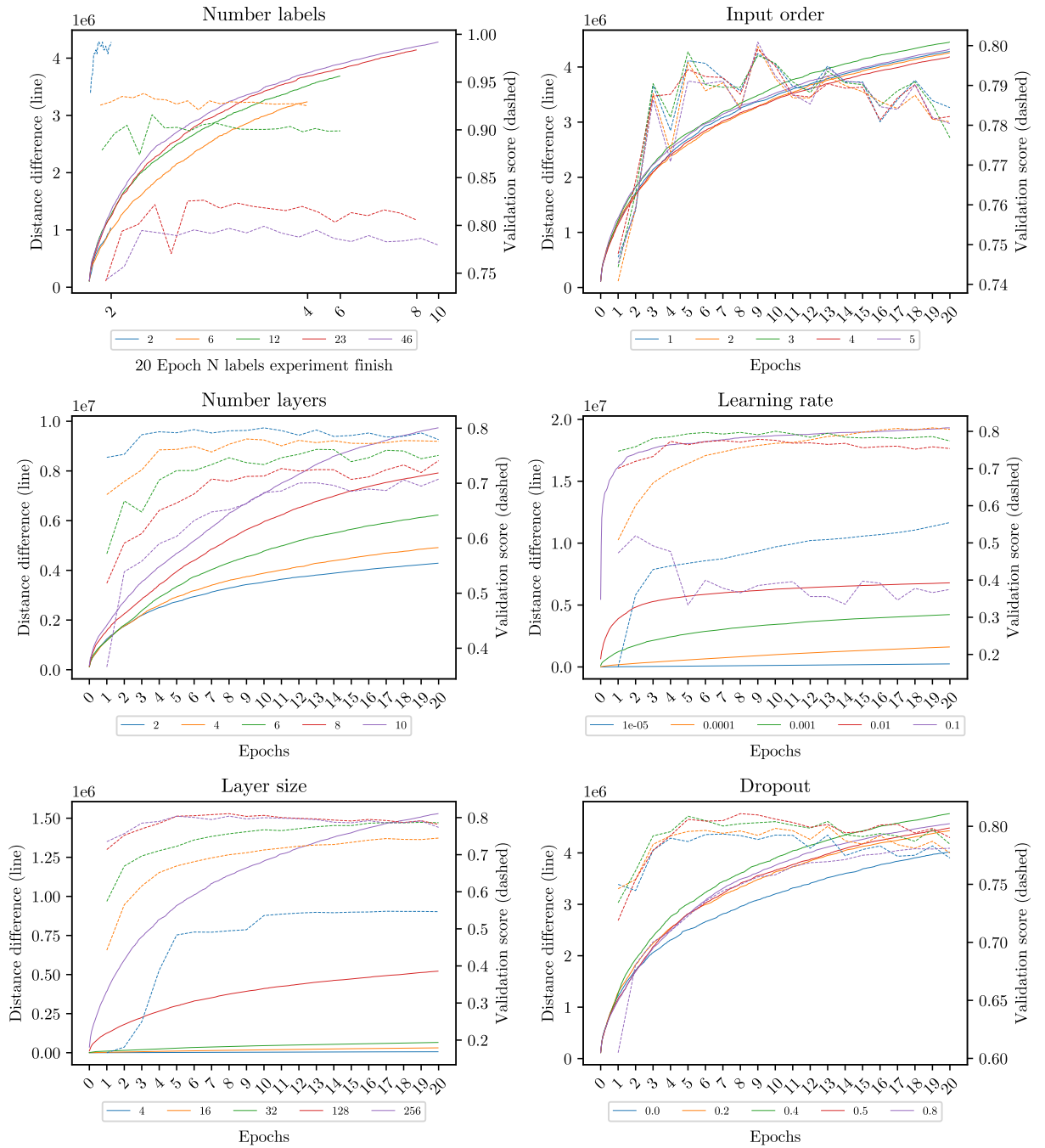


Figure 20: Reuters cumulative using Heat discretization.

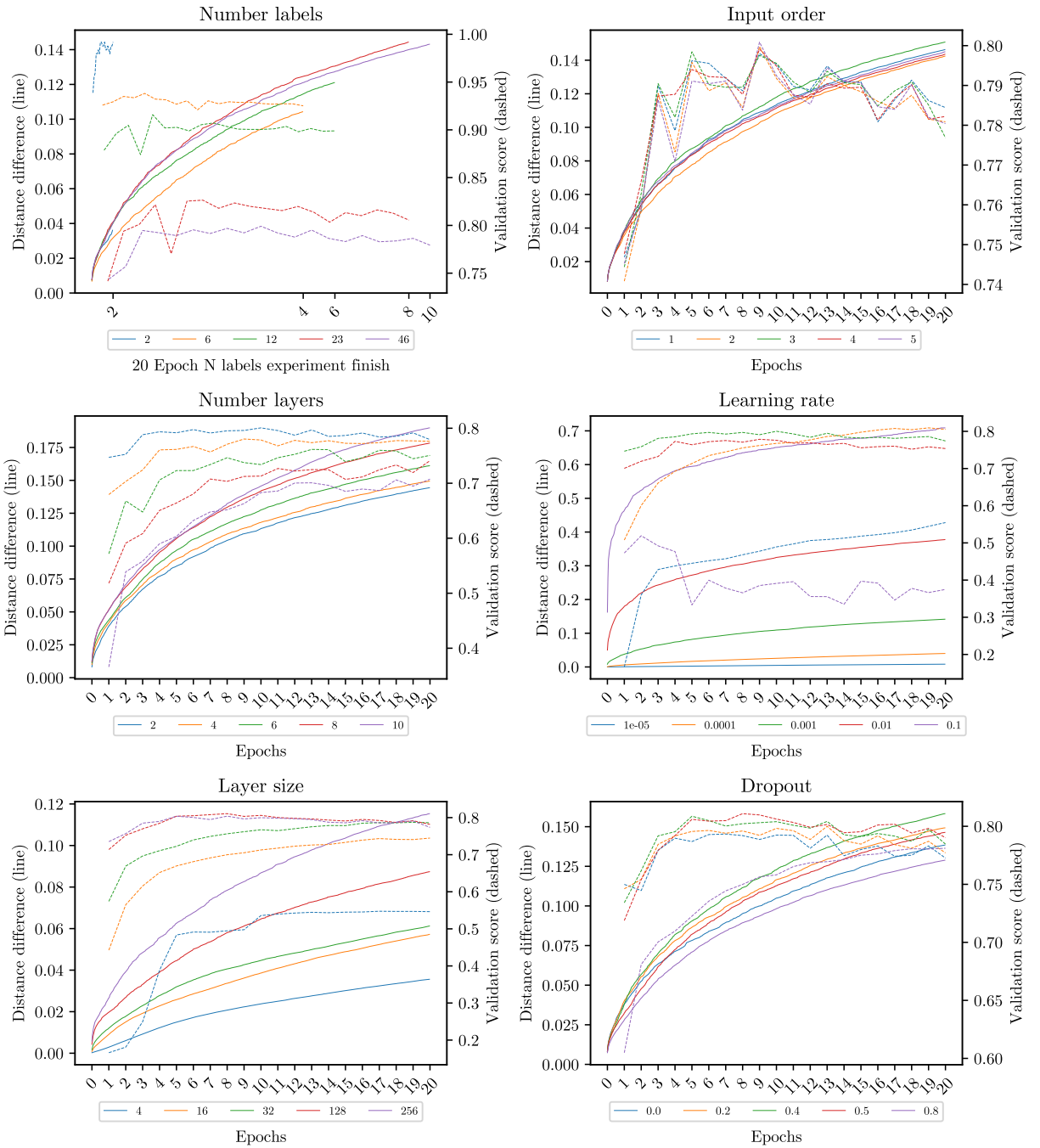


Figure 21: Reuters cumulative using Silhouette discretization.

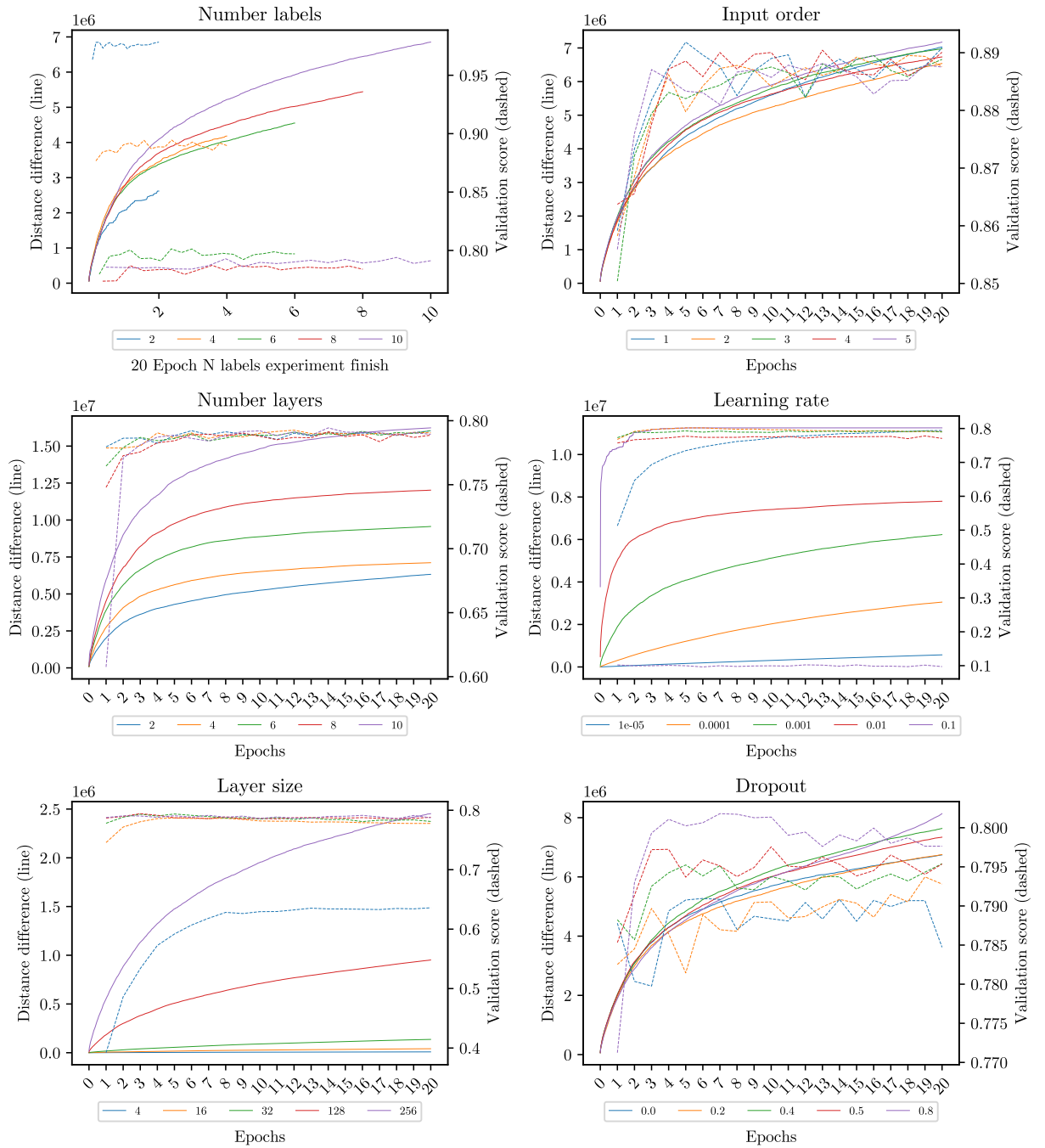


Figure 22: CIFAR-10 CNN cumulative no normalized using Heat discretization.

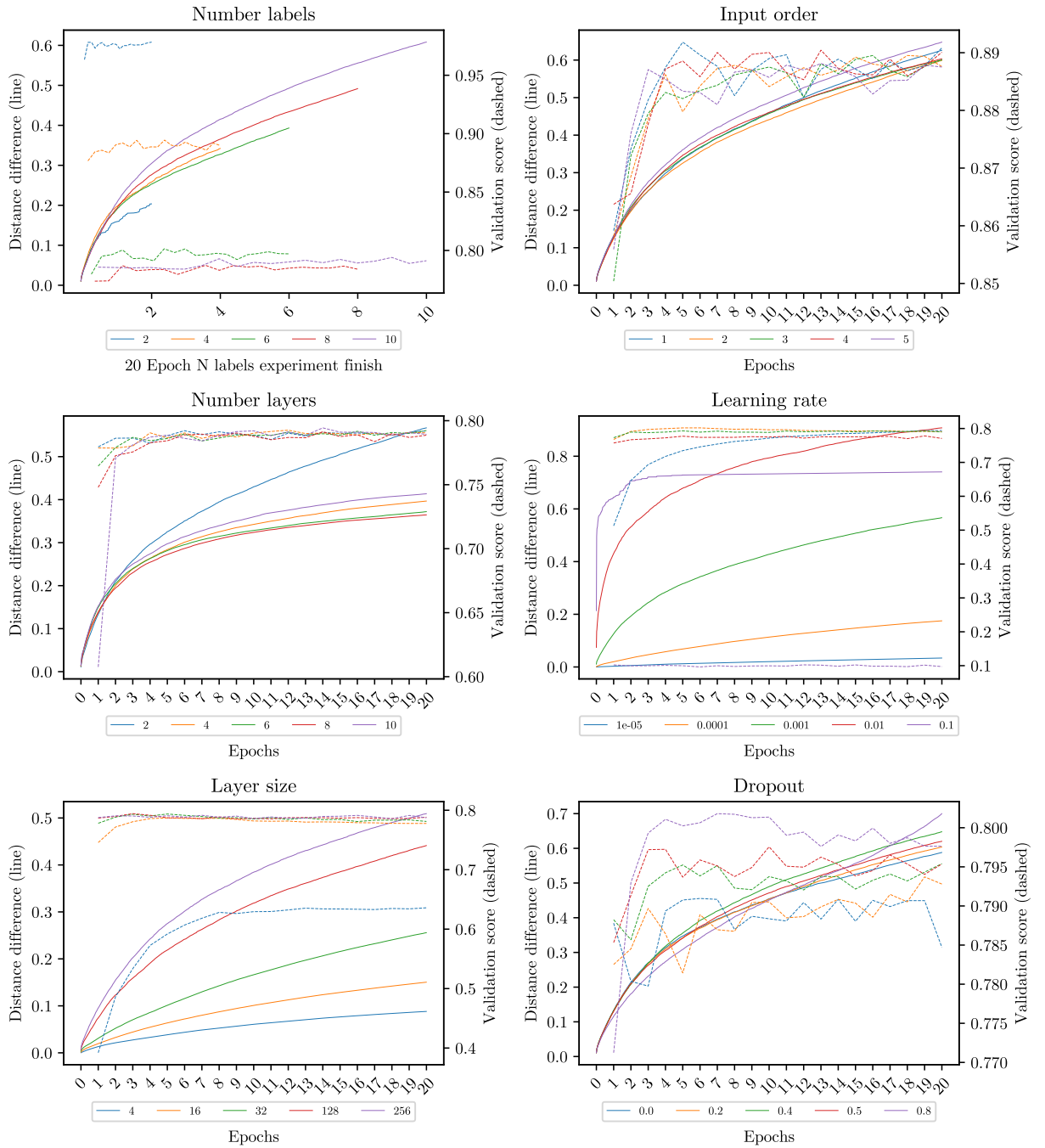


Figure 23: CIFAR-10 CNN cumulative no normalized using Silhouette discretization.

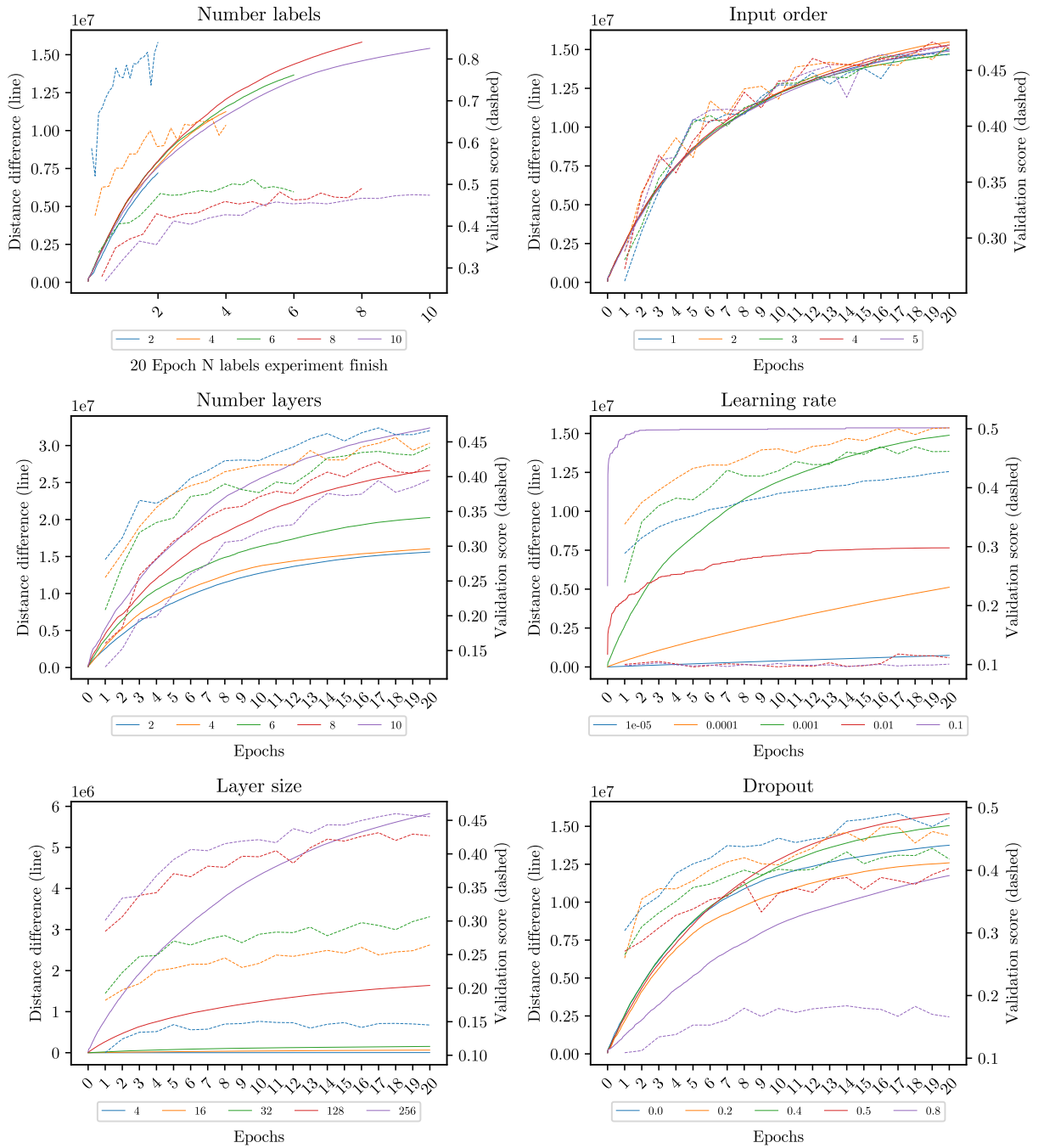


Figure 24: CIFAR-10 MLP cumulative no normalized using Heat discretization.

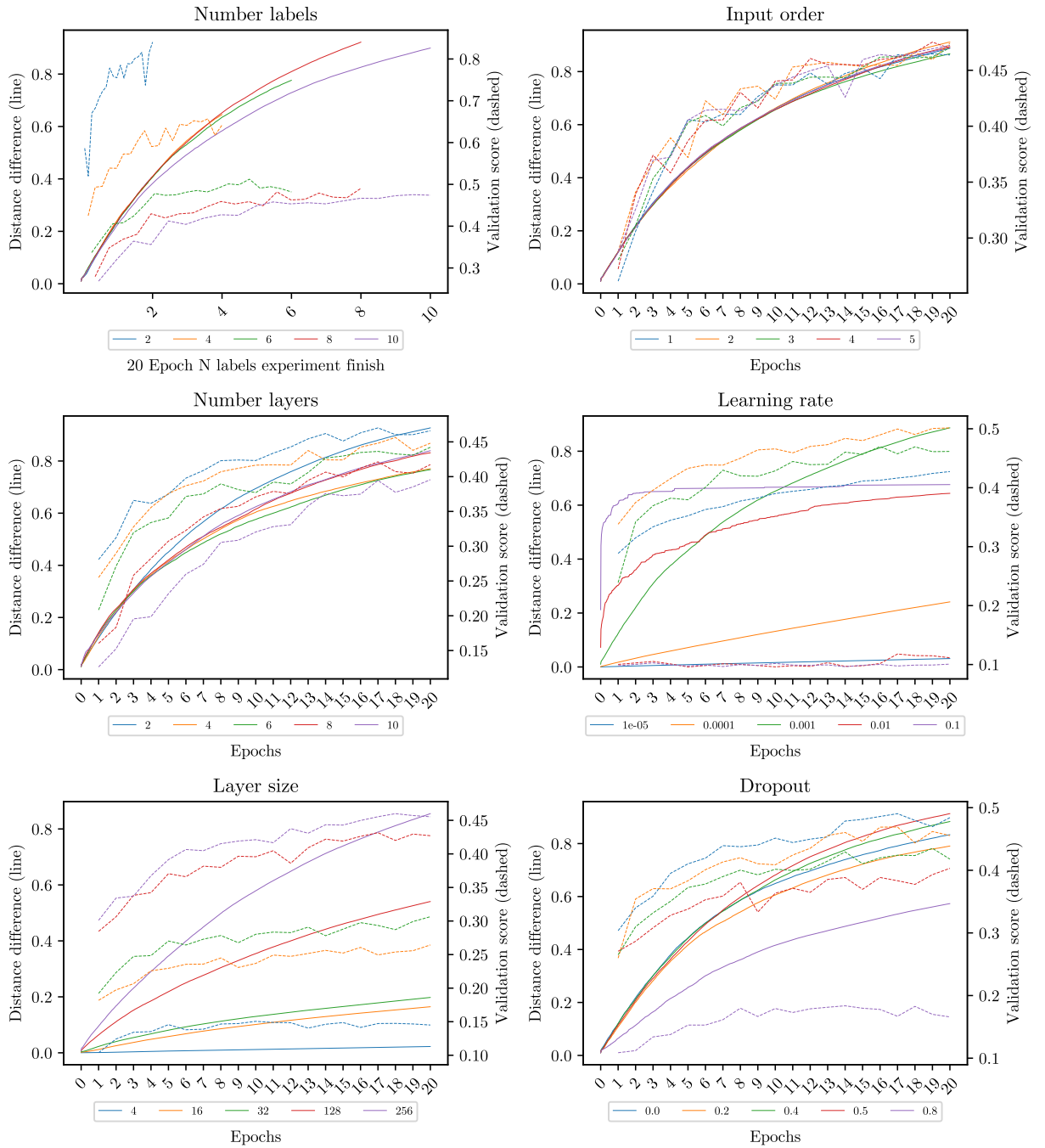


Figure 25: CIFAR-10 MLP cumulative no normalized using Silhouette discretization.

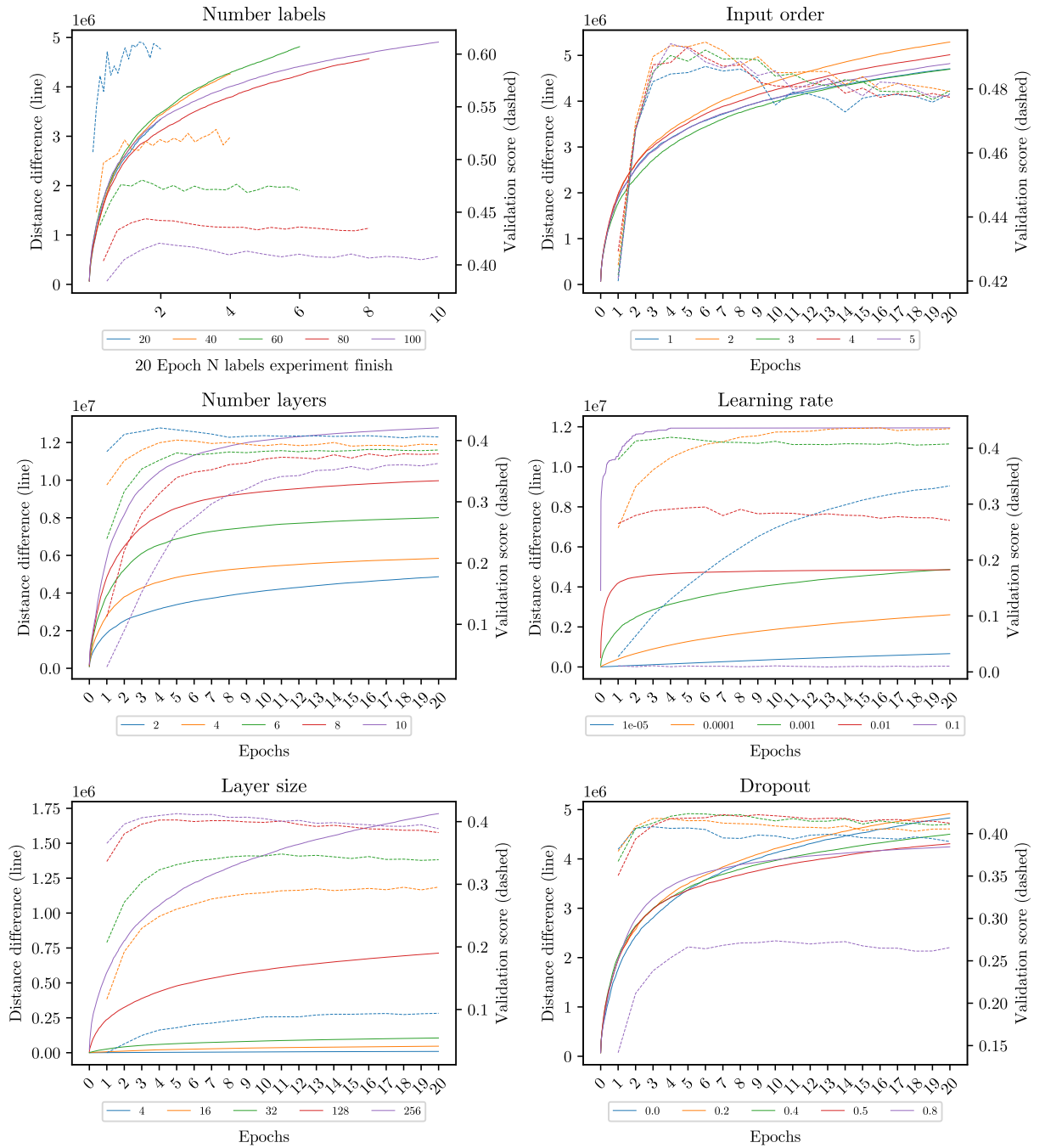


Figure 26: CIFAR-100 CNN cumulative no normalized using Heat discretization.

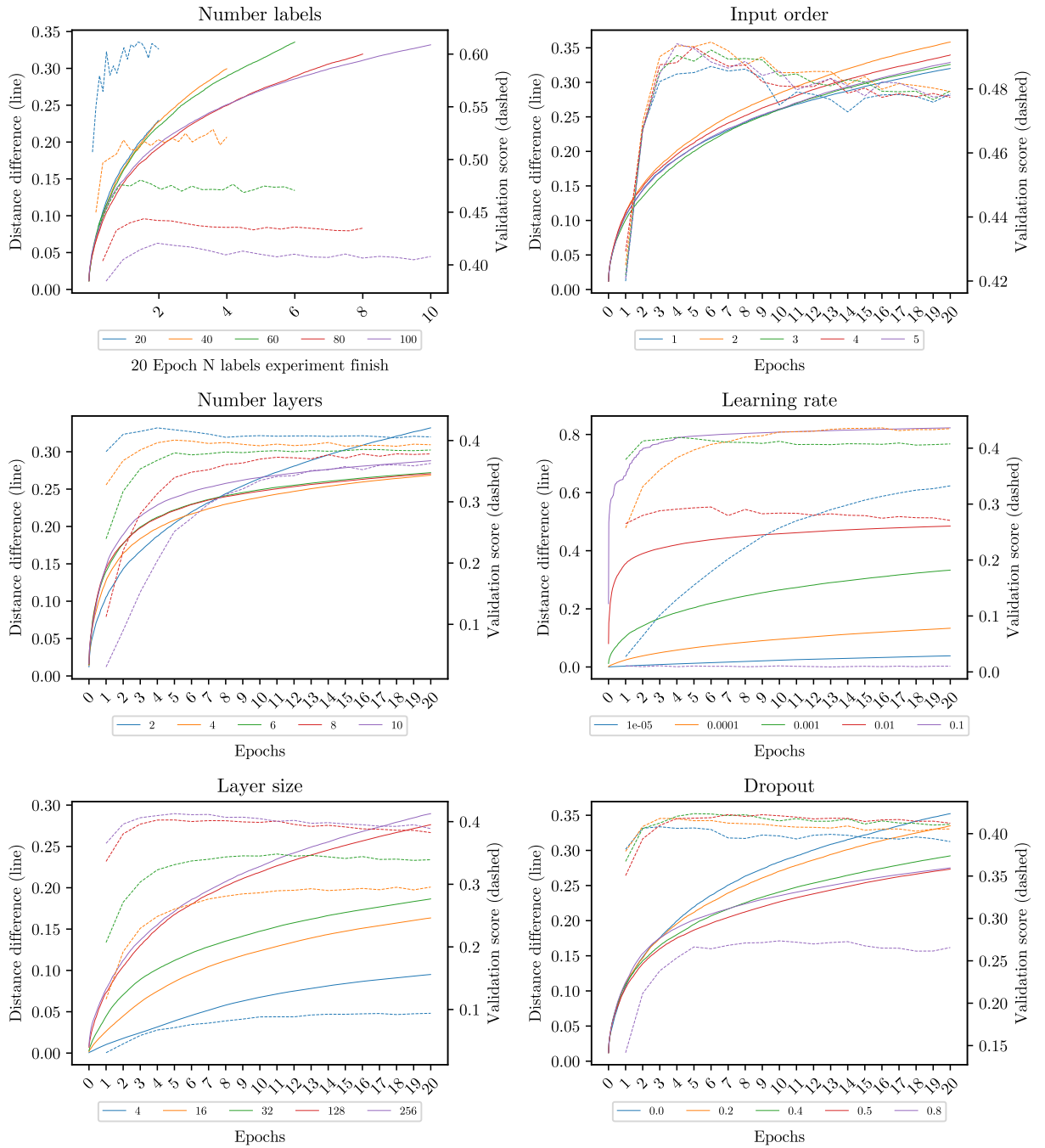


Figure 27: CIFAR-100 CNN cumulative no normalized using Silhouette discretization.

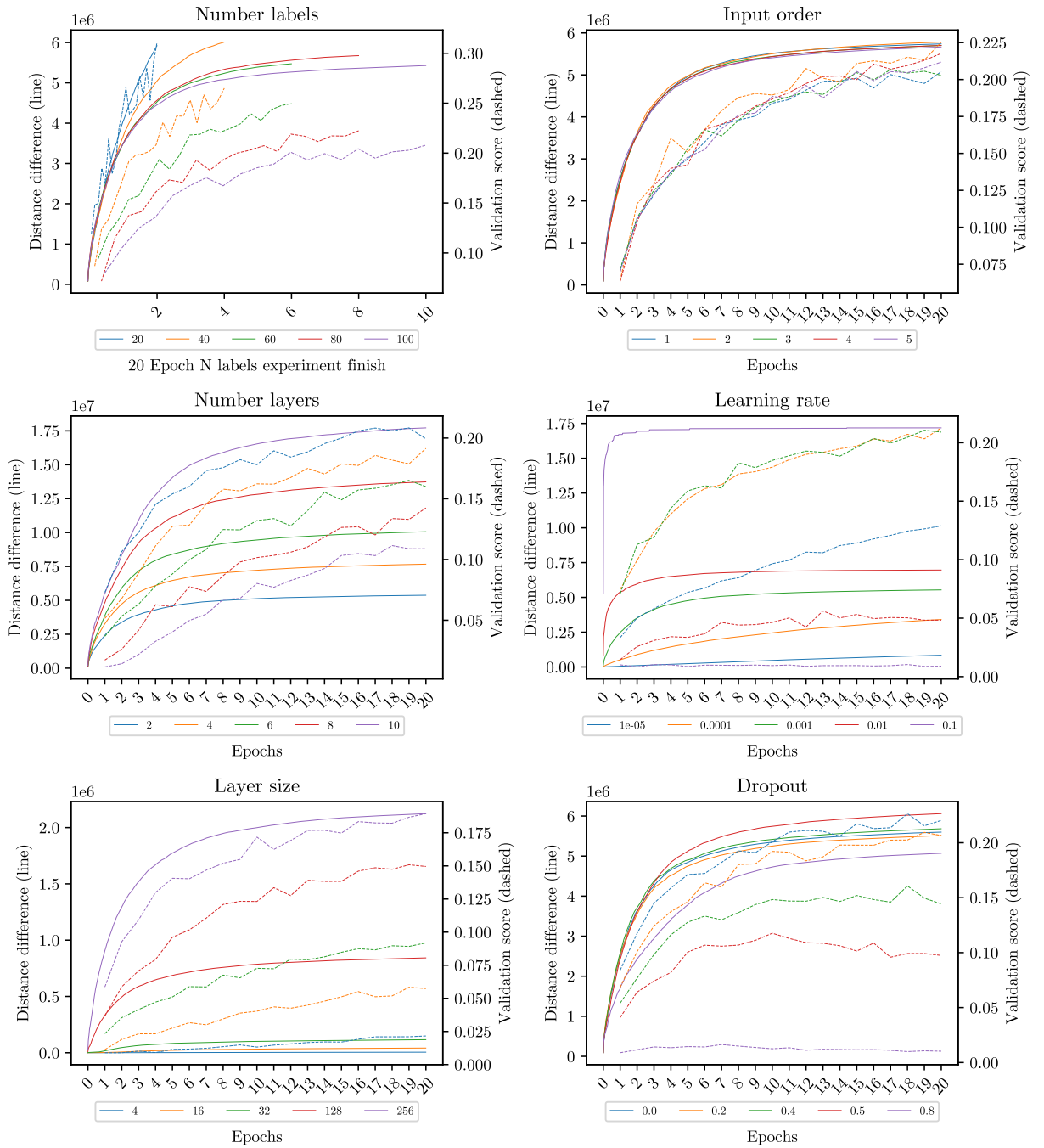


Figure 28: CIFAR-100 MLP cumulative no normalized using Heat discretization.

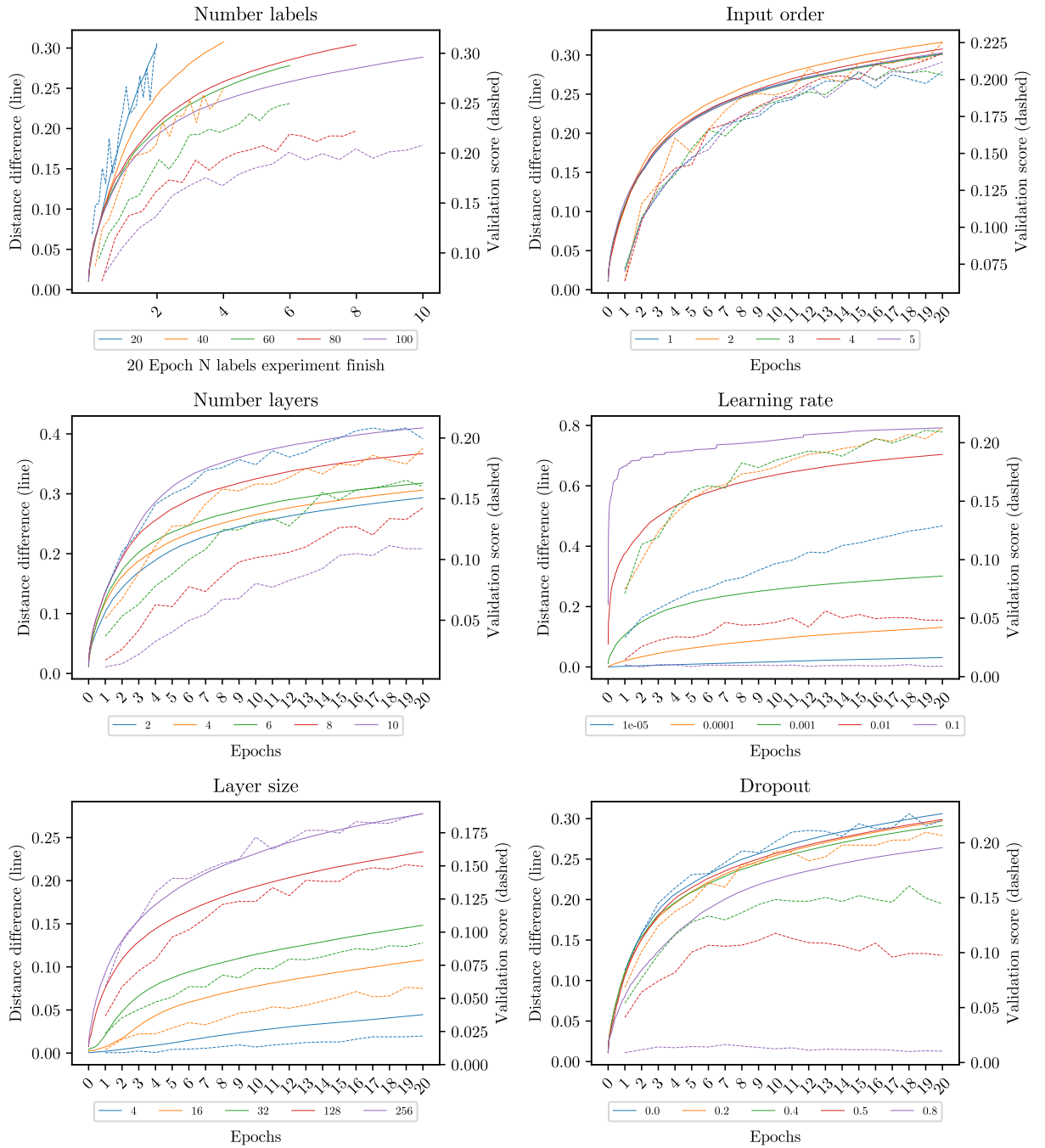


Figure 29: CIFAR-100 MLP cumulative no normalized using Silhouette discretization.

Non-cumulative plots

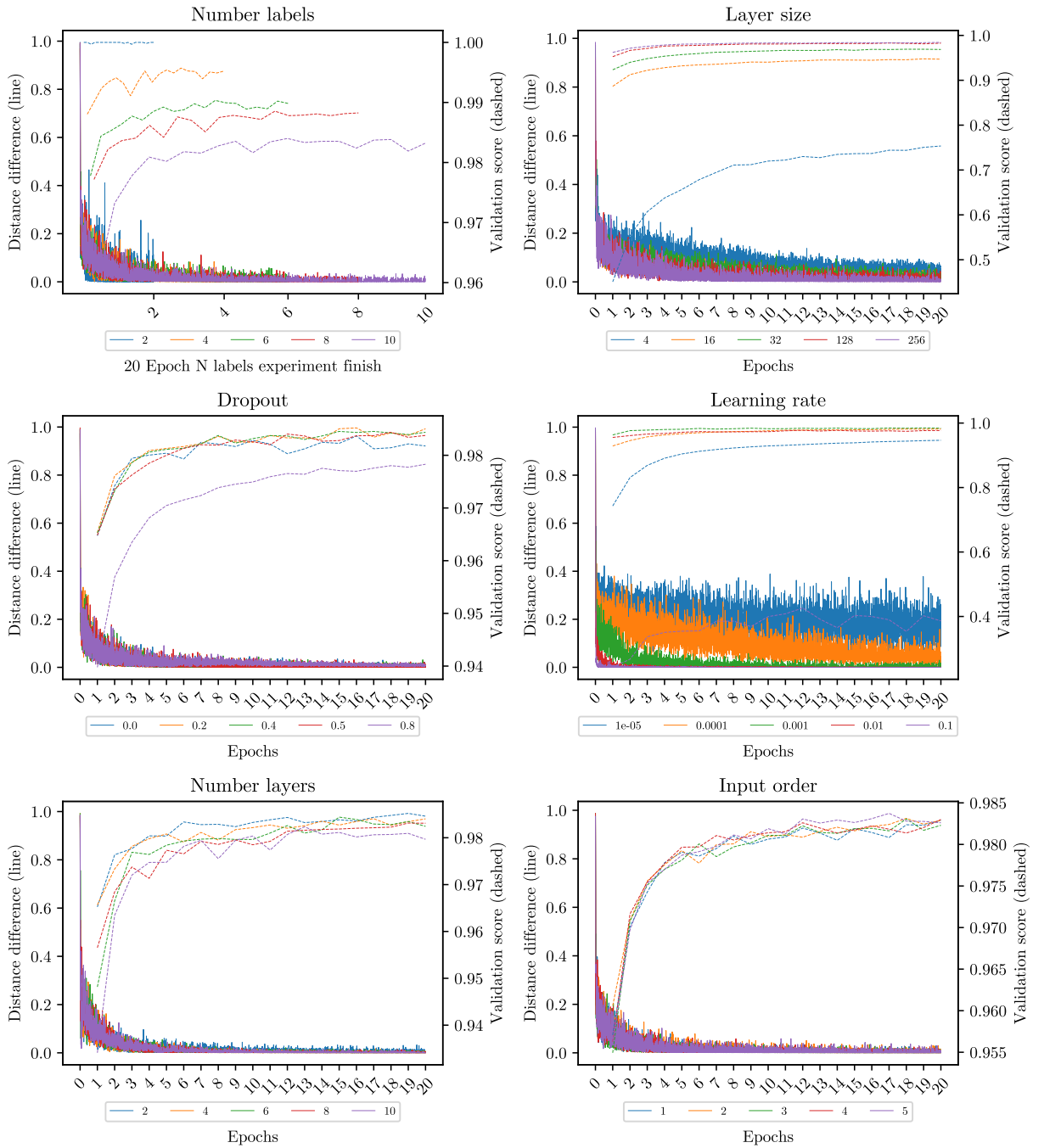


Figure 30: MNIST non-cumulative using Heat discretization.

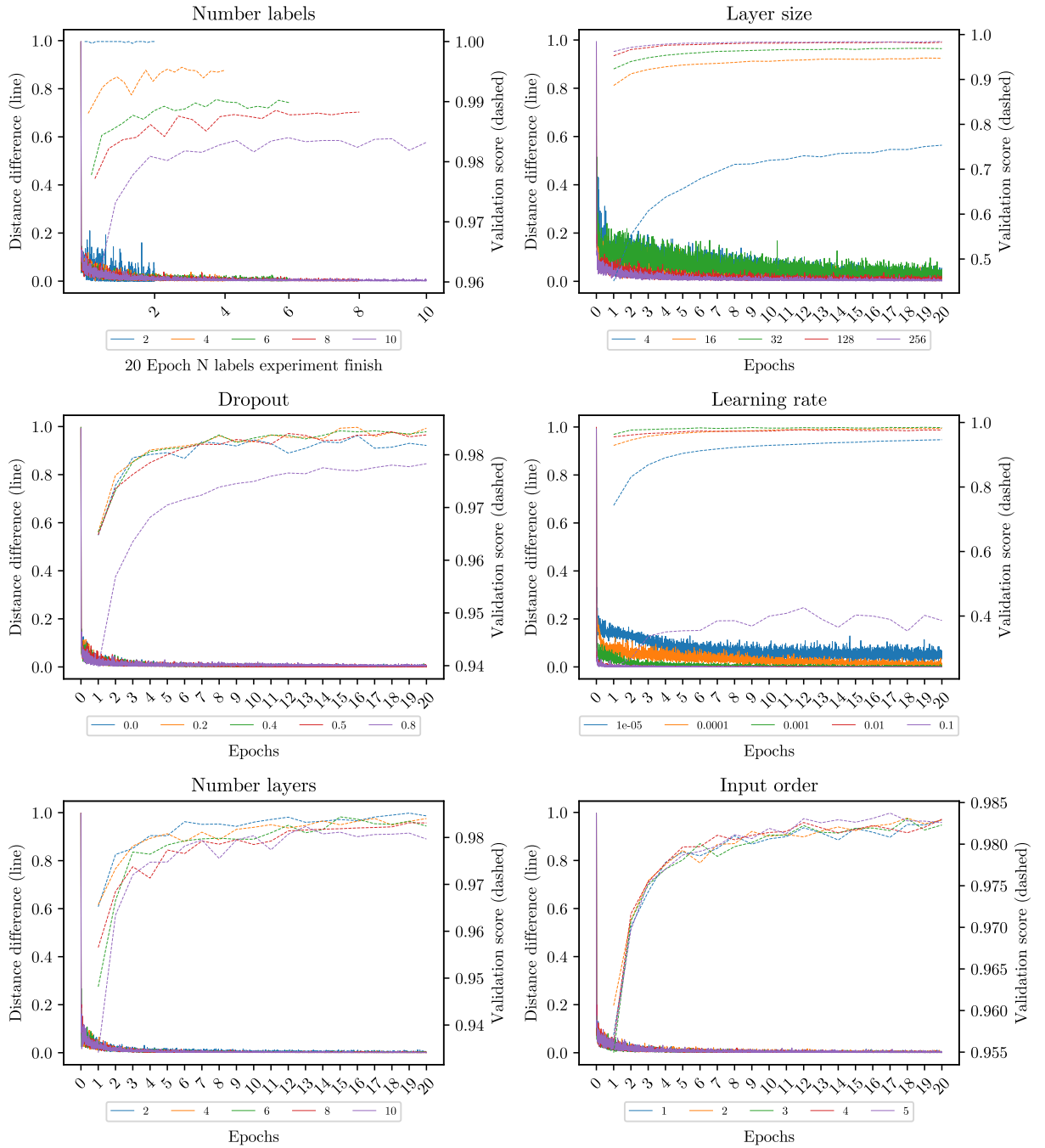


Figure 31: MNIST non-cumulative using Silhouette discretization.

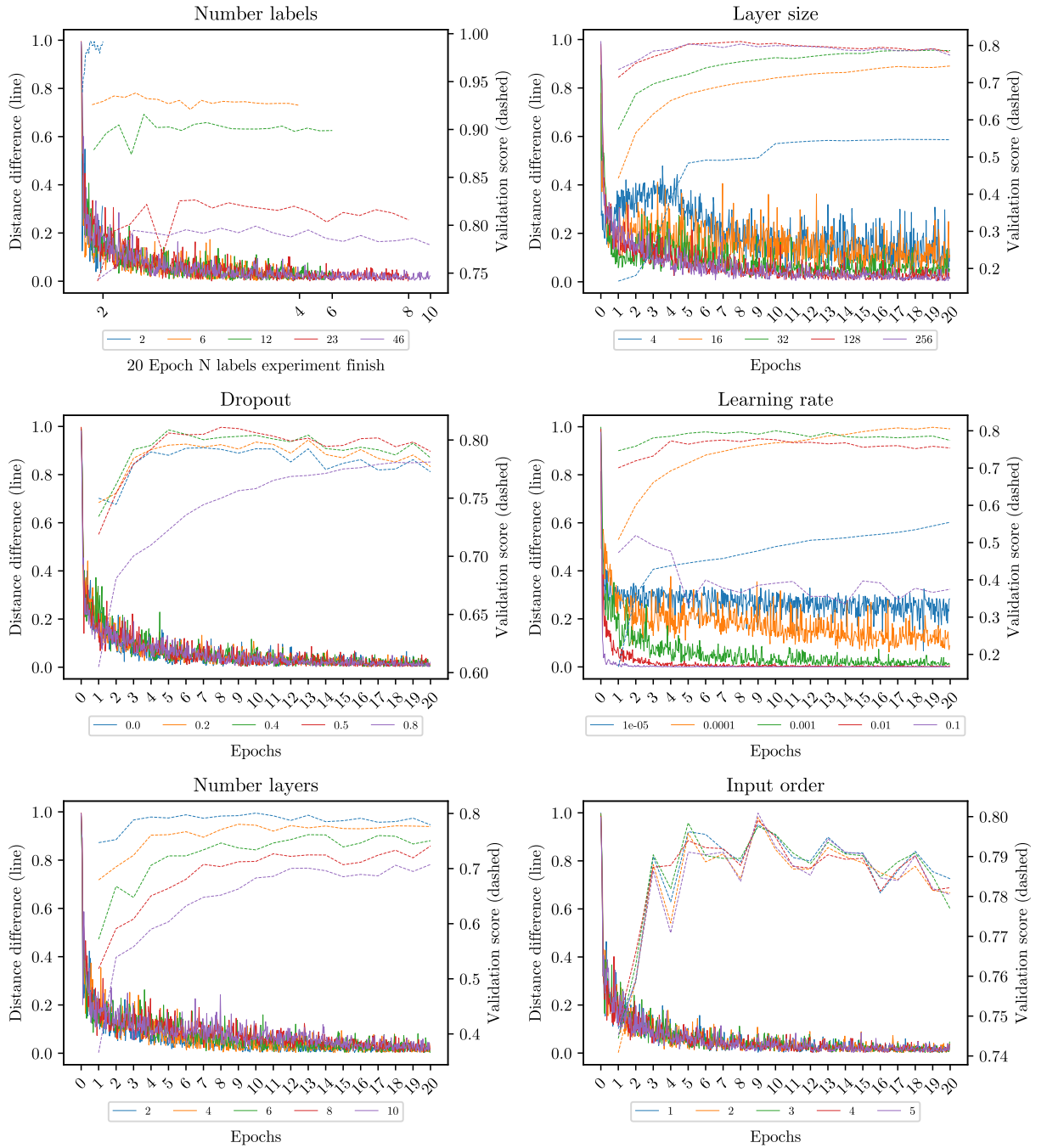


Figure 32: Reuters non-cumulative using Heat discretization.

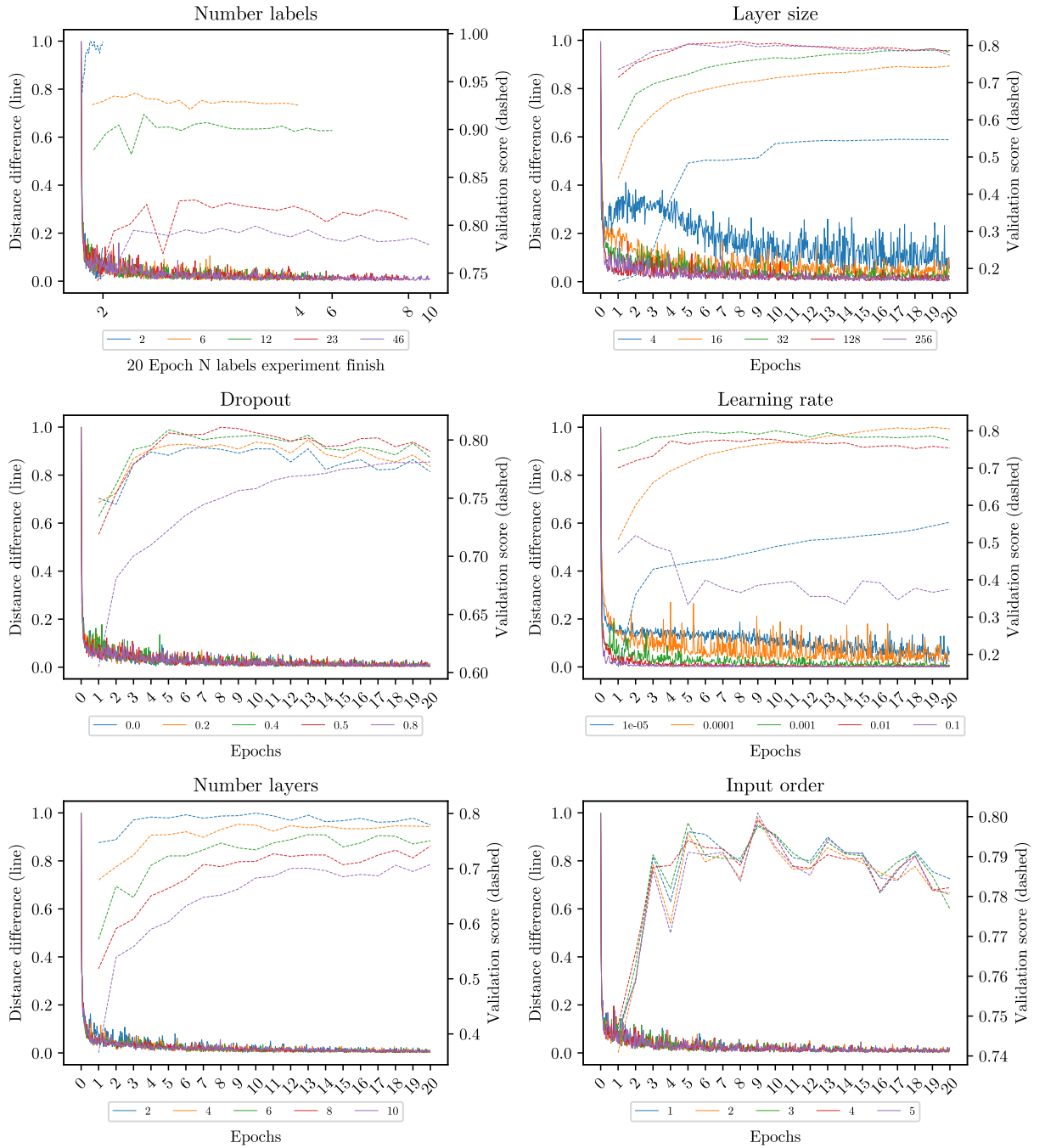


Figure 33: Reuters non-cumulative using Silhouette discretization.

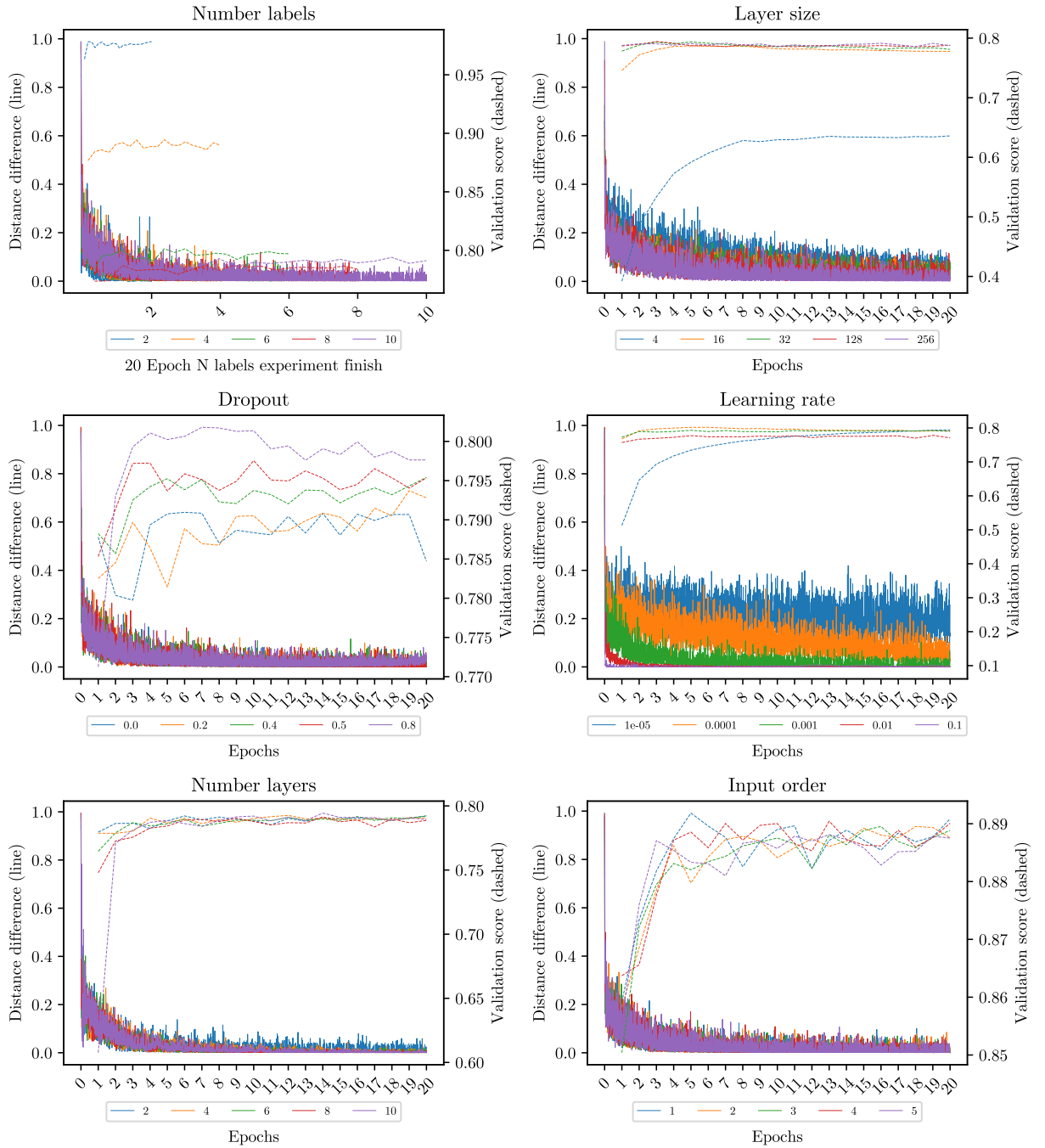


Figure 34: CIFAR-10 CNN non-cumulative using Heat discretization.

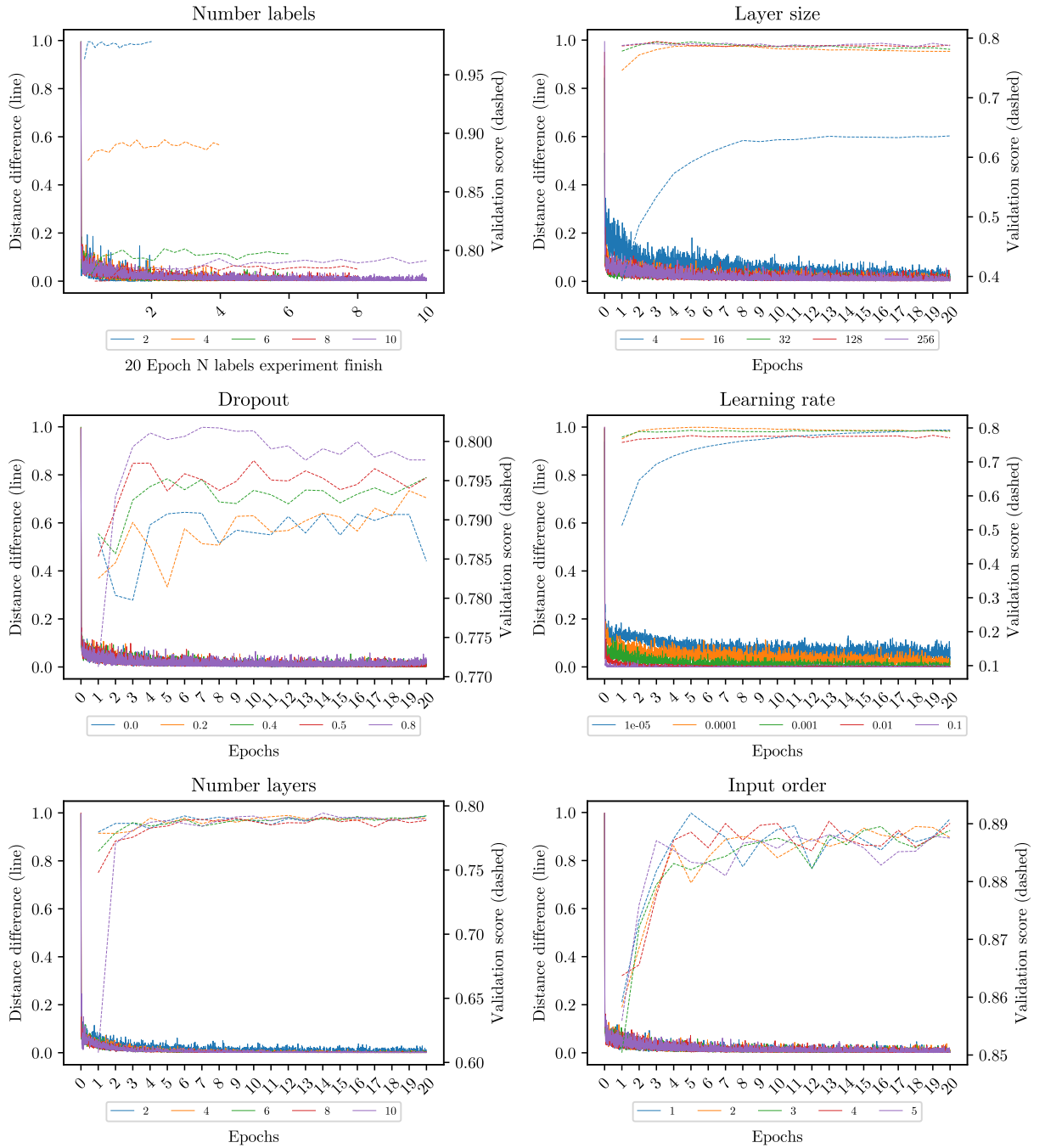


Figure 35: CIFAR-10 CNN non-cumulative using Silhouette discretization.

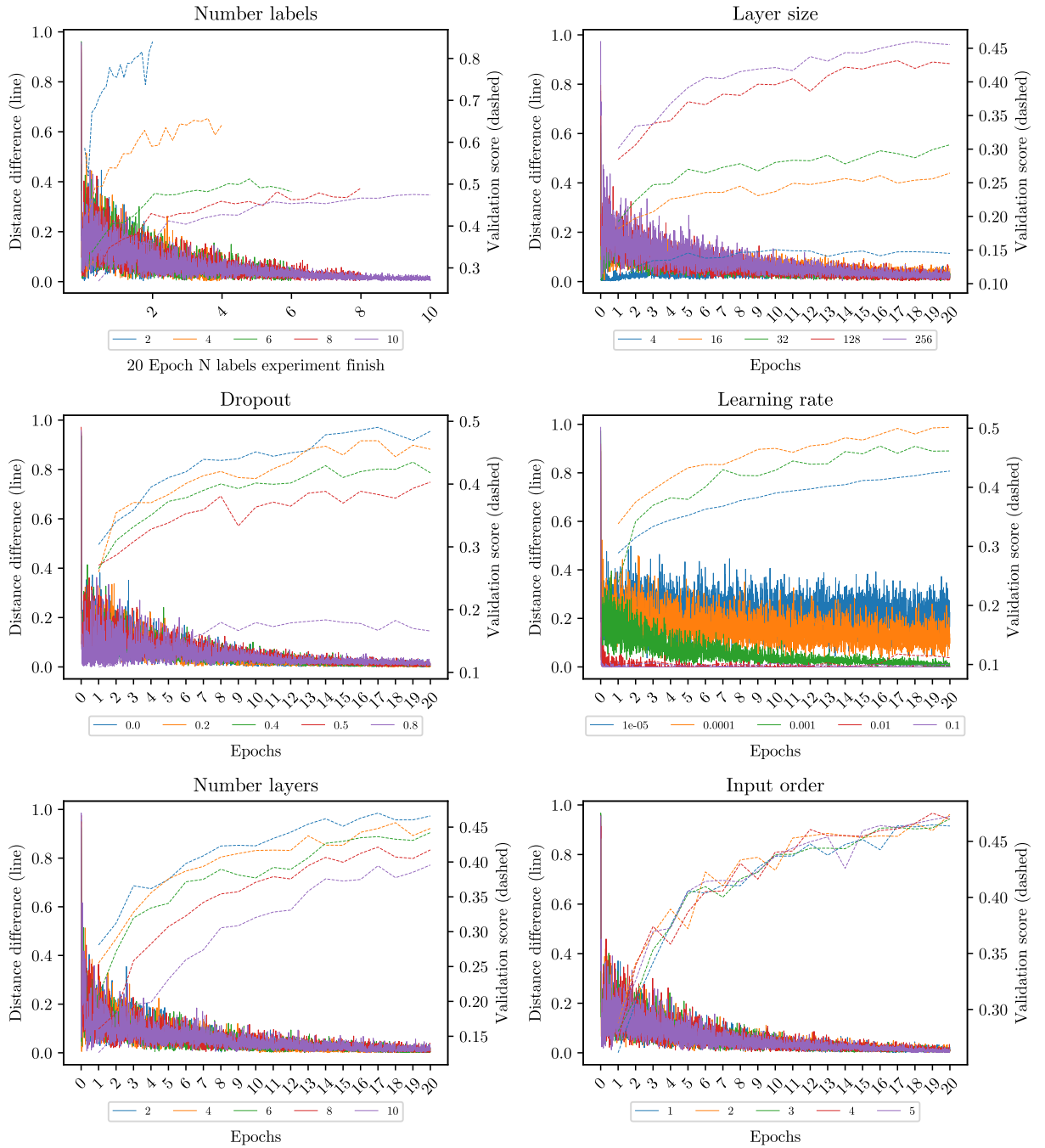


Figure 36: CIFAR-10 MLP non-cumulative using Heat discretization.

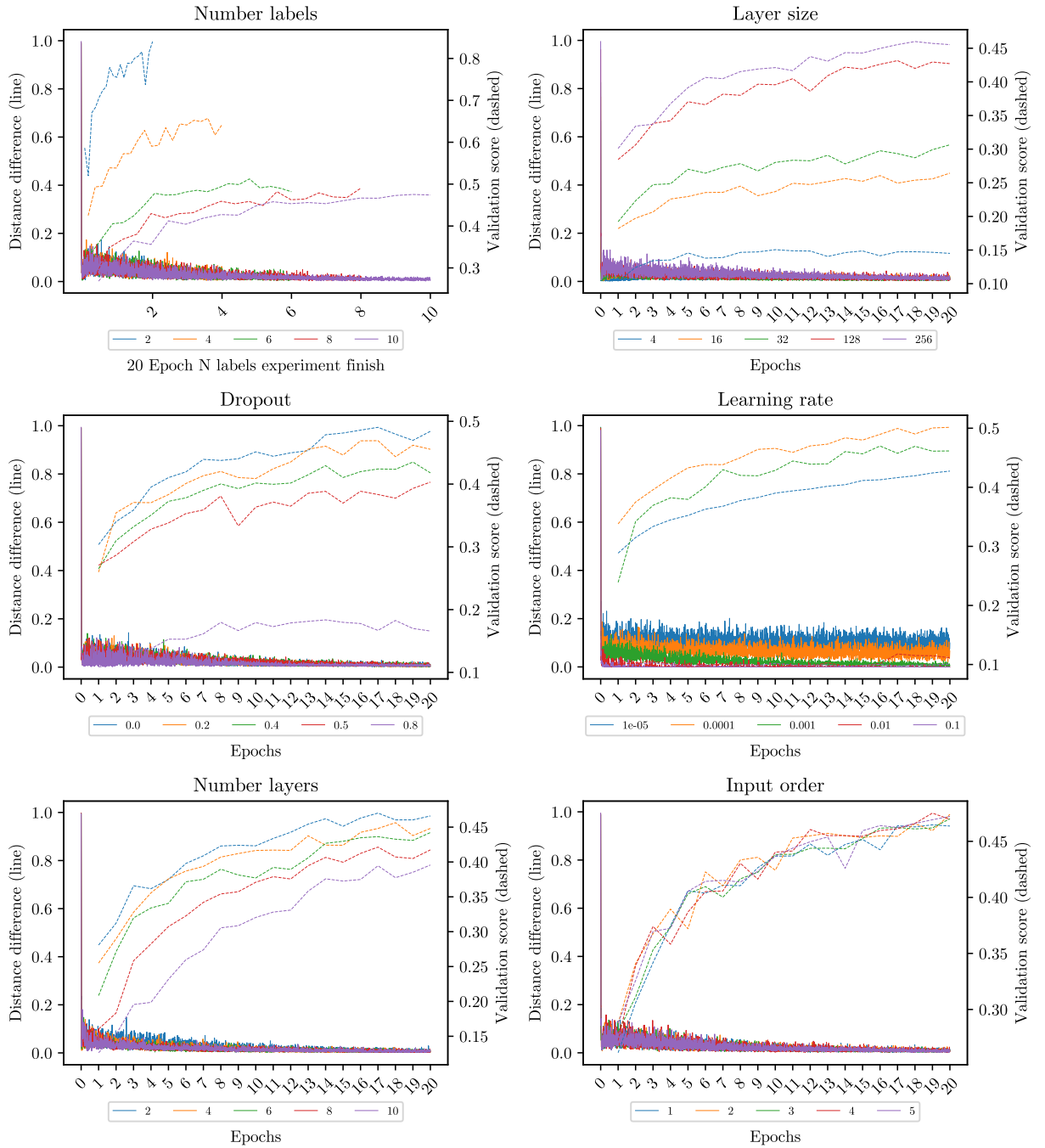


Figure 37: CIFAR-10 MLP non-cumulative using Silhouette discretization.

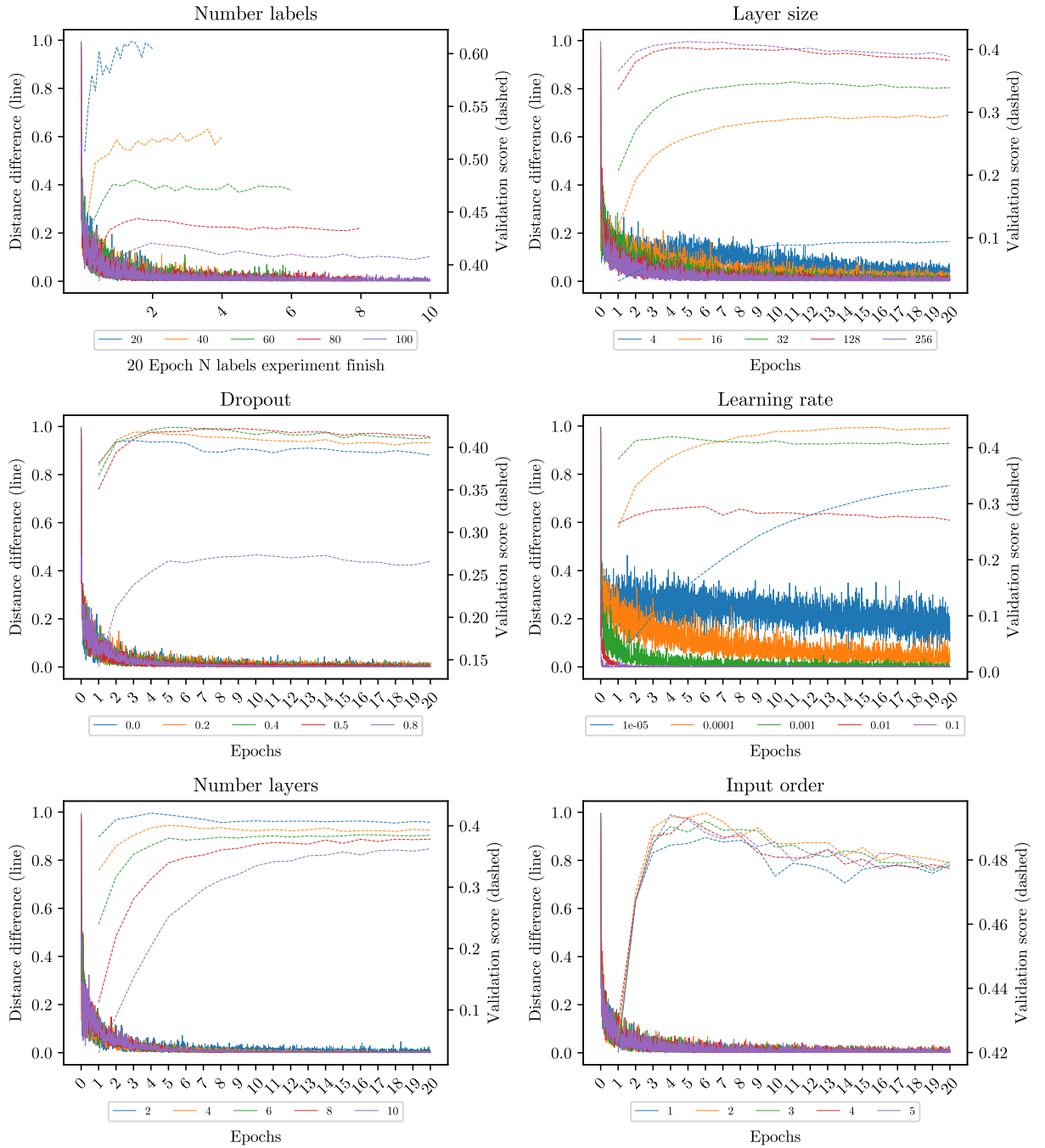


Figure 38: CIFAR-100 CNN non-cumulative using Heat discretization.

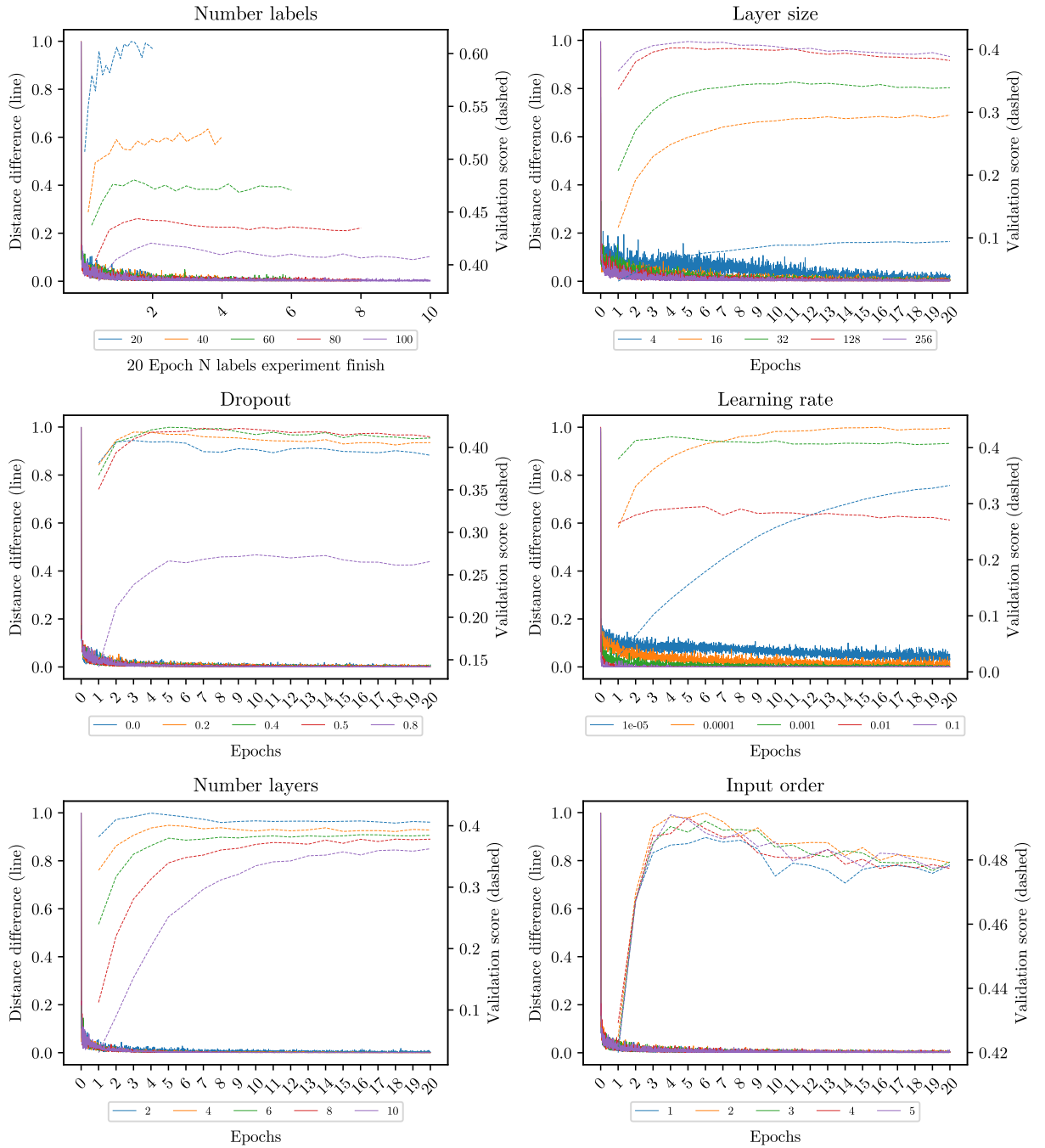


Figure 39: CIFAR-100 CNN non-cumulative using Silhouette discretization.

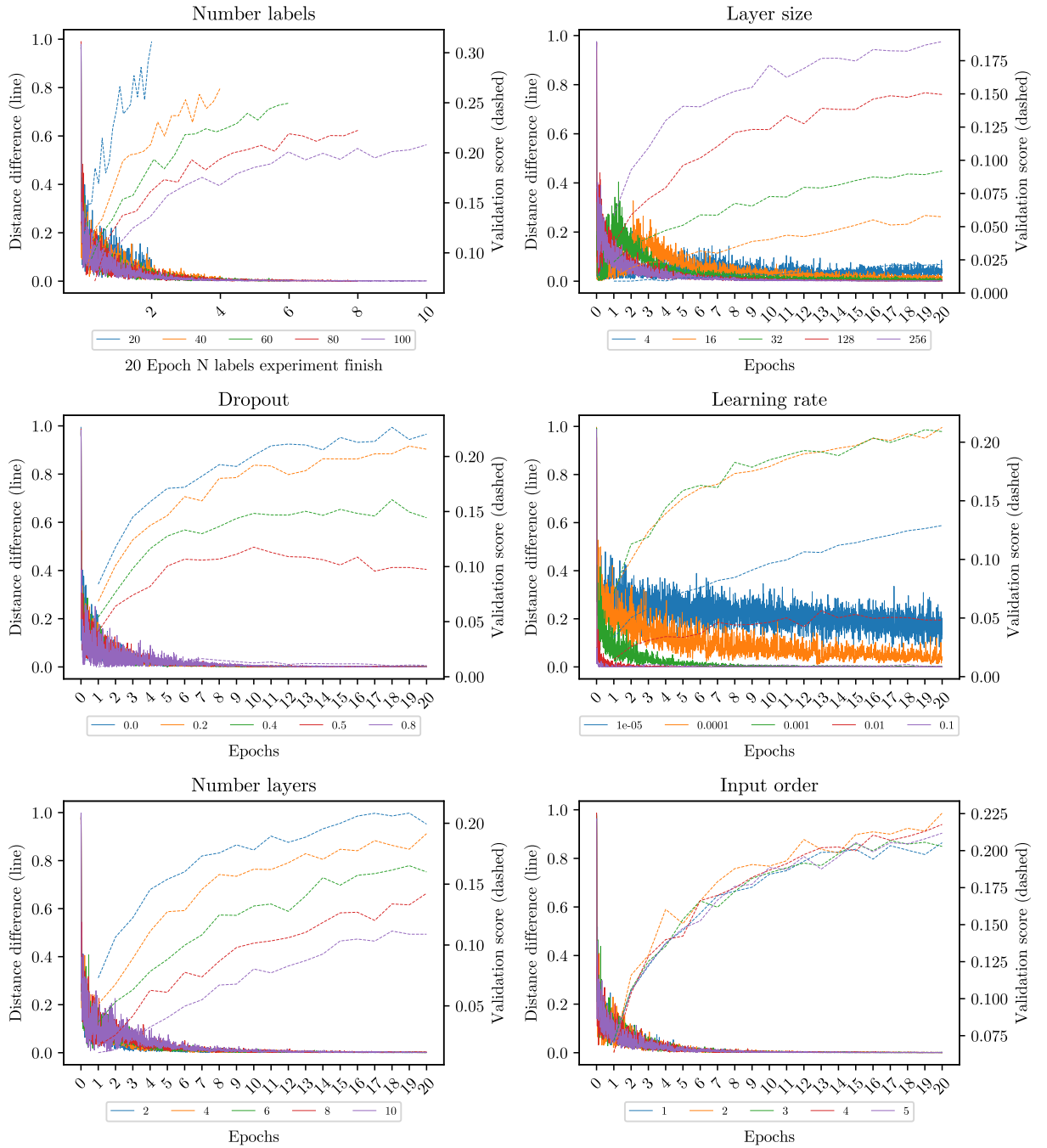


Figure 40: CIFAR-100 MLP non-cumulative using Heat discretization.

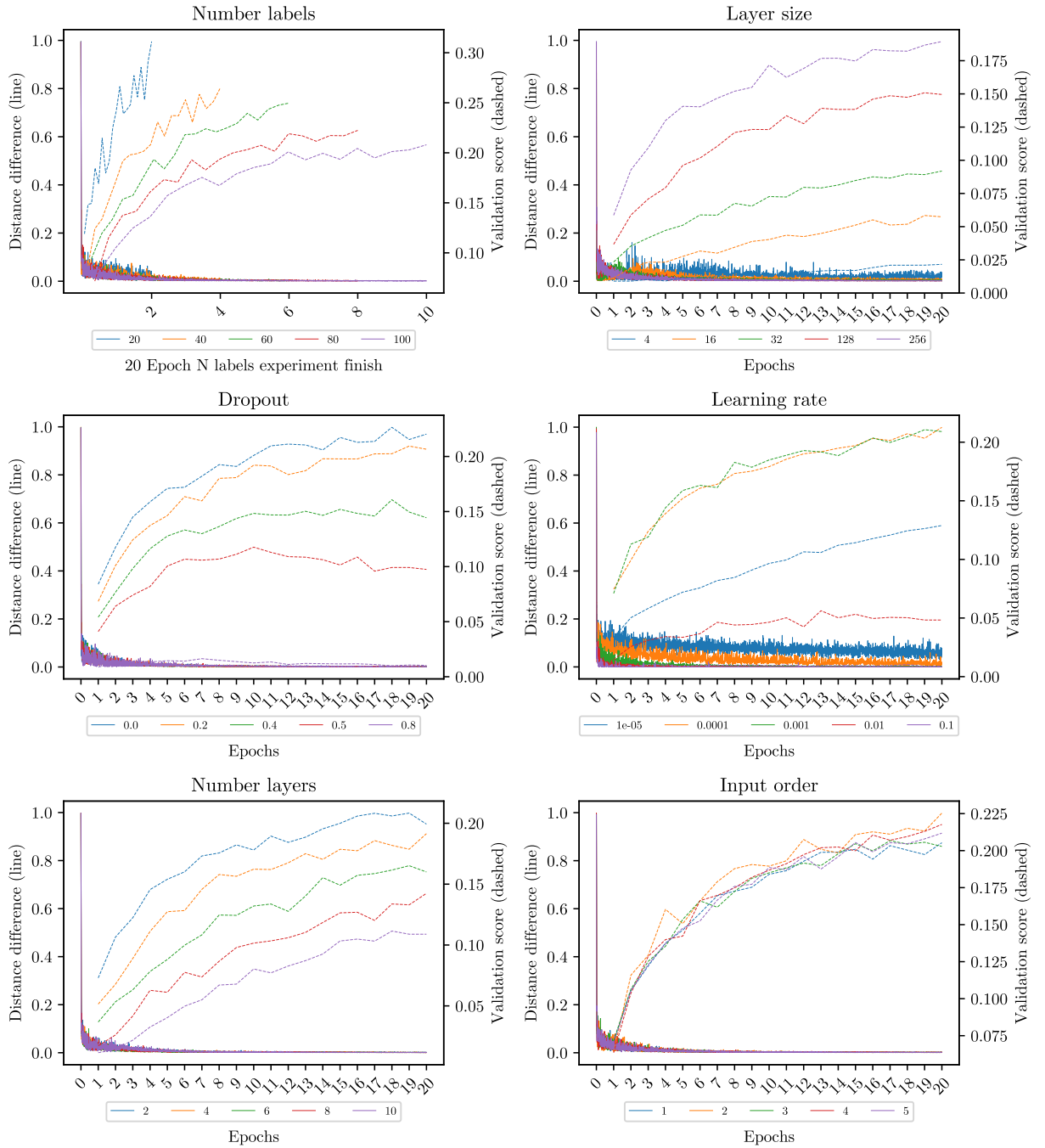


Figure 41: CIFAR-100 MLP non-cumulative using Silhouette discretization.

Correlation Tables

Analysis type	Analysis Value	Pearson's r mean	Pearson's r standard deviation
Layer size	4	0.8080	0.1270
Layer size	16	0.9120	0.0416
Layer size	32	0.9182	0.0327
Layer size	128	0.9224	0.0234
Layer size	256	0.9302	0.0328
Number labels	2	ERROR	ERROR
Number labels	4	0.6805	0.1218
Number labels	6	0.8525	0.0394
Number labels	8	0.8081	0.0835
Number labels	10	0.9197	0.0235
Learning rate	1e-05	0.8035	0.0158
Learning rate	0.0001	0.9165	0.0136
Learning rate	0.001	0.9106	0.0283
Learning rate	0.01	0.8258	0.0615
Learning rate	0.1	0.6516	0.2004
Dropout	0.0	0.8855	0.0251
Dropout	0.2	0.9399	0.0344
Dropout	0.4	0.9567	0.0097
Dropout	0.5	0.9487	0.0057
Dropout	0.8	0.9085	0.0494
Input order	1	0.9416	0.0212
Input order	2	0.9376	0.0233
Input order	3	0.9461	0.0290
Input order	4	0.9401	0.0190
Input order	5	0.9517	0.0124
Number layers	2	0.9244	0.0307
Number layers	4	0.8943	0.0431
Number layers	6	0.9428	0.0131
Number layers	8	0.9322	0.0360
Number layers	10	0.9290	0.0313

Table 1: MNIST Pearson's correlation using Heat distance.

Analysis type	Analysis Value	Pearson's r mean	Pearson's r standard deviation
Layer size	4	0.8232	0.1269
Layer size	16	0.8992	0.0428
Layer size	32	0.8976	0.0403
Layer size	128	0.8866	0.0246
Layer size	256	0.8882	0.0417
Number labels	2	ERROR	ERROR
Number labels	4	0.6691	0.1120
Number labels	6	0.8039	0.0325
Number labels	8	0.7982	0.0716
Number labels	10	0.8668	0.0179
Learning rate	1e-05	0.8542	0.0125
Learning rate	0.0001	0.9309	0.0117
Learning rate	0.001	0.8701	0.0496
Learning rate	0.01	0.8666	0.0283
Learning rate	0.1	0.6576	0.2068
Dropout	0.0	0.8172	0.0247
Dropout	0.2	0.9073	0.0483
Dropout	0.4	0.9274	0.0160
Dropout	0.5	0.9237	0.0148
Dropout	0.8	0.8574	0.0575
Input order	1	0.9039	0.0268
Input order	2	0.9000	0.0320
Input order	3	0.9018	0.0492
Input order	4	0.8907	0.0262
Input order	5	0.9159	0.0209
Number layers	2	0.8903	0.0445
Number layers	4	0.8872	0.0303
Number layers	6	0.9236	0.0169
Number layers	8	0.9384	0.0318
Number layers	10	0.9057	0.0348

Table 2: MNIST Pearson's correlation using Silhouette distance.

Analysis type	Analysis Value	Pearson's r mean	Pearson's r standard deviation
Layer size	4	0.8322	0.0319
Layer size	16	0.8581	0.0788
Layer size	32	0.9122	0.0252
Layer size	128	0.6472	0.0350
Layer size	256	0.5612	0.0534
Number labels	2	0.7383	0.0774
Number labels	6	-0.2842	0.2590
Number labels	12	0.3378	0.0808
Number labels	23	0.5743	0.0610
Number labels	46	0.5203	0.0883
Learning rate	1e-05	0.7949	0.1165
Learning rate	0.0001	0.8973	0.0077
Learning rate	0.001	0.5292	0.1114
Learning rate	0.01	0.7052	0.0696
Learning rate	0.1	-0.4898	0.1535
Dropout	0.0	0.4508	0.0532
Dropout	0.2	0.5700	0.0740
Dropout	0.4	0.6080	0.0378
Dropout	0.5	0.7262	0.0242
Dropout	0.8	0.9752	0.0076
Input order	1	0.6251	0.1389
Input order	2	0.6323	0.0630
Input order	3	0.6109	0.1181
Input order	4	0.5771	0.1141
Input order	5	0.6703	0.0275
Number layers	2	0.5752	0.0677
Number layers	4	0.8567	0.0320
Number layers	6	0.8669	0.0235
Number layers	8	0.8962	0.0155
Number layers	10	0.8843	0.0548

Table 3: REUTERS Pearson's correlation using Heat distance.

Analysis type	Analysis Value	Pearson's r mean	Pearson's r standard deviation
Layer size	4	0.8443	0.0372
Layer size	16	0.9011	0.0668
Layer size	32	0.9353	0.0222
Layer size	128	0.5695	0.0463
Layer size	256	0.4760	0.0581
Number labels	2	0.7434	0.0785
Number labels	6	-0.3016	0.2553
Number labels	12	0.3083	0.0873
Number labels	23	0.5370	0.0666
Number labels	46	0.4552	0.0830
Learning rate	1e-05	0.8071	0.1153
Learning rate	0.0001	0.9187	0.0073
Learning rate	0.001	0.4635	0.1232
Learning rate	0.01	0.6082	0.0751
Learning rate	0.1	-0.5837	0.1366
Dropout	0.0	0.3854	0.0561
Dropout	0.2	0.5108	0.0767
Dropout	0.4	0.5380	0.0508
Dropout	0.5	0.6617	0.0143
Dropout	0.8	0.9554	0.0112
Input order	1	0.5739	0.1468
Input order	2	0.5711	0.0738
Input order	3	0.5591	0.1282
Input order	4	0.5220	0.1145
Input order	5	0.6216	0.0352
Number layers	2	0.5207	0.0712
Number layers	4	0.8503	0.0348
Number layers	6	0.8823	0.0234
Number layers	8	0.9220	0.0110
Number layers	10	0.9068	0.0409

Table 4: REUTERS Pearson's correlation using Silhouette distance.

Analysis type	Analysis Value	Pearson's r mean	Pearson's r standard deviation
Layer size	4	0.8066	0.0480
Layer size	16	0.2882	0.3050
Layer size	32	-0.3713	0.2989
Layer size	128	-0.2872	0.1714
Layer size	256	-0.1035	0.2905
Number labels	2	0.2517	0.2946
Number labels	4	0.3307	0.3197
Number labels	6	0.2712	0.3099
Number labels	8	0.5009	0.2813
Number labels	10	0.3501	0.1339
Learning rate	1e-05	0.7876	0.0099
Learning rate	0.0001	0.1131	0.0572
Learning rate	0.001	0.5346	0.2875
Learning rate	0.01	0.4672	0.1593
Learning rate	0.1	-0.1287	0.3295
Dropout	0.0	0.2901	0.2357
Dropout	0.2	0.5089	0.2655
Dropout	0.4	0.3915	0.2252
Dropout	0.5	0.3815	0.2564
Dropout	0.8	0.5608	0.1693
Input order	1	0.6134	0.1403
Input order	2	0.7551	0.1070
Input order	3	0.7949	0.0424
Input order	4	0.7134	0.1470
Input order	5	0.6552	0.1582
Number layers	2	0.3803	0.2913
Number layers	4	0.5976	0.0911
Number layers	6	0.6576	0.1912
Number layers	8	0.8081	0.0917
Number layers	10	0.8050	0.0364

Table 5: CIFAR10CNN Pearson's correlation using Heat distance.

Analysis type	Analysis Value	Pearson's r mean	Pearson's r standard deviation
Layer size	4	0.8365	0.0410
Layer size	16	0.2859	0.3022
Layer size	32	-0.3900	0.2913
Layer size	128	-0.2940	0.1659
Layer size	256	-0.1073	0.2823
Number labels	2	0.2326	0.2877
Number labels	4	0.2942	0.3251
Number labels	6	0.2448	0.2918
Number labels	8	0.4721	0.2600
Number labels	10	0.3736	0.0926
Learning rate	1e-05	0.8300	0.0094
Learning rate	0.0001	0.1090	0.0606
Learning rate	0.001	0.4838	0.2909
Learning rate	0.01	0.4343	0.1867
Learning rate	0.1	-0.1287	0.3343
Dropout	0.0	0.2839	0.2095
Dropout	0.2	0.5217	0.2303
Dropout	0.4	0.3686	0.2129
Dropout	0.5	0.3344	0.2336
Dropout	0.8	0.4527	0.1747
Input order	1	0.5628	0.1471
Input order	2	0.7108	0.1276
Input order	3	0.7470	0.0569
Input order	4	0.6606	0.1529
Input order	5	0.5970	0.1521
Number layers	2	0.3759	0.2634
Number layers	4	0.5952	0.0978
Number layers	6	0.6525	0.1865
Number layers	8	0.7839	0.0942
Number layers	10	0.7738	0.0317

Table 6: CIFAR10CNN Pearson's correlation using Silhouette distance.

Analysis type	Analysis Value	Pearson's r mean	Pearson's r standard deviation
Layer size	4	0.2950	0.3612
Layer size	16	0.7703	0.2399
Layer size	32	0.8268	0.1422
Layer size	128	0.9307	0.0079
Layer size	256	0.9245	0.0157
Number labels	2	0.7327	0.0660
Number labels	4	0.8480	0.0572
Number labels	6	0.8443	0.0502
Number labels	8	0.8792	0.0411
Number labels	10	0.9536	0.0217
Learning rate	1e-05	0.9596	0.0051
Learning rate	0.0001	0.9317	0.0198
Learning rate	0.001	0.9270	0.0250
Learning rate	0.01	-0.0373	0.2588
Learning rate	0.1	0.0838	0.2118
Dropout	0.0	0.9411	0.0264
Dropout	0.2	0.9144	0.0229
Dropout	0.4	0.9365	0.0154
Dropout	0.5	0.8564	0.0743
Dropout	0.8	0.7389	0.0910
Input order	1	0.9468	0.0101
Input order	2	0.9232	0.0301
Input order	3	0.9482	0.0099
Input order	4	0.9168	0.0415
Input order	5	0.9327	0.0282
Number layers	2	0.9425	0.0178
Number layers	4	0.9511	0.0151
Number layers	6	0.9466	0.0150
Number layers	8	0.9613	0.0139
Number layers	10	0.9741	0.0119

Table 7: CIFAR10MLP Pearson's correlation using Heat distance.

Analysis type	Analysis Value	Pearson's r mean	Pearson's r standard deviation
Layer size	4	0.3302	0.3375
Layer size	16	0.7520	0.2474
Layer size	32	0.8016	0.1655
Layer size	128	0.9163	0.0208
Layer size	256	0.9124	0.0205
Number labels	2	0.7272	0.0622
Number labels	4	0.8307	0.0630
Number labels	6	0.8269	0.0517
Number labels	8	0.8627	0.0425
Number labels	10	0.9403	0.0262
Learning rate	1e-05	0.9611	0.0041
Learning rate	0.0001	0.9235	0.0213
Learning rate	0.001	0.9088	0.0284
Learning rate	0.01	-0.0310	0.2815
Learning rate	0.1	0.0566	0.2259
Dropout	0.0	0.9342	0.0274
Dropout	0.2	0.9082	0.0165
Dropout	0.4	0.9213	0.0247
Dropout	0.5	0.8486	0.0679
Dropout	0.8	0.7399	0.0910
Input order	1	0.9312	0.0117
Input order	2	0.9080	0.0294
Input order	3	0.9395	0.0071
Input order	4	0.9077	0.0343
Input order	5	0.9267	0.0272
Number layers	2	0.9351	0.0172
Number layers	4	0.9427	0.0178
Number layers	6	0.9419	0.0147
Number layers	8	0.9593	0.0135
Number layers	10	0.9788	0.0069

Table 8: CIFAR10MLP Pearson's correlation using Silhouette distance.

Analysis type	Analysis Value	Pearson's r mean	Pearson's r standard deviation
Layer size	4	0.8908	0.0707
Layer size	16	0.8926	0.0230
Layer size	32	0.8653	0.0332
Layer size	128	0.5020	0.1325
Layer size	256	0.2174	0.1214
Number labels	20	0.7607	0.0742
Number labels	40	0.7704	0.0761
Number labels	60	0.5372	0.2043
Number labels	80	0.4041	0.1317
Number labels	100	0.3615	0.1028
Learning rate	1e-05	0.9694	0.0067
Learning rate	0.0001	0.8980	0.0166
Learning rate	0.001	0.3175	0.0993
Learning rate	0.01	0.3461	0.2098
Learning rate	0.1	-0.1318	0.1987
Dropout	0.0	-0.0528	0.1971
Dropout	0.2	0.3034	0.0576
Dropout	0.4	0.6674	0.0835
Dropout	0.5	0.8462	0.0514
Dropout	0.8	0.9509	0.0168
Input order	1	0.6445	0.0834
Input order	2	0.5699	0.0830
Input order	3	0.6100	0.0477
Input order	4	0.5651	0.0729
Input order	5	0.6246	0.0409
Number layers	2	0.2756	0.1057
Number layers	4	0.8624	0.0419
Number layers	6	0.9706	0.0089
Number layers	8	0.9931	0.0020
Number layers	10	0.9572	0.0063

Table 9: CIFAR100CNN Pearson's correlation using Heat distance.

Analysis type	Analysis Value	Pearson's r mean	Pearson's r standard deviation
Layer size	4	0.9129	0.0642
Layer size	16	0.8940	0.0274
Layer size	32	0.8530	0.0325
Layer size	128	0.4209	0.1335
Layer size	256	0.1129	0.1202
Number labels	20	0.7450	0.0777
Number labels	40	0.7361	0.0734
Number labels	60	0.4762	0.2142
Number labels	80	0.3103	0.1319
Number labels	100	0.2614	0.0929
Learning rate	1e-05	0.9806	0.0052
Learning rate	0.0001	0.9015	0.0188
Learning rate	0.001	0.2212	0.1084
Learning rate	0.01	0.2032	0.2316
Learning rate	0.1	-0.1386	0.2254
Dropout	0.0	-0.1262	0.1812
Dropout	0.2	0.1994	0.0553
Dropout	0.4	0.5566	0.0944
Dropout	0.5	0.7549	0.0621
Dropout	0.8	0.8843	0.0347
Input order	1	0.5514	0.0865
Input order	2	0.4804	0.0842
Input order	3	0.5161	0.0472
Input order	4	0.4686	0.0772
Input order	5	0.5282	0.0374
Number layers	2	0.1789	0.1113
Number layers	4	0.8221	0.0507
Number layers	6	0.9577	0.0124
Number layers	8	0.9850	0.0032
Number layers	10	0.9531	0.0066

Table 10: CIFAR100CNN Pearson's correlation using Silhouette distance.

Analysis type	Analysis Value	Pearson's r mean	Pearson's r standard deviation
Layer size	4	0.5640	0.6287
Layer size	16	0.9096	0.0500
Layer size	32	0.9275	0.0152
Layer size	128	0.9253	0.0191
Layer size	256	0.9348	0.0208
Number labels	20	0.8612	0.0283
Number labels	40	0.9361	0.0188
Number labels	60	0.9233	0.0178
Number labels	80	0.9515	0.0120
Number labels	100	0.9314	0.0204
Learning rate	1e-05	0.9864	0.0056
Learning rate	0.0001	0.9813	0.0046
Learning rate	0.001	0.9385	0.0084
Learning rate	0.01	0.7182	0.0230
Learning rate	0.1	-0.1033	0.1915
Dropout	0.0	0.9298	0.0307
Dropout	0.2	0.9274	0.0101
Dropout	0.4	0.9372	0.0133
Dropout	0.5	0.8675	0.0518
Dropout	0.8	0.0635	0.3428
Input order	1	0.9278	0.0135
Input order	2	0.9425	0.0066
Input order	3	0.9315	0.0251
Input order	4	0.9221	0.0259
Input order	5	0.9172	0.0133
Number layers	2	0.9346	0.0112
Number layers	4	0.9135	0.0315
Number layers	6	0.8876	0.0143
Number layers	8	0.8980	0.0140
Number layers	10	0.8733	0.0297

Table 11: CIFAR100MLP Pearson's correlation using Heat distance.

Analysis type	Analysis Value	Pearson's r mean	Pearson's r standard deviation
Layer size	4	0.5423	0.6368
Layer size	16	0.9261	0.0409
Layer size	32	0.9602	0.0092
Layer size	128	0.9689	0.0162
Layer size	256	0.9669	0.0103
Number labels	20	0.8617	0.0284
Number labels	40	0.9375	0.0194
Number labels	60	0.9484	0.0095
Number labels	80	0.9697	0.0048
Number labels	100	0.9706	0.0076
Learning rate	1e-05	0.9882	0.0053
Learning rate	0.0001	0.9792	0.0047
Learning rate	0.001	0.9754	0.0065
Learning rate	0.01	0.7968	0.0622
Learning rate	0.1	-0.0751	0.2187
Dropout	0.0	0.9635	0.0155
Dropout	0.2	0.9689	0.0056
Dropout	0.4	0.9405	0.0117
Dropout	0.5	0.8099	0.0619
Dropout	0.8	-0.0034	0.3426
Input order	1	0.9659	0.0147
Input order	2	0.9740	0.0051
Input order	3	0.9722	0.0131
Input order	4	0.9652	0.0135
Input order	5	0.9656	0.0068
Number layers	2	0.9708	0.0090
Number layers	4	0.9512	0.0235
Number layers	6	0.9330	0.0079
Number layers	8	0.9272	0.0122
Number layers	10	0.8917	0.0236

Table 12: CIFAR100MLP Pearson's correlation using Silhouette distance.

0.1 Correlation Points

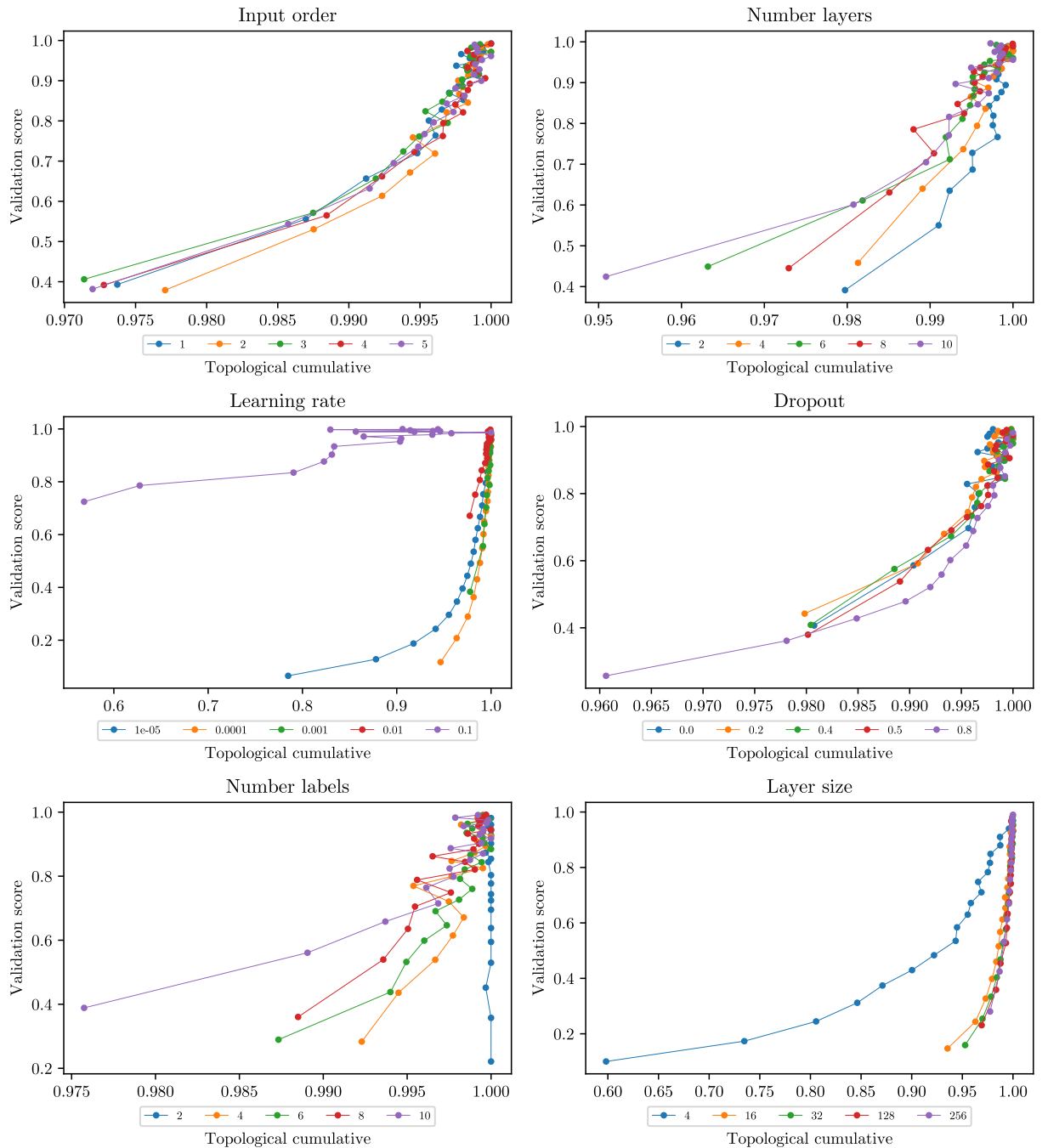


Figure 42: MNIST points relationship across epochs using Heat discretization.

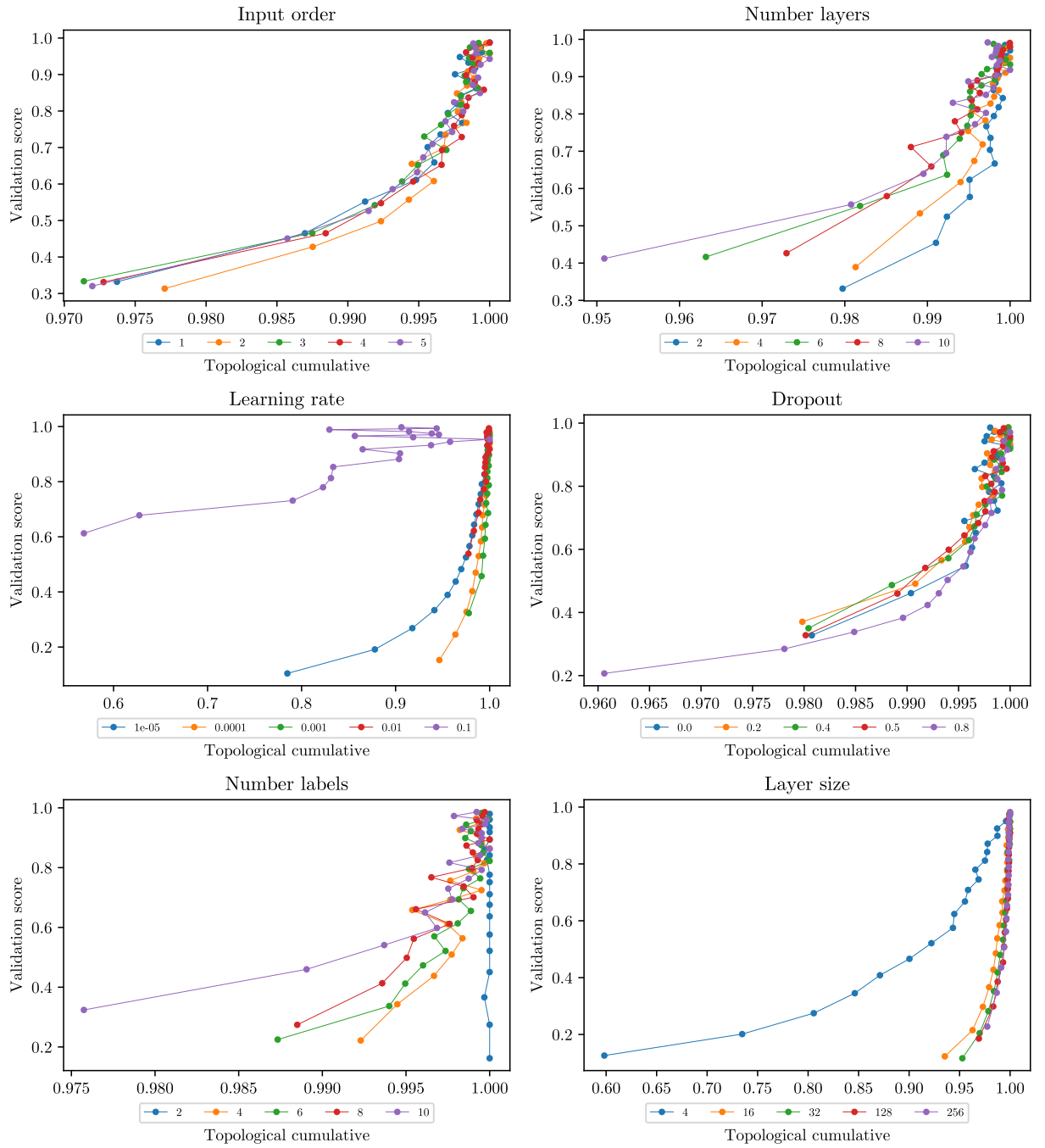


Figure 43: MNIST points relationship across epochs using Silhouette discretization.

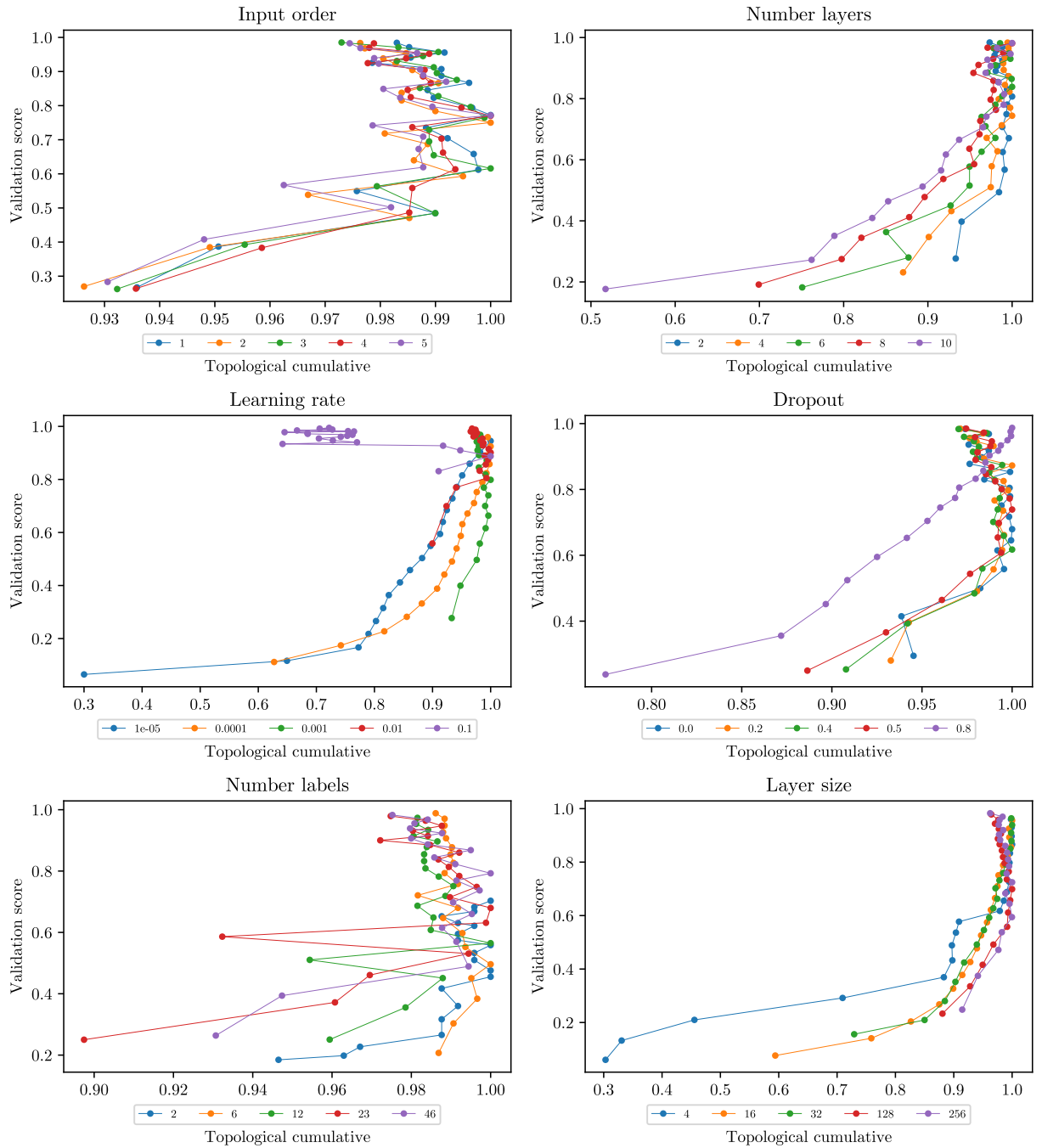


Figure 44: Reuters points relationship across epochs using Heat discretization.

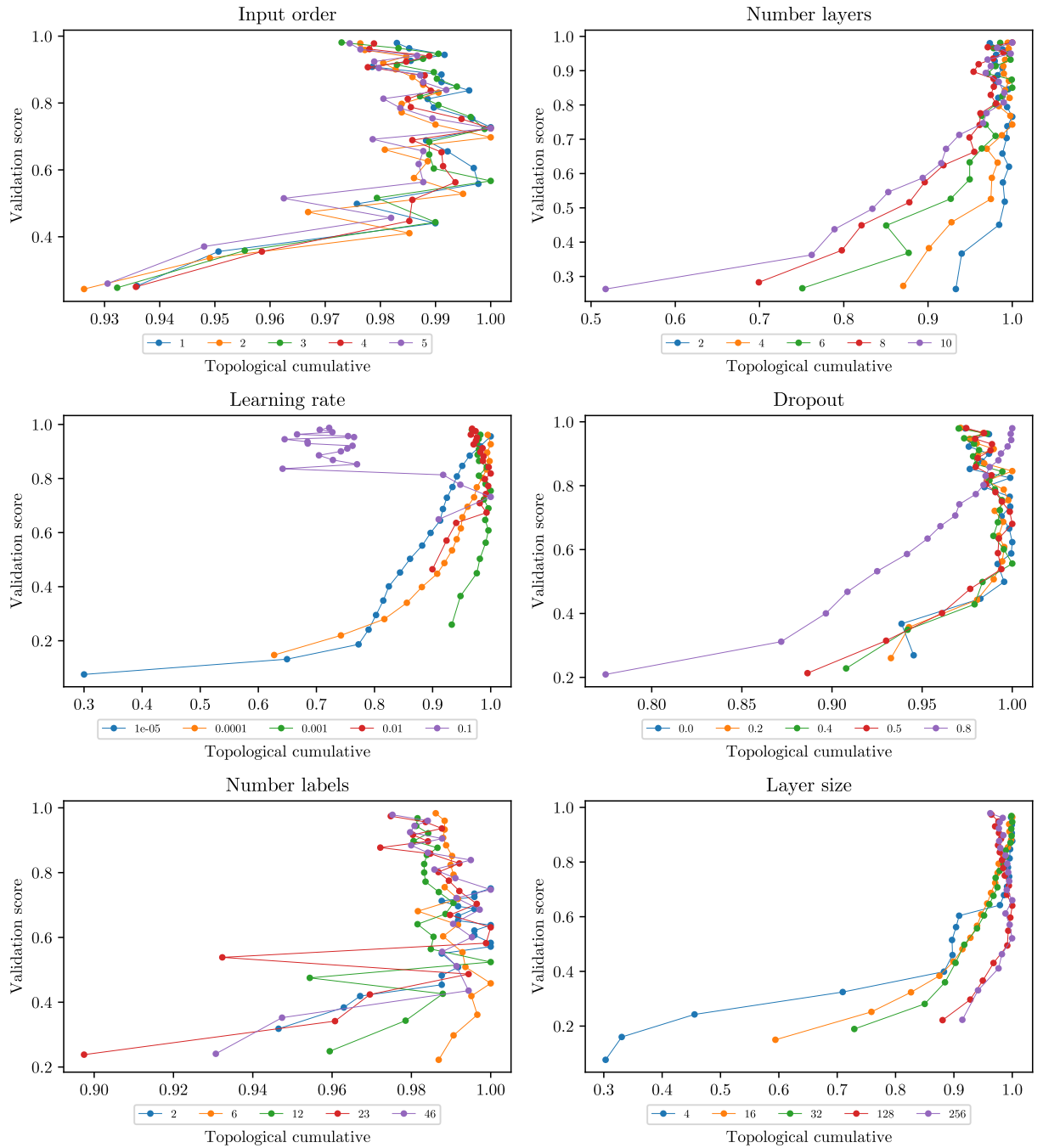


Figure 45: Reuters points relationship across epochs using Silhouette discretization.

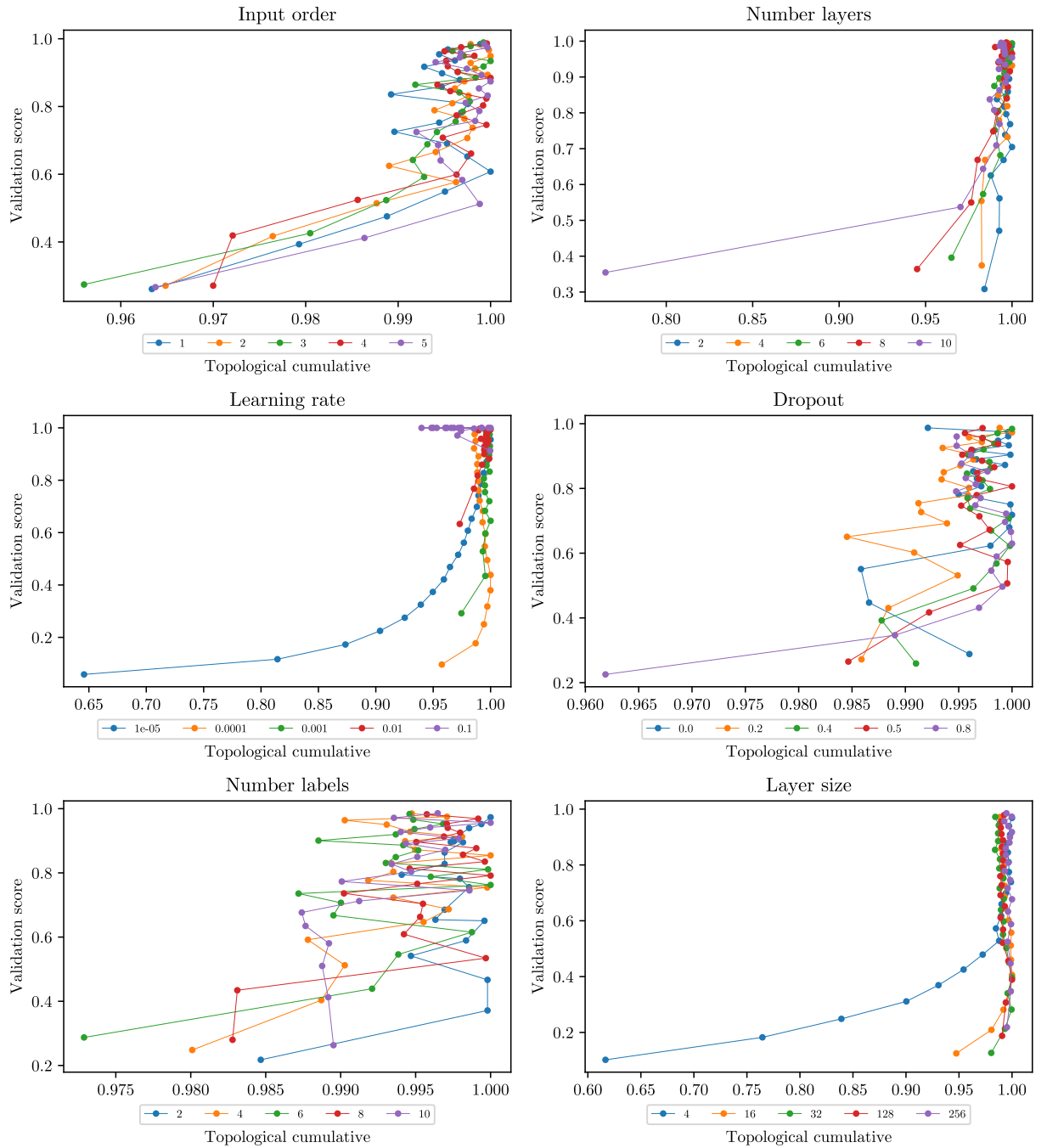


Figure 46: CIFAR-10 CNN points relationship across epochs using Heat discretization.

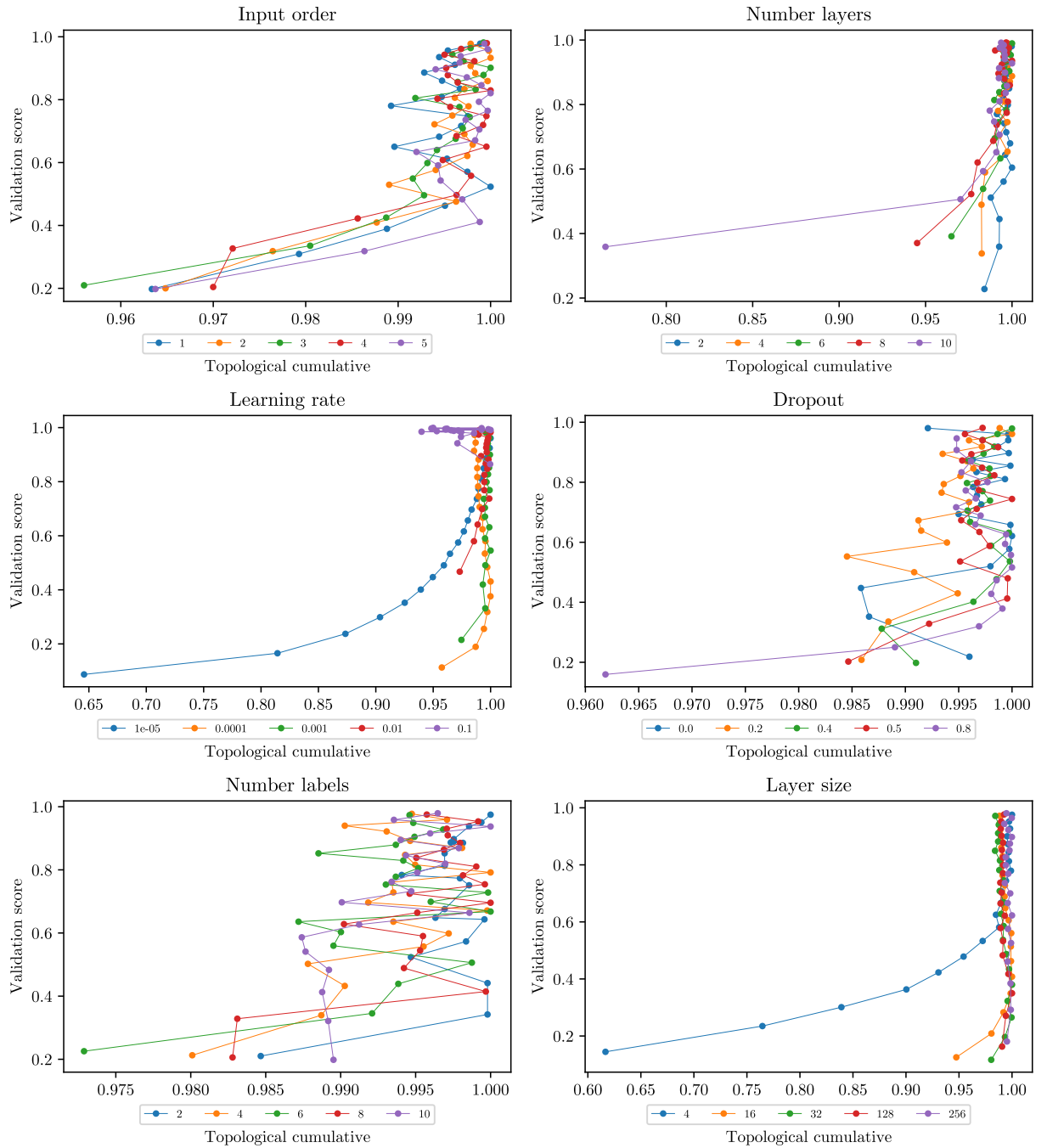


Figure 47: CIFAR-10 CNN points relationship across epochs using Silhouette discretization.

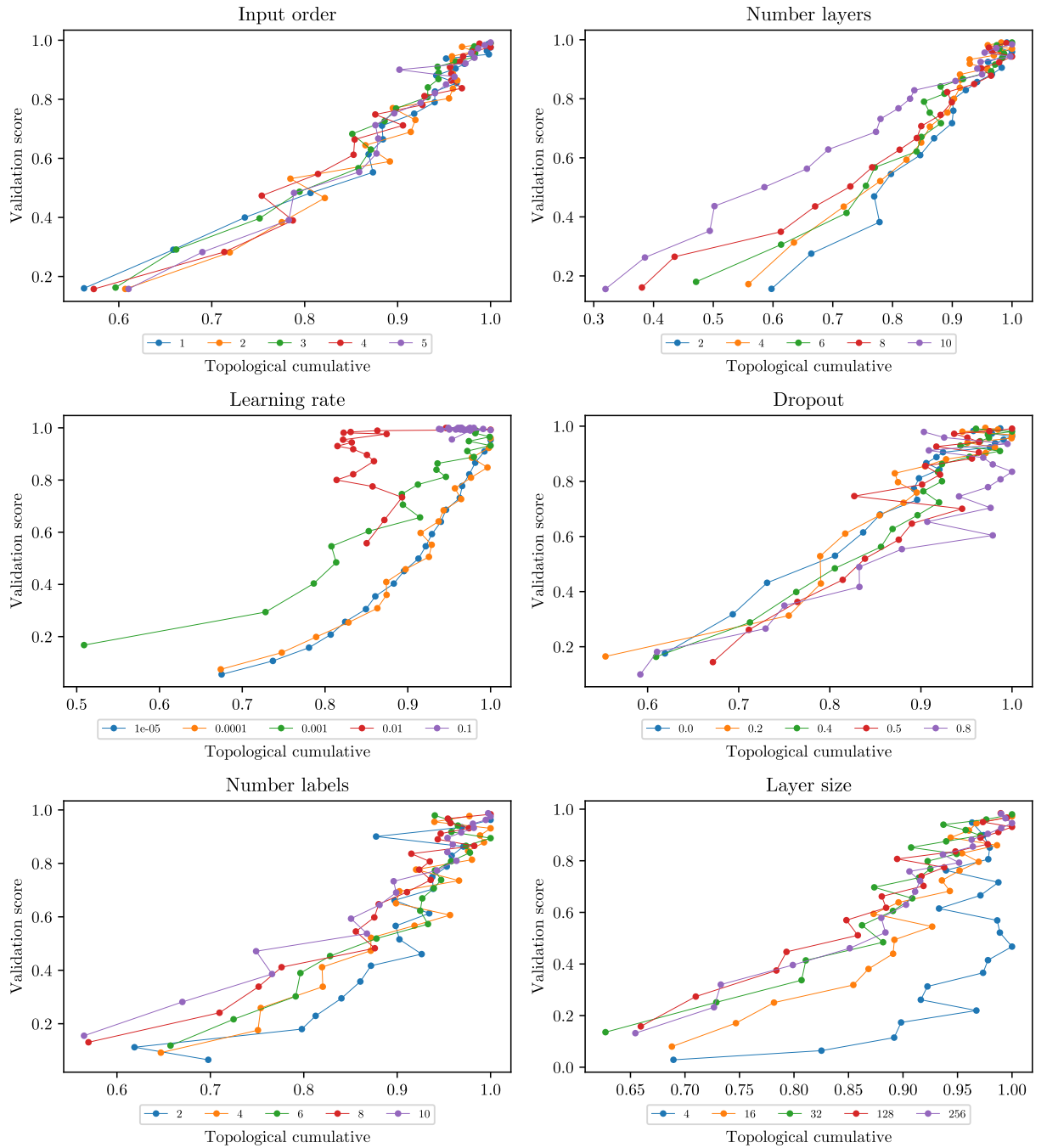


Figure 48: CIFAR-10 MLP points relationship across epochs using Heat discretization.

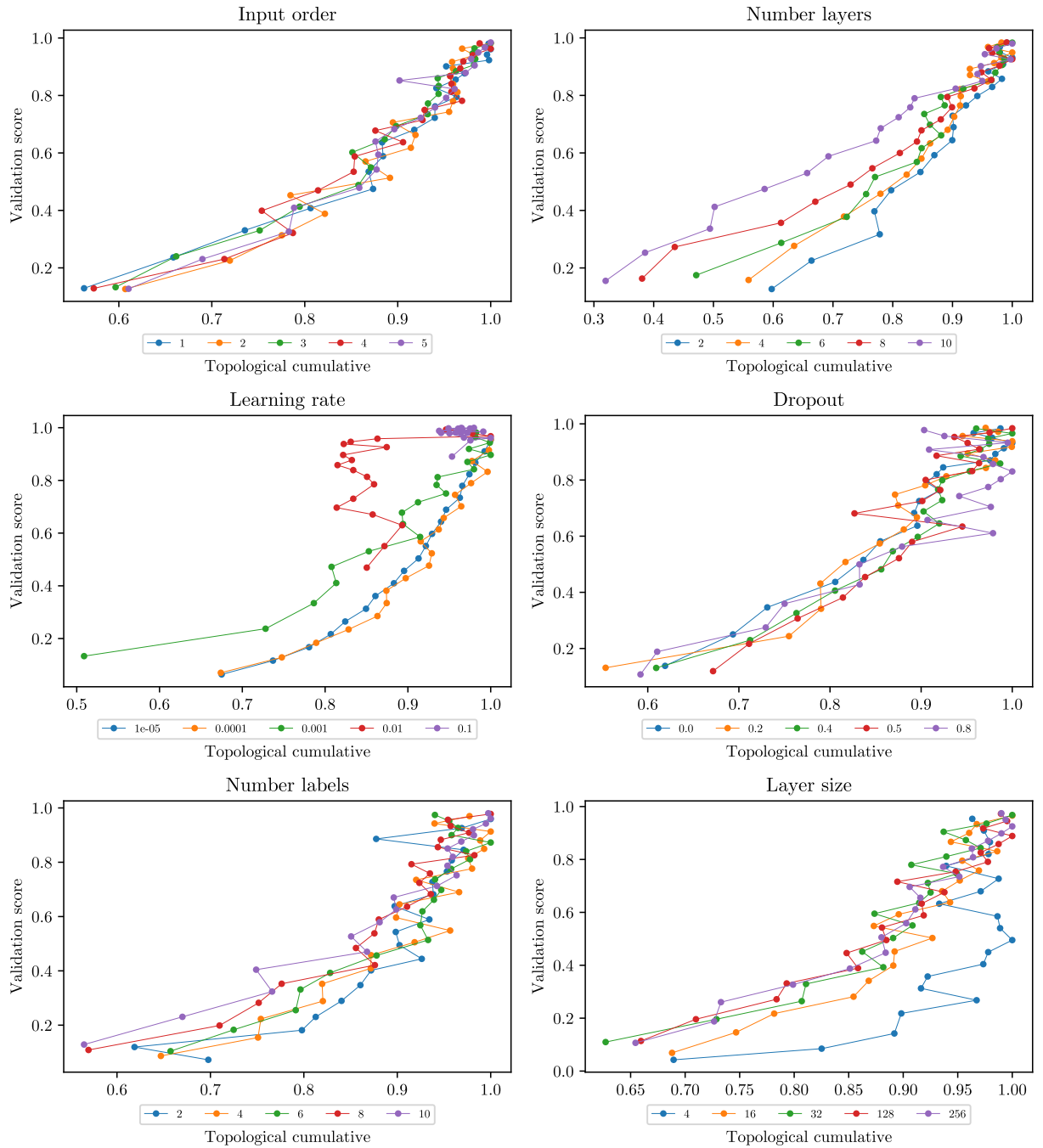


Figure 49: CIFAR-10 MLP points relationship across epochs using Silhouette discretization.

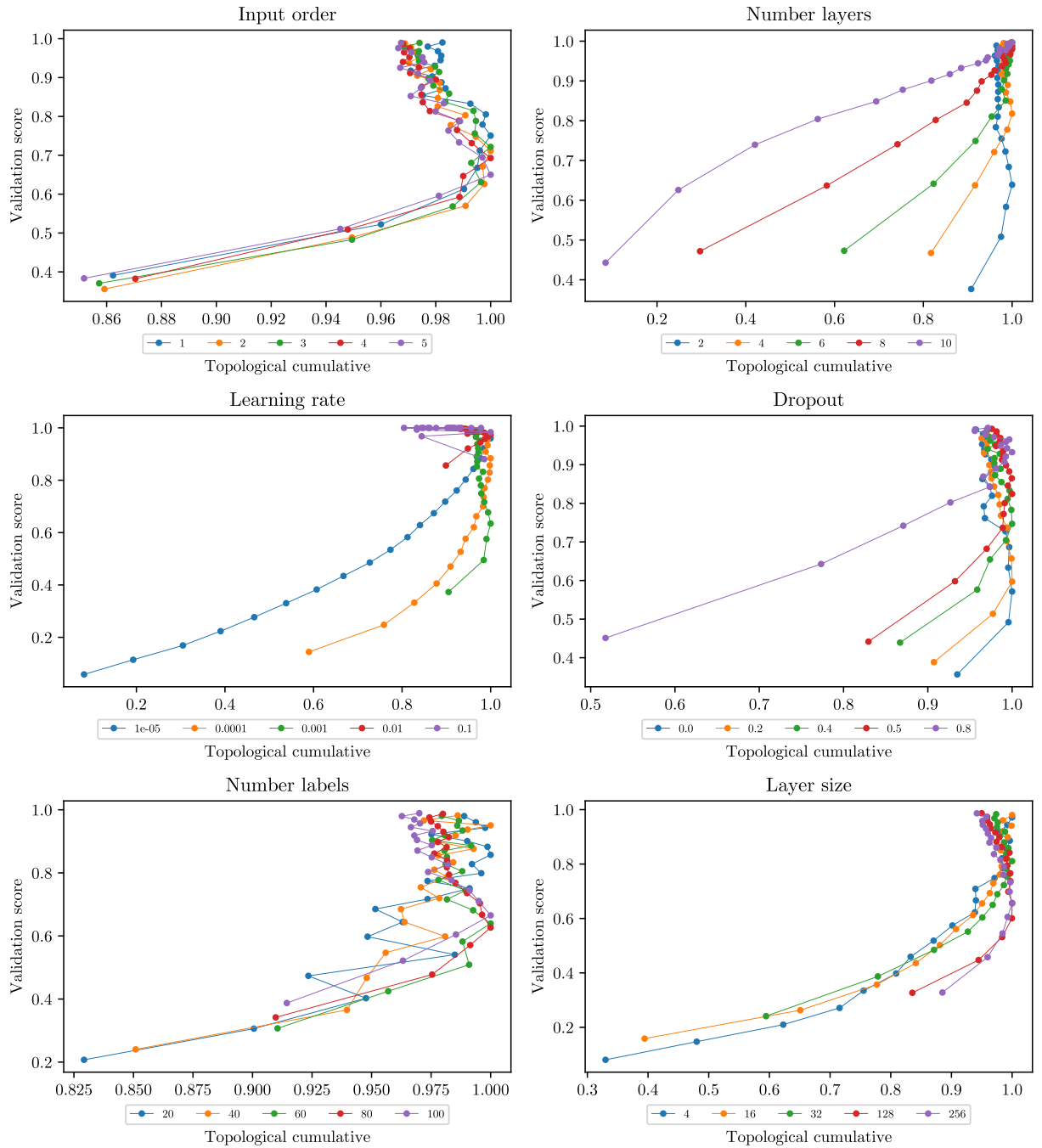


Figure 50: CIFAR-100 CNN points relationship across epochs using Heat discretization.

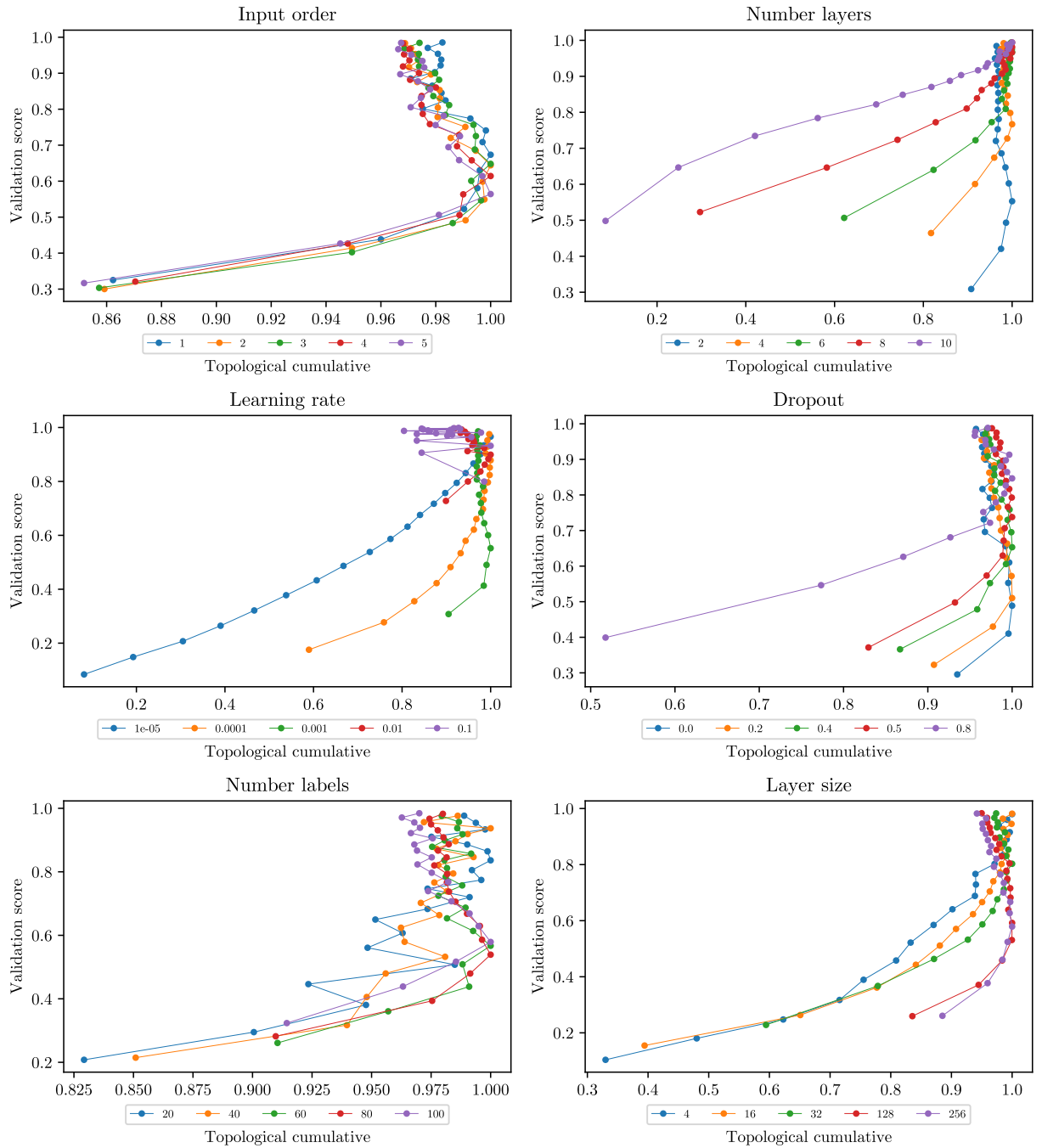


Figure 51: CIFAR-100 CNN points relationship across epochs using Silhouette discretization.

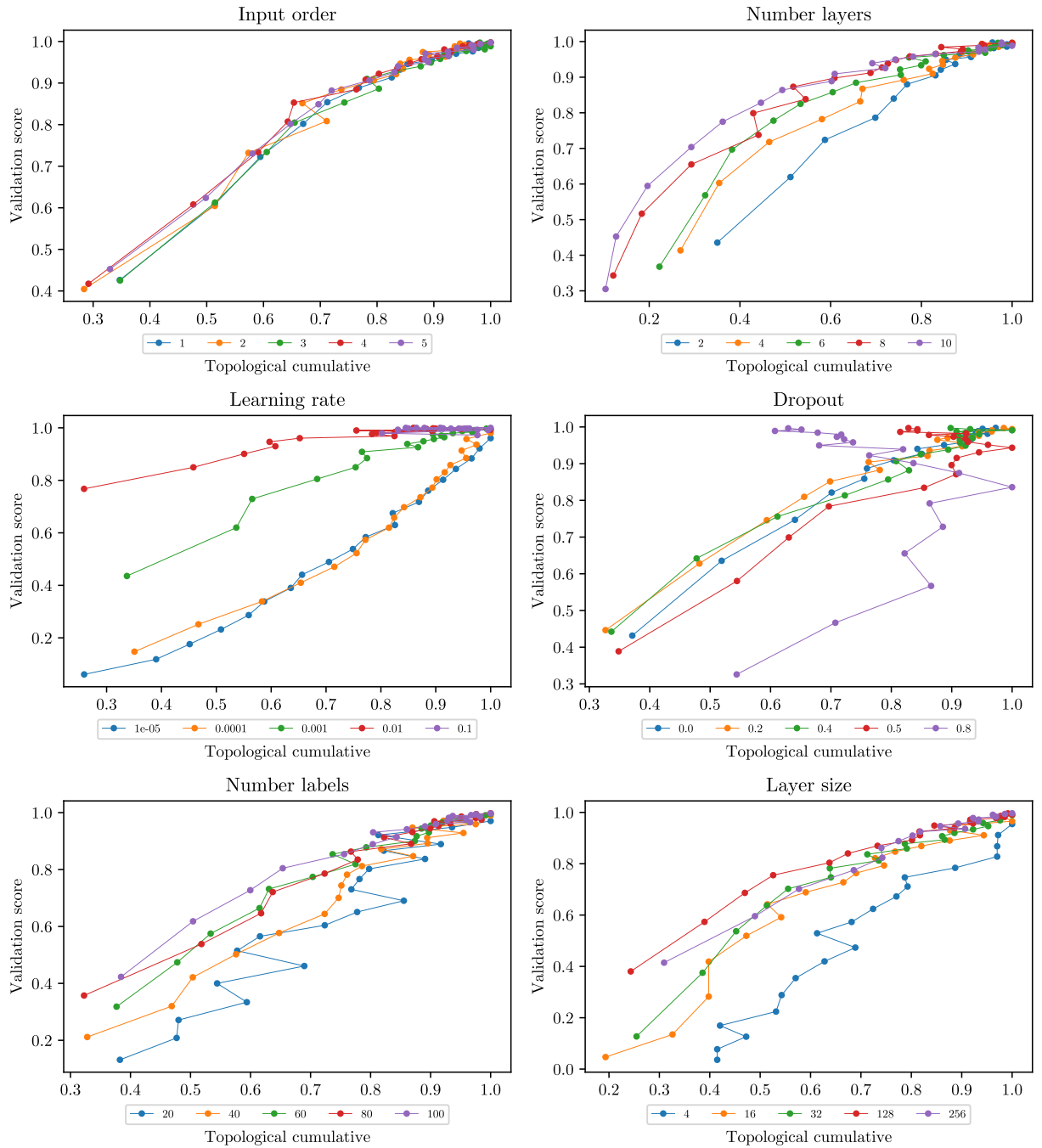


Figure 52: CIFAR-100 MLP points relationship across epochs using Heat discretization.

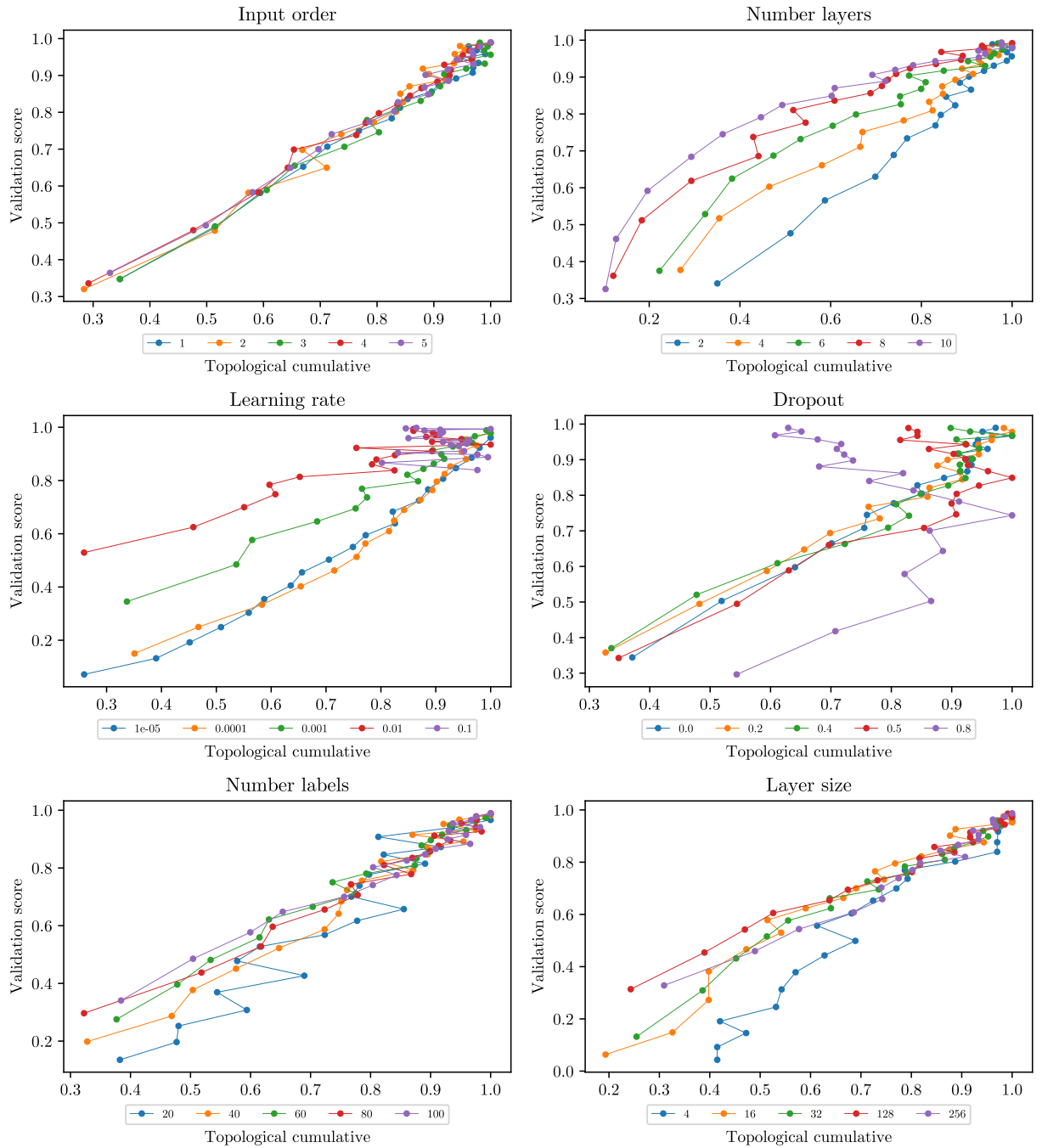


Figure 53: CIFAR-100 MLP points relationship across epochs using Silhouette discretization.